

128407

**DYNAMIC RESPONSE OF HAGIA SOPHIA  
CONSIDERING CRACKS**

**DOKTORA TEZİ**

**Meltem ŞAHİN**

**İnşaat Yüksek Mühendisi**

**YÜKSEKÖĞRETİM KURULU  
BAŞKANLIĞI'NA  
GÖNDERİLMİŞTİR**

**YAPI MÜHENDİSLİĞİ PROGRAMI**

**Jüri Üyeleri: Prof. Dr. İhsan Mungan**

**Prof. Dr. Sadettin Ökten**

**Prof. Dr. Mustafa Erdik**

**Prof. Dr. Özal Yüzügüllü**

**Yrd. Doç. Dr. Fevzi Dansık**

128407



To my father Hüsnu Şahin,  
my mother Yıldız Şahin,  
my sister Çiğdem Şahin,  
and my brother Hidayet Şahin

## ACKNOWLEDGEMENT

This Thesis has been performed in Mimar Sinan University, in the Institute for Graduate Studies in Science and Engineering, in Structural Engineering Program. In this Thesis, Hagia Sophia has been investigated from both static and dynamic points of view. During the static analysis, the crack propagation through the structure under the increasing vertical static loads has been investigated, and during the dynamic analysis, the dynamic response of the structure including cracks occurring under its self-weight has been examined.

I would like to thank to my supervisor, Prof. Dr. İhsan Mungan for his worthy suggestions and guiding.

I must also express my deepest gratitude to Prof. Dr. Sadettin Ökten for his support in technical details and guiding.

I also thank to Prof. Dr. Mustafa Erdik for his worthy suggestions about the Thesis.

I also would like to thank to Dr. Fevzi Dansık for his support and encouragement during the courses of the Thesis.

I thank to Ahmet Şenoğulları for his contributions in solving problems with the computer program and also thank to his family for their sincere hospitality.

I would also like to thank all who encouraged me to complete this thesis.

January, 2002

Meltem Şahin

## TABLE of CONTENTS

LIST of FIGURES.....	vii
LIST of TABLES .....	ix
LIST of INDEX.....	x
SUMMARY .....	xiv
ÖZET .....	xvi
<b>1. INTRODUCTION.....</b>	<b>1</b>
<b>1.1. Significance of the Subject.....</b>	<b>1</b>
<b>1.2. Previous Works on the Subject.....</b>	<b>1</b>
<b>1.3. Objectives of the Research.....</b>	<b>6</b>
<b>2. STRUCTURAL ANALYSIS of HISTORICAL MASONRY STRUCTURES.....</b>	<b>8</b>
<b>2.1. Basic Concepts, Definitions and Stress-Strain Behaviour of Masonry.....</b>	<b>8</b>
2.1.1. Material Properties of Historical Masonry.....	10
2.1.2. Testing Techniques used in Masonry .....	11
<b>2.2. Methods of Structural Evaluation of Historical Masonry Structures .....</b>	<b>13</b>
2.2.1. Development of a Physical Model and its Analysis .....	14
2.2.2. Methods for Modelling of Cracks .....	15
A. Smearred Crack Modelling Method.....	15
B. Discrete Crack Modelling Method .....	18
C. Comparing the Methods.....	20
D. An Example for the Smearred and Discrete Crack Modelling Methods.....	20
<b>3. STRUCTURAL PROPERTIES of HAGIA SOPHIA.....</b>	<b>27</b>
<b>3.1. Architectural Features of Hagia Sophia.....</b>	<b>28</b>
<b>3.2. Materials used in the Structural System of Hagia Sophia .....</b>	<b>31</b>
<b>3.3. Structural System of Hagia Sophia .....</b>	<b>33</b>
<b>3.4. Previous Restorations and Renovations on Hagia Sophia .....</b>	<b>40</b>
<b>4. ANALYSIS of the STRUCTURAL SYSTEM of HAGIA SOPHIA .....</b>	<b>50</b>
<b>4.1. Finite Element Models used in the Analyses .....</b>	<b>50</b>
4.1.1. Material Properties .....	59



4.1.2.	Supports .....	60
4.1.3.	Types and Properties of the Elements chosen in the Models .....	62
	Frame Elements.....	62
	Shell Elements.....	64
	Solid Elements.....	67
<b>4.2.</b>	<b>Assumptions of SAP2000 .....</b>	<b>69</b>
4.2.1.	Force-Deformation Relationships.....	69
4.2.2.	Anisotropic Materials .....	70
4.2.3.	Dynamic Analysis .....	72
	A. Eigen-value Analysis .....	72
	B. Definition of Response Spectrum.....	73
<b>4.3.</b>	<b>Methods of Analysis and Solution Techniques.....</b>	<b>74</b>
4.3.1.	Load Increment Method.....	74
4.3.2.	Spectral Analysis .....	78
<b>5.</b>	<b>RESULTS AND FINDINGS .....</b>	<b>85</b>
<b>5.1.</b>	<b>Results of the Static Analysis .....</b>	<b>85</b>
5.1.1.	Static Analysis of the First Model .....	85
	The Main Dome .....	86
	Semidomes.....	86
	Arches, Pendentives and Piers .....	88
5.1.2.	Static Analysis of the Second Model.....	92
	The Main Dome .....	92
	Semidomes.....	93
	Arches, Pendentives and Piers .....	93
5.1.3.	Static Analysis of the Third Model.....	99
	The Main Dome .....	100
	Semidomes.....	100
	Arches, Pendentives and Piers .....	101
5.1.4.	Static Analysis of the Fourth Model.....	108
<b>5.2.</b>	<b>Results of the Spectral Analysis.....</b>	<b>110</b>
5.2.1.	Spectral Analysis of the First Model .....	110
	A. Earthquake in the X-Direction .....	110
	The Main Dome .....	112

Semidomes.....	113
Arches, Pendentives and Piers .....	114
B. Earthquake in the Y-Direction .....	115
The Main Dome and Semidomes.....	115
Arches, Pendentives and Piers .....	116
5.2.2. Spectral Analysis of the Third Model.....	129
A. Earthquake in the X-Direction .....	129
B. Earthquake in the Y-Direction .....	130
<b>6. DISCUSSION OF THE RESULTS AND CONCLUSIONS .....</b>	<b>138</b>
REFERENCES.....	144



## LIST of FIGURES

Figure 2.1-1	Different Kinds of Masonry .....	9
Figure 2.1-2	The $\sigma$ - $\varepsilon$ , $\tau$ - $\nu$ Relationships in Uniaxial Compression for Masonry.....	9
Figure 2.2-1	Plane Stresses Case.....	16
Figure 2.2-2	Idealised Representation of a Single Crack in the Smearred Crack Modelling.....	18
Figure 2.2-3	The Representation of Cracks in the Discrete Crack Modelling Approach....	19
Figure 2.2-4	Simple Beam Example.....	21
Figure 2.2-5	The Maximum Principal Stress Distribution through the Beam for the Smearred Crack Modelling Method .....	25
Figure 2.2-6	The Maximum Principal Stress Distribution through the Beam for the Discrete Crack Modelling Method.....	26
Figure 3-1	Hagia Sophia today .....	27
Figure 3.1-1	The Plan of the Entrance Floor of Hagia Sophia .....	29
Figure 3.1-2	The Elevations of Hagia Sophia .....	30
Figure 3.3-1	Isometric Plan, Longitudinal Section and Cross Section of Hagia Sophia.....	34
Figure 3.3-2	The Main Structural System with the Secondary Systems.....	35
Figure 3.3-3	The Five Secondary Structural Systems of Hagia Sophia.....	36
Figure 3.3-4	Thrust Lines in the Main Vaulting System and the General Pattern of Associated Cracking .....	38
Figure 3.4-1	The Join between the Fourteenth-Century Reconstruction of the Dome and the Surviving Sixth-Century Work.....	42
Figure 3.4-2	Isometric View of the Arches.....	42
Figure 3.4-3	The Buttresses at the South .....	44
Figure 3.4-4	The Buttresses at the East .....	45
Figure 3.4-5	The Flying Buttresses at the East.....	45
Figure 3.4-6	The Buttresses at the North .....	46
Figure 3.4-7	The Flying Buttresses at the West .....	46
Figure 3.4-8	The Structure from the South .....	47
Figure 3.4-9	The Structure from the South-West in 1847.....	49
Figure 4.1-1	The 3 Dimensional and Top Views of M1 .....	52
Figure 4.1-2	The 3 Dimensional and Top Views of M2 .....	54
Figure 4.1-3	The Top Views of M3 (a) and M1 (b) .....	56
Figure 4.1-4	The 3 Dimensional and Top Views of M4 .....	57

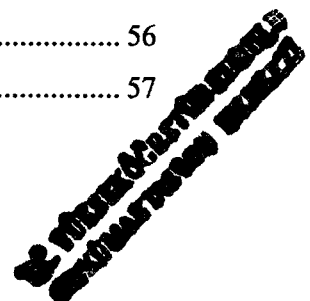


Figure 4.1-5	Four Models used in the Analyses: M1, M2, M3 and M4 .....	58
Figure 4.1-6	The Views of M1 from the South and West.....	59
Figure 4.1-7	The Directions of the Springs used in M2.....	61
Figure 4.1-8	The Position of the Supports .....	61
Figure 4.1-9	The Positive Axes, Forces and Moments of Frame Elements.....	63
Figure 4.1-10	General Types of Shell Elements.....	65
Figure 4.1-11	Forces and Moments in Shell Elements .....	66
Figure 4.1-12	Solid Elements.....	68
Figure 4.2-1	Definition of Positive Stresses.....	71
Figure 4.3-1	The Flow Chart of the Load Increment Method for the Smearred Crack Modelling.....	76
Figure 4.3-2	The Flow Chart of the Load Increment Method for the Discrete Crack Modelling.....	77
Figure 4.3-3	Stresses at Section of an Element .....	79
Figure 4.3-4	The Flow Chart to Determine the Cracks occurring under the Self-weight of the Structure .....	81
Figure 4.3-5	The Flow Chart of the Spectral Analysis for the Smearred Crack Modelling....	83
Figure 4.3-6	The Curve of Spectrum Coefficient according to the Turkish Earthquake Code.....	84
Figure 5.1-1	The Crack Propagation through M1 for the Collapse Load Factor .....	88
Figure 5.1-2	The Maximum Principal Stress Distribution through M1, $\lambda=0.8$ .....	89
Figure 5.1-3	The Maximum Principal Stress Distribution through M1, $\lambda=1$ .....	90
Figure 5.1-4	The Maximum Principal Stress Distribution through M1, $\lambda=1.2$ .....	91
Figure 5.1-5	The Crack Propagation through M2 for the Collapse Load Factor .....	94
Figure 5.1-6	The Maximum Principal Stress Distribution through M2, $\lambda=0.8$ .....	95
Figure 5.1-7	The Maximum Principal Stress Distribution through M2, $\lambda=1.2$ .....	96
Figure 5.1-8	The Maximum Principal Stress Distribution through M2, $\lambda=1.6$ .....	97
Figure 5.1-9	The Maximum Principal Stress Distribution through M2, $\lambda=1.8$ .....	98
Figure 5.1-10	The Crack Propagation through M3 for the Collapse Load Factor .....	102
Figure 5.1-11	The Maximum Principal Stress Distribution through M3, $\lambda=0.8$ .....	103
Figure 5.1-12	The Maximum Principal Stress Distribution through M3, $\lambda=1$ .....	104
Figure 5.1-13	The Maximum Principal Stress Distribution through M3, $\lambda=1.2$ .....	105
Figure 5.1-14	The Crack Propagation through M1, M2, and M3 for the Static Analysis .....	106
Figure 5.1-15	The Collapse Conditions for M1 and M3 for the Static Analysis.....	107

Figure 5.1-16	The Variation of the Vertical Displacement versus Load Factors for M1, M2, M3 and M4 .....	109
Figure 5.2-1	The Variation of the Horizontal Displacements in the X-direction at the Apex of the Main Dome versus the Accelerations for M1 under the Earthquake in the X-Direction.....	117
Figure 5.2-2	The Variation of the Period versus the Accelerations for M1 under the Earthquake in the X-Direction.....	117
Figure 5.2-3	The Crack Propagation through M1 for the Spectral Accelerations.....	118
Figure 5.2-4	$S_{11}$ Stresses of M1 for Acceleration 0.1g in the X-Direction .....	119
Figure 5.2-5	$S_{11}$ Stresses of M1 for Acceleration 0.2g in the X-Direction .....	120
Figure 5.2-6	$S_{11}$ Stresses of M1 for Acceleration 0.3g in the X-Direction .....	121
Figure 5.2-7	$S_{11}$ Stresses of M1 for Acceleration 0.4g in the X-Direction .....	122
Figure 5.2-8	$S_{22}$ Stresses of M1 for Acceleration 0.1g in the X-Direction .....	123
Figure 5.2-9	$S_{22}$ Stresses of M1 for Acceleration 0.2g in the X-Direction .....	124
Figure 5.2-10	$S_{22}$ Stresses of M1 for Acceleration 0.3g in the X-Direction .....	125
Figure 5.2-11	$S_{22}$ Stresses of M1 for Acceleration 0.4g in the X-Direction .....	126
Figure 5.2-12	$S_{11}$ Stresses of M1 for Acceleration 0.4g in the Y-Direction .....	127
Figure 5.2-13	$S_{22}$ Stresses of M1 for Acceleration 0.4g in the Y-Direction .....	128
Figure 5.2-14	$S_{11}$ Stresses of M3 for Acceleration 0.4g in the X-Direction .....	132
Figure 5.2-15	$S_{22}$ Stresses of M3 for Acceleration 0.4g in the X-Direction .....	133
Figure 5.2-16	$S_{11}$ Stresses of M3 for Acceleration 0.4g in the Y-Direction .....	134
Figure 5.2-17	$S_{22}$ Stresses of M3 for Acceleration 0.4g in the Y-Direction .....	135
Figure 5.2-18	$S_{11}$ Stresses of M1 and M3 for Acceleration 0.4g in the X-Direction.....	136
Figure 5.2-19	$S_{22}$ Stresses of M1 and M3 for Acceleration 0.4g in the X-Direction.....	137

## LIST of TABLES

Table 4.1-1	The Characteristic Values of the Materials used in the Analyses.....	60
-------------	--	----

## LIST of INDEX

$\sigma$ :	Axial Stress
$\tau$ :	Shear Stress
$\varepsilon$ :	Strain
$\gamma$ :	Shear Strain
[K]:	Elastic Stiffness Matrix
$\sigma_x$	Normal Stress in the X-Direction
$\sigma_y$ :	Normal Stress in the Y-Direction
$\sigma_z$ :	Normal Stress in the Z-Direction
$\tau_{xy}$ :	Shear Stress in the Y-Direction in the X Plane
$\tau_{yz}$ :	Shear Stress in the Z-Direction in the Y Plane
$\tau_{zx}$ :	Shear Stress in the X-Direction in the Z Plane
$\varepsilon_x$ :	Strain in the X-Direction
$\varepsilon_y$ :	Strain in the Y-Direction
$\varepsilon_z$ :	Strain in the Z-Direction
$\gamma_{xy}$ :	Shear Strain in the Z Plane
$\gamma_{yz}$ :	Shear Strain in the X Plane
$\gamma_{zx}$ :	Shear Strain in the Y Plane
E:	Young's Modulus
$\nu$ :	Poisson's Ratio
[C <sub>cr</sub> ]:	Tangent Material Stiffness for Cracked Elements
$d\sigma_n$ :	Normal Stress Increment in the n-Direction
$d\sigma_t$ :	Normal Stress Increment in the t-Direction
$d\tau_{nt}$ :	Shear Stress Increment
$d\varepsilon_n$ :	Lateral Strain Increment in the n-Direction
$d\varepsilon_t$ :	Lateral Strain Increment in the t-Direction
$d\gamma_{nt}$ :	Shear Strain Increment in the n-t Plane
$\beta$ :	Shear Retention Factor
G:	Shear Modulus
M:	Bending Moment
W:	Section Modulus
$\sigma_{limit}$ :	Crack Limit Strength
q:	Load

$l$	Span of the Beam
$q_c$	Collapse Load Value
$\lambda_c$	Collapse Load Factor
$b$	Element Width
$h$	Element Thickness
$M1$	First Model
$M2$	Second Model
$M3$	Third Model
$M4$	Fourth Model
$F, N$	Axial Force for Frame Elements
$V_2$	Shear Force in the 1-2 Plane
$V_3$	Shear Force in the 1-3 Plane
$T$	Torsion for Frame Elements
$M_2$	Bending Moment in the 2-Direction for Frame Elements
$M_3, M$	Bending Moment in the 3-Direction for Frame Elements
$\Theta_x$	Rotation around the X-Axis
$\Theta_y$	Rotation around the Y-Axis
$\Theta_z$	Rotation around the Z-Axis
$u$	Displacement in the X-Direction
$v$	Displacement in the Y-Direction
$w$	Displacement in the Z-Direction
$F_{11}$	Axial Plane Force in the 1-Direction for Shell Elements
$F_{12}$	Shear Force in the 1-2 Plane for Shell Elements
$F_{22}$	Axial Plane Force in the 2-Direction for Shell Elements
$F_{MIN}$	Minimum Principal Force for Shell Elements
$F_{MAX}$	Maximum Principal Force for Shell Elements
$M_{11}$	Bending Moment in the 2-Direction for Shell Elements
$M_{12}$	Twisting Moment in the 1-2 Plane for Shell Elements
$M_{22}$	Bending Moment in the 1-Direction for Shell Elements
$M_{MIN}$	Minimum Principal Moment for Shell Elements
$M_{MAX}$	Maximum Principal Moment for Shell Elements
$S_{11}, \sigma_1$	Stress in the Local 1-Axis in the 2-3 Plane for both Shell and Solid Elements

$S_{22}, \sigma_2$ :	Stress in the Local 2-Axis in the 1-3 Plane for both Shell and Solid Elements
$S_{MIN}$ :	Minimum Principal Stress for both Shell and Solid Elements
$S_{MAX}$ :	Maximum Principal Stress for both Shell and Solid Elements
$S_{33}, \sigma_3$ :	Stress in the Local 3-Axis in the 1-2 Plane for Solid Elements
$S_{12}, \tau_{12}$ :	Stresses in the Local 2-Axis in the 2-3 Plane for Solid Elements
$S_{21}, \tau_{21}$ :	Stresses in the Local 1-Axis in the 1-3 Plane for Solid Elements
$S_{13}, \tau_{13}$ :	Stresses in the Local 3-Axis in the 2-3 Plane for Solid Elements
$S_{31}, \tau_{31}$ :	Stresses in the Local 1-Axis in the 1-2 Plane for Solid Elements
$S_{23}, \tau_{23}$ :	Stresses in the Local 2-Axis in the 1-2 Plane for Solid Elements
$S_{32}, \tau_{32}$ :	Stresses in the Local 3-Axis in the 1-3 Plane for Solid Elements
$\Delta$ :	Total Deformation
$L$ :	Length of the Element
$A$ :	Cross-Sectional Area
$k_a$ :	Axial Stiffness
$f_a$ :	Axial Flexibility
$\{u\}$ :	Displacement Vector
$\{R\}$ :	Force Vector
$\alpha_i$ :	Thermal Expansion
$\omega$ :	Unit Weight
$\rho$ :	Unit Mass
$\{f\}$ :	Stress Matrix
$\{d\}$ :	Strain Matrix
$\epsilon_1, \epsilon_2, \epsilon_3$	Unit Lengthening in the 1,2, and 3-Directions, respectively
$\gamma_{21}$ :	Unit Rotation in the 1-2 Plane
$\gamma_{31}$ :	Unit Rotation in the 1-3 Plane
$\gamma_{23}$ :	Unit Rotation in the 2-3 Plane
$\Delta T$ :	Temperature Change
$\alpha_1, \alpha_2, \dots$ :	Thermal Expansions in the 1,2,... Directions
$\nu_{14}, \nu_{12}, \dots$ :	Poisson Ratios
$[\acute{C}]$ :	Compliance Matrix
$\{a\}$ :	Strain Matrix due to Unit Temperature Increment
$\{f_0\}$ :	Stress Matrix due to Temperature Change
$[M]$ :	Mass Vector



$\{\ddot{u}\}$ :	Acceleration Vector
$\{u\}$ :	Displacement Vector
$[\Omega^2]$ :	Modal Frequencies
$\{\phi\}$ :	Mode Shapes
$[C]$ :	Damping Matrix
$\{\dot{u}\}$ :	Velocity Vector
$\ddot{u}_{gx}$ :	X-Component of Uniform Ground Acceleration
$\ddot{u}_{gy}$ :	Y-Component of Uniform Ground Acceleration
$\ddot{u}_{gz}$ :	Z-Component of Uniform Ground Acceleration
$P_v$ :	Vertical Load Applied to the Structure
$\lambda$ :	Load Factor
$W_s$ :	Self-weight of the Structure
$h_{cr}$ :	Crack Depth
$\sigma_{tlimit}$ :	Crack Limit Tension Strength
$\sigma_t$ :	Tension Strength
$\sigma_c$ :	Compression Strength
$x$ :	Depth of the Tension Region in an Element
$x'$ :	Depth of the Uncracked Section in the Tension Region
$E_{cr}$ :	Modulus of Elasticity of the Cracked Region
$a$ :	Acceleration
$T_A, T_B$ :	Characteristic Periods depend on the Soil Type
$T$ :	Period
$S(T)$ :	Spectrum Coefficient

## **SUMMARY**

### **DYNAMIC RESPONSE OF HAGIA SOPHIA CONSIDERING CRACKS**

Hagia Sophia attracts the interest of structural engineers, architects, and art historians because of its unique structural system and size considering its nearly 1500 years age. In order to understand the features and the behaviour of the structure, many studies have been carried out for many years until today

Hagia Sophia had held the record of being the world's largest domed building for some 800 years. In order to preserve this historical structure, it is necessary to understand its earthquake response in its current condition. Therefore, it is important to study the dynamic vulnerability of Hagia Sophia, which includes cracks already.

In this study, four different computational models are used. The First Model taken from the Kandilli Earthquake Observatory and Research Institute was originally developed in Princeton University. Both static and dynamic analyses are performed with this model, and the cracks are taken into account using the Smeared Crack Modelling Method. However, the crack propagation through the main structural elements cannot be detected clearly with this model, since initial cracks start at the connection region between the secondary semidomes and the main semidomes. The purpose of this study is to investigate the crack propagation through the main structural elements. Hence, the Second Model, which consists of only the main load bearing elements, is also investigated in the first part of the study. The Second Model is derived from the First Model by letting the secondary load bearing elements out of consideration. Only static analysis is performed with the Second Model. The cracks are imposed on the model using the Discrete Crack Modelling Method. Since the procedure of the discrete crack modelling is time consuming, it is used only in the Second Model, which has relatively small number of elements as compared to the other models used in this study.

As an alternative to the First Model, the size of the weak east and west arches is increased to be equal to the size of the strong north and south arches to study the effect of the arch stiffness on the crack propagation. Both static and dynamic analyses are performed with this model, namely the Third Model, and again, the Smearred Crack Modelling Method is used to take cracks into account.

Furthermore, as another alternative to the First Model, a steel ring is placed between the top of the windows and the main dome to find out its effect on crack propagation. This model, namely the Fourth Model, is investigated with only static analysis, since there is not a big difference between the results of the First and Fourth Models.

The analyses performed in this study are divided into two parts. At the first part, static analysis is performed using the Load Increment Method and the crack propagation through the structure under increasing vertical static loads. Basically, the Smearred Crack Modelling Method is used in modelling of cracks, but as an example, the Discrete Crack Modelling Method is also considered at the first part of the analyses. When cracks cover one third of the surface of the main load bearing elements, the structure is considered as collapsed, and the iterations are finished. In this study, the main objective is not to assess the collapse load of the structure, but to follow the propagation of cracks through the structure, and hence to determine its collapse behaviour. For this end, the Smearred Crack Modelling Method is preferred in the analyses, because, it is a good method to determine the collapse behaviour and sufficient enough to obtain the approximate collapse load of the structural system.

At the second part, the dynamic vulnerability of the structure including cracks caused by self-weight, is studied using the spectral analysis method. The cracked state of the structure under self-weight is obtained applying the Load Increment Method. Cracks occurring at each step are imposed on the structure using the Smearred Crack Modelling Method for different assumptions. After the propagation of these cracks stop, the spectral accelerations are applied to the structure with the starting value of 0.04g. Using the Acceleration Increment Method, the crack propagation of the structure is obtained at each increased acceleration value. This iteration is ceased, when the crack propagation stops at acceleration 0.4g.

## ÖZET

### ÇATLAKLARIN GÖZÖNÜNDE TUTULMASI DURUMUNDA AYASOFYA'NIN DİNAMİK DAVRANIŞI

Ayasofya, yapı sistemi ile yaklaşık 1500 yıllık geçmişi boyunca yapı mühendisleri ve mimarların büyük ölçüde ilgisini çekmiştir. Ancak, yapı sistemi gerek uğradığı doğal afetlerden, gerekse onarım ve takviye çalışmalarından günümüze gelene kadar bir takım değişikliklere uğramıştır. Yapının daha uzun yıllar ayakta kalmasını sağlamak amacıyla üzerinde araştırmalar yapılmaya devam edilmekte ve onarım çalışmaları sürmektedir.

Bu çalışmada, bugüne kadar yapılan çalışmalardan farklı olarak, yapıda oluşabilecek çatlakların yapı içinde yayılışı ve çatlakların kesit zayıflaması olarak ele alınması durumunda yapının depreme karşı göstereceği direnç incelenmiştir.

Bu amaçla çalışmanın ilk bölümünde, ele alınan konunun önemi anlatılıp konu tanıtılmaya çalışılmış ve ayrıca, konu ile ilgili daha önce yapılan çalışmalar özetlenmiştir.

İkinci bölümde, tarihi yığma yapılar üzerinde yapılan çalışmalar ve bunların analizinde kullanılan metodlar anlatılmıştır. Yapının davranışını gerçeğe en yakın şekilde elde etmek, yapının inşasında kullanılan malzemelerin özelliklerinin belirlenmesindeki hassasiyete bağlıdır. Bu nedenle, öncelikle tarihi yapıların malzeme özellikleri genel olarak anlatılmış, gerilme şekil değiştirme diyagramları hakkında bilgiler verilmiştir.

İkinci bölümde ayrıca, tarihi yapılarda uygulanan test teknikleri incelenmiştir. Tarihi yapılarda yapılan testlerde göz önüne alınması gereken en önemli kriter yapıya hasar vermemektir. Bu nedenle, bu tür yapılarda tahribatsız veya en azından az tahribatlı deneylerin uygulanması tercih edilir. Bu bölümde ayrıca, bu deney

tekniklerinden kısaca bahsedilmiştir. Bundan sonraki kısımda ise teorik çalışmalara ışık tutacak fiziksel modellerin oluşturulması ve bunun önemi anlatılmıştır.

Ayrıca, analizlerde kullanılan metodlar hakkında genel bilgi verilmiştir. Çatlaklar, Çatlak Modelleme Metodları kullanılarak modellenmiştir. Bu nedenle, bu metodları uygulayarak basit bir giriş için göçme yüküne kadar çatlak yayılımı incelenmiştir.

Çalışmanın üçüncü bölümünde, Ayasofya'nın mimari, yapısal ve malzeme özellikleri anlatılmış, ayrıca, yapıdaki daha önceki restorasyon çalışmalarından da detaylı olarak bahsedilmiştir.

Dördüncü bölümde, bu çalışmada kullanılan modeller tanıtılmış, hesaplarda göz önüne alınan yaklaşımlar ve malzeme özellikleri anlatılmıştır. Ayrıca, uygulanan çözüm teknikleri de bu bölümde detaylı olarak açıklanmıştır.

Yapılan analizler iki kısma ayrılmıştır. Birinci kısımda, statik analiz uygulanarak yük artımı metodu ile çatlak yayılımı saptanmıştır. Çatlaklar 2. bölümde bahsedilen Çatlak Modelleme Metodları kullanılarak hesaba katılmıştır. İkinci kısımda ise, önce yapının kendi ağırlığı altında oluşan çatlaklar, hesapların birinci kısmında olduğu gibi, yük artımı metodu ile tesbit edilmiştir. Yapının ağırlığının 0.8 katı altında bile çatlak oluşması nedeni ile iterasyona bu değerden başlanmıştır. Yapının kendi ağırlığı altında oluşan çatlaklarının yayılımı durduğunda, yapıya 0.04g'lik ivme değerinden başlayarak spektral ivme değerleri, hem doğu-batı hem de kuzey-güney yönlerinde ayrı ayrı uygulanmıştır. İvme artımı yöntemi uygulanarak her 0.02g'lik ivme artışı için çatlakların yayılımı incelenmiştir. Bu analiz 0.4g'lik ivme değerinde çatlak yayılımı durana kadar devam ettirilmiştir. Çatlaklar yapıya, ikinci bölümde bahsedilen yöntemlerden Yayılı Çatlak Modelleme Metodu kullanılarak dahil edilmiştir. Bu metod uygulanırken çatlayan elemanların elastisite modüllerinin çatlamamış kalınlıklarının 3/2'inci kuvveti ile orantılı olarak azaldığı kabulü yapılmıştır. Bu şekilde, çatlayan elemanlarda eleman kalınlığı ve çatlak kalınlığı arasındaki orandan, çatlak derinliğine bağlı olarak çatlayan elemanların yeni elastisite modülleri hesaplanmıştır. Çatlayan elemanlar için iterasyonun bir sonraki adımında bu elastisite

modülleri kullanılmıştır. Çatlak etkisi bu şekilde azaltılan elastisite modülleri ile kesit zayıflaması şeklinde hesaba katılmıştır.

Analizlerde Ayasofya'nın dört farklı modeli kullanılmıştır. Birinci Model Kandilli Deprem İnceleme ve Araştırma Merkezi'nden alınmıştır. Bu model ilk olarak Princeton Üniversitesi'nde hazırlanmış olup modelde Kandilli Deprem İnceleme ve Araştırma Merkezi'nde birtakım değişiklikler yapılmıştır. Birinci Model'de çatlak yayılışı, Yayılı Çatlak Modelleme Metodu kullanılarak tespit edilmiştir. İlk çatlaklar, ikinci derece yarı kubbelerin ana yarı kubbelere birleştiği yerde başlayıp ana yarı kubbelerin içine doğru ilerlemiş ve bu elemanların yıkılmasına neden olmuştur. Bu modelde, kalınlıkları ana yarı kubbelerin kalınlıklarının yarısı kadar olan ikinci derece yarı kubbelere yapıdaki çatlak yayılışını kontrol etmektedir. Bu durum, çalışmanın asıl amacı olan ana yarı kubbelere beraber üst ana taşıyıcı elemanlardaki çatlak yayılışının tesbit edilmesini güçleştirmektedir. Bu nedenle Birinci Model, sadece ana taşıyıcı elemanlardan oluşmak üzere sınırlandırılarak ikinci bir model oluşturulmuş ve bu modelin çatlak yayılışı incelenmiştir. Çatlak Ayırma Modelleme Metodunda çatlakların modele uygulanması için gerekli işlemler çok zaman gerektirdiğinden, bu metod sadece, bu çalışmada kullanılan diğer modellere göre daha küçük olan İkinci Modelde uygulanmıştır. İkinci Modelde statik analiz uygulanarak yük artımı metodu ile göçme davranışı tesbit edilmiştir. Bu modelde çatlaklar ana kubbede oluşmuş, ana yarı kubbelere ise tepe noktalarının ana kemerlere bağlandıkları yerler dışında çatlama oluşmamıştır.

Ayrıca, yapının dayanımını arttırıcı iki öneri geliştirilmiş ve bu öneriler için iki alternatif model hazırlanmıştır. Birinci alternatif modelde, Üçüncü Model, doğu ve batıdaki zayıf kemerlerin yerine kuzey ve güney kemerleri ile aynı rijitlikte kemerler yerleştirilmiş, ikinci öneride ise ana kubbe ile oturduğu pencerelerin arasına çelikten yapılmış bir kasnak yerleştirilmiştir. Her iki alternatif model için çatlak yayılışı Yayılı Çatlak Modelleme Metodu ile saptanmıştır. İkinci alternatif modelde elde edilen sonuçların Birinci Modelde elde edilen sonuçlarla hemen hemen aynı olması nedeni ile bu model sadece statik açıdan incelenmiştir. Buna karşılık, ilk alternatif model hem statik hem de dinamik analizler uygulanarak incelenmiştir.

Beşinci bölümde, yapılan analizlerin sonuçları grafikler yardımıyla detaylı olarak anlatılmıştır. Buna göre, Birinci, Üçüncü ve Dördüncü Modellerde göçme ana taşıyıcı elemanlardan ilk olarak batı yarı kubbede gözlenmiştir. Diğer yandan, İkinci Modelde göçme ana kubbede görülmüştür. Statik yükler altında çatlak yayılışlarında farklılıklar olmasına karşın Üçüncü Modelin göçme mekanizması İlk Modelle aynıdır. Buna rağmen, Üçüncü Modelde dinamik yükler altında gerilme değerleri İlk Modeldeki değerlere göre çok küçük çıkmıştır. Buna göre, yapının doğu ve batısındaki ana kemerleri kuzey ve güneyindeki ana kemerleri kadar büyük yapılmış olsaydı, yapının günümüze gelene kadar geçirmiş olduğu depremlerde yıkılmayacağı söylenebilir.

Altıncı bölümde, çatlak yayılışı uygulanarak elde edilen statik ve dinamik analiz sonuçlarına göre, 5. Bölümde anlatılan göçme riski en fazla olan bölgeler özetlenmiş ve elde edilen sonuçlara göre yapının onarımı ve güçlendirilmesine yönelik öneriler verilmeye çalışılmıştır. Bu bölümde ayrıca, bu çalışmayı takip edecek ileriki çalışmalara yön verecek öneriler getirilmiştir.



# CHAPTER 1

## INTRODUCTION

### 1.1. Significance of the Subject

Many historic structures still survive, although they have experienced many natural disasters during their lives. These structures are the heritage of mankind. Hence, a big attention has to be given to their preservation and restoration to ensure that they will survive with minimum damage for coming centuries. For this aim structural analyses are performed to understand their load carrying behaviour. These analyses are generally carried out in two steps:

- The first step consists of observations and tests related with the structural elements and the soil-structure interaction. In this phase, the foundations, soil conditions, structural behaviour, the material behaviour, density and ratio of humidity are determined. In this way, it is possible to develop the model, which represents the structure best, and to determine the characteristic values used in calculations.
- In the second step, static and dynamic analyses are performed. In addition the effects of heat, support settlements and environment are thoroughly investigated. With the help of these analyses, the structural behaviour and the stress distribution through the structure is determined. When the response of a structure is investigated under loads, either static or dynamic, some proposals and methods for its restoration and retrofitting can easily be developed.

### 1.2. Previous Works on the Subject

Because of its unique structural system and size considering its age of nearly 1500 years, Hagia Sophia attracts the interest of structural engineers, architects, and

Dr. Mustafa Kemal University  
Engineering Faculty



art historians. In order to understand the features and the behaviour of the structure many studies have been carried out until today. The aim of this study is mainly to observe the effect of the cracks on the response of the structure due to both static and dynamic loading. Hence first, the previous works related to the subject are reviewed. Selected studies are briefly explained in chronological order in the following:

Kato, Aoki, Hidaka and Nakamura (1991) have prepared a finite element model for the dome of Hagia Sophia composed of 9-node Heterosis shell elements. They have investigated the structure utilising an elastic analysis. The result of the analysis has seemed to reveal the fundamental structural behaviour of the dome. The deformation pattern of the elastic analysis has been similar to that observed in the structure, but there are differences in the magnitudes of the displacements. The displacements have been completely of different order. The authors have also performed elasto-plastic analysis to investigate the effectiveness of the analysis to simulate the magnitude of the deformations. At the stage of self-weight loading, the magnitude and the pattern of the global deformation are almost the same as those in the former analysis. However, according to the results of the second analysis they have concluded that the dome could endure a load, which is 1.9 times of the self-weight. They have observed that the north to south arches between the main dome and the semidomes and the west foot of the main dome deform progressively. Moreover, it has been obtained that the displacements of the north to south arches are higher than that of the west to east arches.

Durukal (1992) has prepared a thesis having the title 'A Study on Structural Identification and Seismic Vulnerability Assessment of Hagia Sophia'. A model frequencies of which matched the results of the ambient vibration survey has been obtained. Using this final model, the structure has been investigated dynamic point of view. According to the results of the dynamic analysis, stress concentrations are observed in the top of the four main arches and at their springing points. The main dome is in good condition, but in the main semidomes, the stresses intensify in areas close to the east and west main arches.

Türkmen (1994) has compared the load carrying mechanisms of the domes of Hagia Sophia, Süleymaniye Mosque, Şehzade Mosque and Mihrimah Sultan Mosque. The solutions have been investigated in respect of different thicknesses for space covers of these structures utilising the finite element method. The models of space covers of the structures have been established for the springing levels of arches resting on the columns and analysed by utilising the structural analysis computer program SAP90. In these solutions, the sub-structure that carries the main dome has been examined considering various sizes or rigidity of the arches. In the solutions obtained for Hagia Sophia, it has been shown that the displacements and stresses in the load carrying elements are higher than those in the other structures investigated. In addition, it has been concluded that cracks caused by either shear or compression stresses may occur parallel to the axes of arches in the regions where the main dome is attached to the pendentives.

Aoki, et. al. (1997) have performed three-dimensional finite element elasto-plastic analysis in the cases of dead and earthquake loads to obtain the effect of the supporting structure to the dome. Two analytical models have been prepared one corresponding to the quarter and the other to half of the actual structure. The difference between these two models affects the treatment of the lowest part of the dome where it is ringed by buttress-like piers. The shape of the base circle is delineated into an ellipse in both cases. The massive double arches on the north and south deflect outwards due to the thrust of the dome. On the eastern and western sides, however, the upper parts of the great semidomes deflect inwards due to the discontinuity present in the rigidity at the north and south arches, while the main dome produces thrust outwards. On the narrowed end of the semidomes, the thrust has pushed down the edge of the adjacent barrel vault. According to the results, the direction of the deformation deviates slightly southward (or northward) from the diagonal of the central square defined by the four piers. This is probably caused by that the magnitude of the component of the thrust transmitted through the western (or eastern) transverse arch and the adjacent area of the pendentives is greater than the other component given primarily by the strong double arches. As a result of this

investigation, it has been found that the critical regions of the whole structure are the connection regions between the east and west arches and the crests of the semidomes.

Çakmak, Moropoulou and Erdik (1998) have performed the structural analysis of Hagia Sophia considering the geotechnical and material investigations to provide an insight in the structure's response to dynamic loads. Material properties of stone and brick masonry have been adjusted for the numerical model to match the mode shapes of the system and the frequencies identified from the measured response to a low-intensity earthquake. The calibrated model has been used to predict the responses by incorporating soil-structure interaction as well. Stresses under simulated severe earthquake loading have been estimated at the critical locations in the arches. The mortar has been examined in detail using a number of microstructural, mineralogical, and chemical tests to support the choice of effective mechanical properties. Moreover, the foundations of the main piers and the soil surrounding them have been investigated through preliminary tomography experiments to model the soil-structure interaction. Earthquake input accelerations in the magnitudes  $M=6.5$  and  $M=7.5$  are generated at the site according to the procedure described by Findell (Findell, 1993). The results of these analyses have given benchmarks for severe response characteristics and highlight the importance of dynamic response to past and potential failures of the primary support structure. According to the results of the analyses, under the dead and earthquake loads together, maximum tension stress values, 1.4 MPa and 2.52 MPa, are obtained for the east arch and 1.72 MPa and 2.73 MPa for the west arch, respectively. The former values are the results of the earthquake  $M=6.5$  and the latter values are those of the one  $M=7.5$ , respectively.

In a technical report performed in Bosphorus University for Spektra Company (1998), the earthquake performance of Hagia Sophia has been investigated using the structural analysis program, LUSAS, based on the finite element method. In this research, both linear and nonlinear analyses have been performed. The linear elastic model has been investigated due to static, dynamic and spectral effects. According to the results of the linear analysis and the ambient vibration survey, the model has been modified for nonlinear analysis. The structural parts, which have shown high

nonlinearity with respect to the other parts, are assessed, and material nonlinearity has been applied only to these parts. Then, the previous analyses have been repeated as the second step. According to the non-linear analysis, it has been indicated that a possible violent earthquake at western part of the North Anatolian Fault Zone could lead to a severe impact and to separation the east and west semidomes from the arches joining them. Moreover, it has been found that, in the case of higher magnitudes than those considered there, the east and west semidomes would be demolished and the east main arch would be damaged, consequently, a part of the main dome would also collapse.

In all these studies, the effect of earthquake is investigated for different assumptions and models. However, only one study has been found considering the effects of cracks on the structure.

Mark, Çakmak, Hill and Davidson (1993a) has performed the structural analysis to derive a better understanding of the structure and determining the current earthquake worthiness of Hagia Sophia. To accomplish these ends, just two of the concurrent efforts are presented in this paper. These are; observation of the building fabric and the deformations, and creation of numerical models to account for material behaviour, including the consequences of cracking. A full model of Hagia Sophia was constructed in three stages, allowing the portions of the structure in each stage to deform and weaken before the portions of subsequent stages were added. Stages of the modelling procedure took into account the cracking and weakening of masonry in regions where tension exceeds 1.4 MPa. Redistribution of stress is obtained where the elastic modulus in highly-stressed tensile regions has been reduced to  $10^9$  Pa. The extent of the regions subject to high tensile stress has been reduced, and accompanying this, the maximum compressive stress is found to be higher than in the uncracked model. According to the results obtained from this study, high tensile stresses are observed at the connection region of the secondary semidomes to the main semidomes and at the crests of the main semidomes to the main arches, and also all over the pendentives.

### **1.3. Objectives of the Research**

Retrofitting of historical structures is an important issue in structural engineering, especially in earthquake regions. In any preservation or restoration attempt, a detailed review should be made on the structural system. The structural system of many historical buildings has been modified because of the damages caused by earthquakes, wars, natural disasters and support settlements along their lives. Moreover, most of them have faced to some retrofittings of their structural system during their lives and this has affected their load carrying mechanisms despite the efforts to keep the original structure not changed.

In order to preserve Hagia Sophia, it is necessary to understand its earthquake response in its current cracked condition. Therefore, it is found to be important to study the dynamic vulnerability of Hagia Sophia including the effects of cracking.

The purposes of the present study are summarised as follows:

- To apply the crack modelling methods to Hagia Sophia in order to find out the crack propagation through the structure,
- To obtain the collapse load factor,
- To get an efficient structural model of Hagia Sophia for a cracked state and,
- Last but not least, to determine the dynamic vulnerability of the structure considering cracking.

During the analyses, cracks occurred or those expected to occur are taken into account using two Crack Modelling Methods. The structural model of Hagia Sophia prepared in Princeton University by Hill, 1991, is used in the analyses. To apply the Crack Modelling Methods effectively, a smaller version of the model, which includes only the main structural load bearing elements, is also considered. Besides, two more models are developed. One of them has a steel ring between the windows and the main dome, whereas, the other one has main arches at east and west with the same rigidity as that of the north and south arches.

The analyses performed in this study are divided into two parts. At the first part, the propagation of cracks throughout the models is investigated using the load increment method. This analysis is performed statically. At the second part, the dynamic vulnerability of the structure, in which some elements have cracks, is investigated using both the Load Increment and the Spectral Analysis Methods.



# CHAPTER 2

## STRUCTURAL ANALYSIS OF HISTORICAL MASONRY STRUCTURES

### 2.1. Basic Concepts, Definitions and Stress-Strain Behaviour of Masonry

Masonry is probably the oldest material, which is still used in constructions. Most historic masonry structures are standing in spite of the disastrous effects. They faced for years with the advantage of durability, which is one of the important characteristics of masonry structures. Another important reason to use masonry as a building material is its simplicity. Aesthetic, low maintenance, versatility, sound absorption, and fire protection are also other reasons that make masonry a preferable material.

Masonry is a composite material that consists of blocks and mortar joints. A large number of possible combinations generated with the geometry, nature and arrangement of units and the characteristics of the mortar casts doubt on the suitability of the generic term 'masonry'. Nevertheless, its mechanical behaviour has one common feature as very low tensile strength. This property is so important that it determines the behaviour of masonry structures (Borrell, 1996).

Generally, the most important factors affecting the stress-strain behaviour and strength of masonry are:

- From the blocks: strength, type, geometry and absorption,
- From the mortar: strength, relative deformation characteristics and thickness,
- From the masonry: bond between units and mortar, direction of stressing (anisotropy) and local stress raisers.



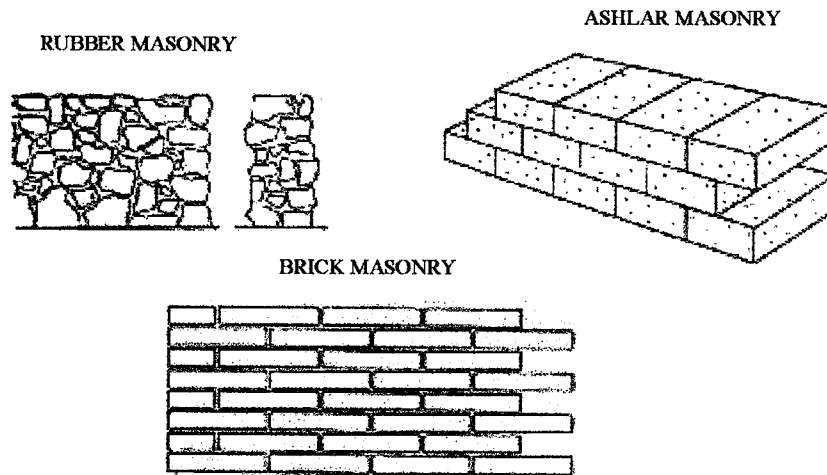


Figure 2.1-1 Different Kinds of Masonry (Borrell, 1996)

It is well known that mortar's bed joints act as planes of weakness inside the masonry. Moreover, biaxial anisotropic behaviour of walls in their own plane is determined by the existence of these planes of weakness. In other words, the stress-strain characteristics of masonry change with the angle between the bed joints and the main loading directions (Borrell, 1996).

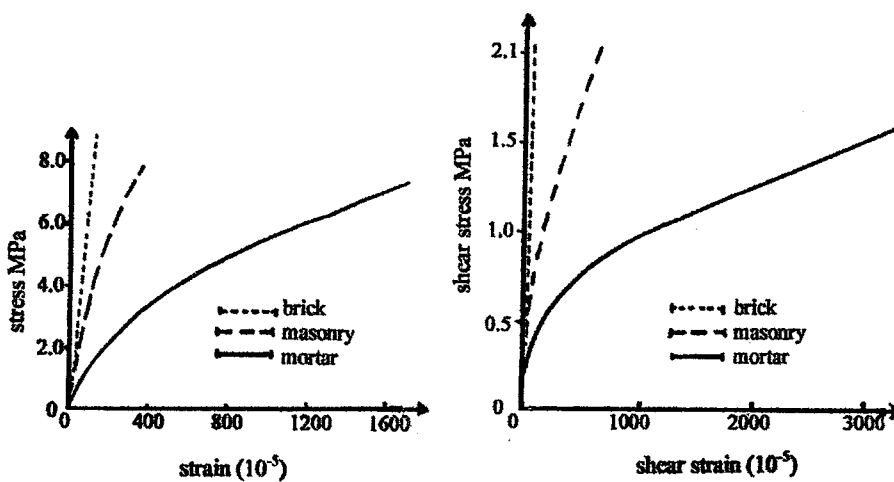


Figure 2.1-2 The  $\sigma$ - $\epsilon$ ,  $\tau$ - $\nu$  Relationships in Uniaxial Compression for Masonry, Brick and Mortar (developed by Page, 1978)



### **2.1.1. Material Properties of Historical Masonry**

Although mortar generally accounts for little percent of the total volume of masonry, it influences the performance far more than its proportion indicates. Its main function is to bind the building blocks together to provide a durable masonry. It also seals against air and moisture penetration and bonds the steel reinforcing, metal ties, and anchor bolts to join the building components structurally. The historical masonry is thus, a composite system durability of which is related both to the nature of its constituents and to the particular interaction between mortar and stone or brick. The adhesion between building units and mortar in structural systems can be different depending on the interaction between binder and load bearing units under various operating conditions, regarding the structure and its environment. This means that, the adhesion and the durability of the masonry are influenced by the workmanship and by the environmental conditions such as pollution. Even, the environmental conditions may favour the activity between the constituents inducing disagreement, modifying the kinetics of the hardening. Moreover, mortar strength and performance are as critical as unit strength and workmanship for engineered construction and load bearing applications (Penelis, 1995; Moropoulou, 1998a).

Egyptian architects of the twenty-seventh century BC witnessed the first known use of masonry mortar, when a mixture of burned gypsum and sand is used in the construction of the Great Pyramid at Giza. Then, Greek and Roman builders later substituted lime or added crushed volcanic materials to it. However, it is not until the nineteenth century with the development of Portland cement that mortar became a true structural component equal in strength to the masonry units it bonded together (Penelis, 1995).

With the aim of reparation or renovation, since Antiquity, natural materials or materials resulting from artisanal transformations are used: sand, lime, natural organic materials and pigments obtained with very little processing. Crushed brick, gravel, bristle and soil have also been found in some

of them. In some cases pozzolona and crushed brick are used in mortars in order to give them hydraulic properties as well. Historic mortars in general do not fit modern standards as their aggregates very often contain a considerable amount of fine components and also relatively high proportions of grains, such as bigger than 4 mm in diameter. While this improves their durability, it also increases their resistance to weathering as well as mechanic resistance along the time (Karaveziroğlu, 1995; Gonçalves, 1998).

Since the late Roman times and during the Byzantine times, the joints in brick and stone masonry became more and more thick reaching a ratio joint/brick thickness greater than 1. In this case, the material of which the joint is made cannot be defined any more as a mortar due to the very large size of the aggregate. Maybe it should be called as 'concrete'.

Thick mortar joint is considered as the weak element for the strength of the masonry. The role of the thick mortar joint on the mechanical behaviour and also the role of brick pebbles and dust in these joints have to be investigated in detail to understand the strength of the mortar clearly. Brick pebbles play important roles within the mortar, which gives special strength and stiffness, special compactness to it, and influencing in general the strength and stiffness of the walls.

### **2.1.2. Testing Techniques used in Masonry**

The first step in any repair or seismic upgrading project of historical monuments is to assess the condition of the structure. This assessment is required first to determine the need for repair or strengthening and then, to determine the type and extent of structural repair or strengthening required. In determining of the condition of an existing masonry building, the quantitative knowledge of the strength and deformation-stiffness properties of the masonry and knowledge of the distribution of these values throughout the building, i.e. structural and mechanical properties, must be determined (Atkinson, 1994).

To detect as much as possible mechanical factors useful for the analytical modelling process and furthermore to compare different test methods and analyses, several tests are carried on. Chemical, optical and physical analyses carried on bricks and hardened mortars, give better knowledge on possible mutual influence of the materials on the masonry behaviour. Compression and flexural tests, shear and tensile bond strength tests are performed on whole bricks, cubes and small prisms built of bricks and mortars (Binda, 1994).

In most cases, since the edifice has to be preserved with minimum intervention, non-destructive testing techniques are favoured. A great variety of information concerning mechanical properties, microstructural characteristics, water vapour, permeability of the treated layers etc., can be easily and fast collected with these techniques (Moropoulou, 1998b-c). While these techniques are very important as they provide important information on homogeneity of the material and the anomalies that may exist, they can only provide very rough idea about the mechanical factors needed for structural analysis. In order to obtain reliable values for determination of the factors related to the behaviour of a structure, some slight interventions, i.e. slightly destructive methods are utilised such as drilling holes and cutting small sections (Durukal, 1998; Rossi, 1997; 1998).

Non-destructive and slightly destructive testing techniques can be summarised as follows:

*Non-Destructive Tests:* Sonic Measurements, Sonic Topography, Radar Investigation, Thermographic Analysis, Rebound Tests, and Magnetometric Analysis.

*Slightly Destructive Tests:* Coring Techniques, Borehole Video Surveys, and Flat Jack Tests (Durukal, 1998).

## **2.2. Methods of Structural Evaluation of Historical Masonry Structures**

In a structure, properties of its construction materials, method of construction and current condition may vary widely over its extent due to different stages of construction, environmental deterioration, loading from past use, past repairs, base settlements and seismic events, etc. The structural condition evaluation of an existing structure requires a carefully planned program of exploration and testing.

A general structural survey should be the first step in any structural condition assessment program. The visual survey identifies zones of different masonry quality and location and extent of structural flaws. Items to be included in the survey are:

- Definition of the geometry,
- Measurement of settlements, tilting and wall movements,
- Examination of connections (wall to roof and floors),
- Environmental deterioration,
- Investigation of crack pattern,
- Corrosion of any metallic elements.

The results of the visual survey are also used in analysis of the structure (Atkinson, 1994).

The steps of analyses can be categorised as follows:

- Measurements of natural frequencies by ambient vibrations,
- Estimation or determination of the characteristics of the materials used in based on dynamic measurements for the structures,
- FEM three-dimensional elasto-plastic analysis, in both cases of dead and earthquake loads to the comprehensive structural system (Aoki. et. al.1997).

### **2.2.1. Development of a Physical Model and its Analysis**

A significant contribution to the knowledge of the static condition of a structure is provided by a physical model, which utilises all the data obtained through in-situ and laboratory investigations and the information coming from the monitoring system. The validation of the model is carried out through the comparison between the calculated values of the state of stress and those measured in-situ investigations (Rossi, 1996).

A physical model provides a reasonable explanation for the present stress distribution. The validity of the model in achieving this aim can be tested by comparing experimental and analytical stress results in certain points of the structure. Moreover, the reduction of stiffness in some structural elements, which could produce in terms of displacement and stress redistribution, can be determined (Leftheris, 1998).

After the physical model of the structure is obtained, first, a finite element configuration of the structure is assessed by choosing appropriate elements for meshing and modelling of the mechanical behaviour of the structure for analysis. Finite element method is a widespread used numerical method, which is also applicable to computer.

The most important problems that can appear in modelling may be the regions where the geometry changes. In these areas important interventions by the investigators are required in order to have small deviations from the actual geometry. Moreover, the precision of the results of analysis depends on the type of elements chosen; the number of elements and the predictions about the behaviour of the elements. However, the more the number of elements, the more the unknowns which cause an increase in the computational time. Accordingly, some parts of the structure like the architectural details that have no significant participation in structural behaviour and some parts that are not critical for the resistance of the structure do not need to be included in the model. On the other hand, some structural parts should be added to the model after detailed investigation.

### 2.2.2. Methods for Modelling of Cracks

One of the most important characteristics of masonry is its low tensile strength, which results in tensile crack at very low tensile stress compared to compressive stress. For these structures, accurate modelling of crack behaviour of the masonry is one of the important factors. Therefore, linear elastic-fracture models have been developed and used by many investigators.

The tension failure of masonry is characterised by a gradual growth of cracks, which accumulate and then, eventually disconnect larger parts from the structure. It is usually assumed that crack formation is a brittle process and that the strength in the tension loading direction abruptly goes to zero after such cracks have formed. When a principal stress or strain exceeds its limit value, a crack is assumed to occur in a plane normal to the direction of the offending principal stress or strain (Chen, 1994).

Cracks in material are modelled either by the discrete approach, which lumps the additional deformation due to cracking into a displacement discontinuity (opening a localised crack), or by the smeared approach, which treats this deformation as cracking strain distributed over a certain material volume. Both techniques have their advantages and drawback (Jirásek, 2000). These will be discussed in Section 2.2.2.C.

#### A. *Smeared Crack Modelling Method*

In this method, the cracked element is assumed to remain continuum; i.e. the cracks are “smeared out” in a continuous fashion. The fissures across the cracked element, rather than representing a single discrete crack. These parallel fissures are assumed to form in the direction perpendicular to the maximum principal tension stress (or strain) direction. Once the first crack occurs, it is assumed that the cracked element becomes orthotropic or transversely isotropic. Also, one of the element principal axes is oriented along the direction of the crack.

An uncracked element is considered as an isotropic elastic material and the stress-strain relations can be written in a matrix form as

$$\{\sigma\}=[K]\{\varepsilon\} \quad (2.2.1)$$

where  $\{\sigma\}$  and  $\{\varepsilon\}$  are the stress and strain vectors, respectively, which are given by

$$\{\sigma\} = \begin{Bmatrix} \sigma_x \\ \sigma_y \\ \sigma_z \\ \tau_{xy} \\ \tau_{yz} \\ \tau_{zx} \end{Bmatrix}, \quad \{\varepsilon\} = \begin{Bmatrix} \varepsilon_x \\ \varepsilon_y \\ \varepsilon_z \\ \gamma_{xy} \\ \gamma_{yz} \\ \gamma_{zx} \end{Bmatrix} \quad (2.2.2)$$

and  $[K]$  is the elastic stiffness matrix, as given in terms of  $\nu$  and  $E$  by

$$[K] = \frac{E}{(1+\nu)(1-2\nu)} \begin{bmatrix} (1-\nu) & \nu & \nu & 0 & 0 & 0 \\ \nu & (1-\nu) & \nu & 0 & 0 & 0 \\ \nu & \nu & (1-\nu) & 0 & 0 & 0 \\ 0 & 0 & 0 & (1-2\nu)/2 & 0 & 0 \\ 0 & 0 & 0 & 0 & (1-2\nu)/2 & 0 \\ 0 & 0 & 0 & 0 & 0 & (1-2\nu)/2 \end{bmatrix} \quad (2.2.3)$$

For plane stress problems (Figure 2.2-1), the stress-strain relations in Equation 2.2.1 can be written in the following form when  $\sigma_z = \tau_{yz} = \tau_{zx} = 0$ .

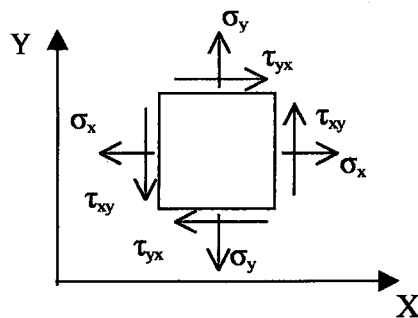


Figure 2.2-1 Plane Stresses Case

$$\begin{Bmatrix} \sigma_x \\ \sigma_y \\ \tau_{xy} \end{Bmatrix} = \frac{E}{(1-\nu^2)} \begin{bmatrix} 1 & \nu & 0 \\ \nu & 1 & 0 \\ 0 & 0 & (1-\nu)/2 \end{bmatrix} \begin{Bmatrix} \varepsilon_x \\ \varepsilon_y \\ \gamma_{xy} \end{Bmatrix} \quad (2.2.4)$$

The values of the elastic modulus,  $E$  and Poisson ratio,  $\nu$  are determined from experimental tests corresponding to simple states of stress.

Cracks occur when a principal stress either compression or tension exceeds the strength limit. This introduces orthotropic material properties and hence, new incremental constitutive relationships must be derived. It is accomplished by modifying the tangent material stiffness matrix, namely  $[K]$ . In the case of plane stress problems, the incremental stress-strain relation in the cracked direction becomes to Equation 2.2.5. In this equation, the cracked direction is given as “t” and the normal direction to t is denoted by “n”. n and t also coincide the directions of the principal stresses (Figure 2.2-2).

$$\begin{Bmatrix} d\sigma_n \\ d\sigma_t \\ d\tau_{nt} \end{Bmatrix} = [C_{cr}] \begin{Bmatrix} d\varepsilon_n \\ d\varepsilon_t \\ d\gamma_{nt} \end{Bmatrix} \quad (2.2.5)$$

In this equation,  $[C_{cr}]$  denotes the tangent stiffness matrix for the cracked element, and is defined in Chen, 1994 as

$$[C_{cr}] = \begin{bmatrix} 0 & 0 & 0 \\ 0 & E & 0 \\ 0 & 0 & \beta G \end{bmatrix} \quad (2.2.6)$$

in which  $\beta$  is the shear retention factor.



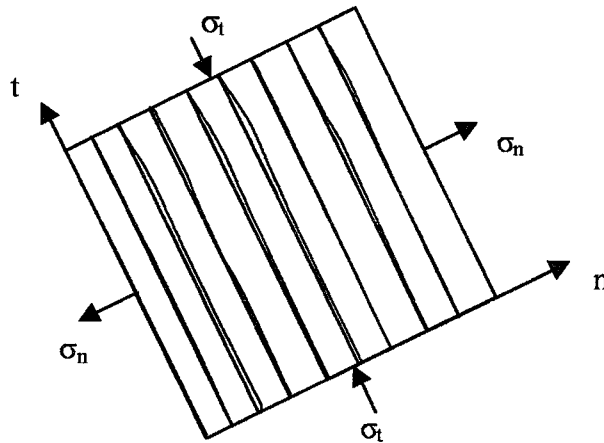


Figure 2.2-2 Idealised Representation of a Single Crack in the Smeared Crack Modelling (Chen, 1994)

In Equation 2.2.6, the modulus of elasticity of the material is reduced to zero in the direction normal to the crack ( $n$ -axis). Further, a reduced shear modulus  $\beta G$  can be assumed on the cracked plane in order to take into account the secondary effects such as aggregate interlocking in the concrete material. The value of  $\beta$  is a preselected constant between 0 and 1 (Chen, 1994).  $\beta$  is taken as '1' in this study.

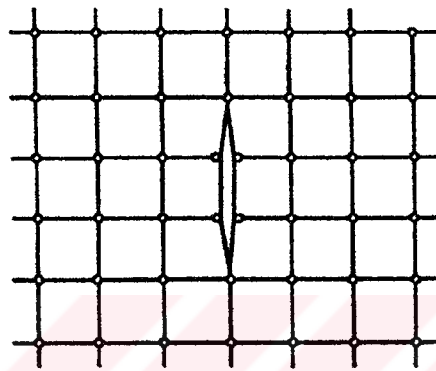
### ***B. Discrete Crack Modelling Method***

An alternative to the continuous smeared crack modelling is the introduction of discrete cracks. This is normally done by disconnecting displacements at nodal points for adjoining elements in a finite element mesh (Figure 2.2-3).

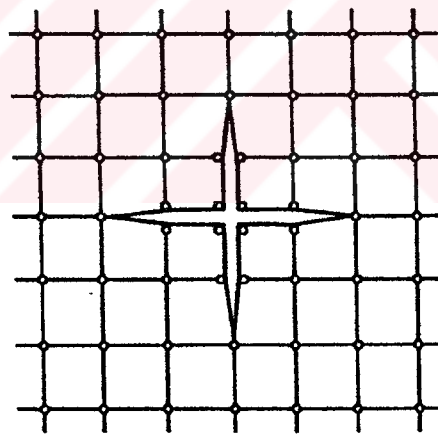
One difficulty in this approach is that the location restrictions imposed by the preselected finite element mesh and this can hardly be avoided. This can be rectified to some extent by redefinition of element nodes; such techniques are unfortunately extremely complex and time consuming. With the change in topology following formation of a crack in discrete crack models, the redefinition of the nodal points destroys the narrow band width in the structural

stiffness matrix and greatly increases the computation effort required in the solution.

Despite these difficulties and limitations, a few dominant cracks, such as the diagonal tension crack in a beam, are more realistically represented as strain discontinuity using the Discrete Crack Modelling Approach (Chen, 1994).



(a)



(b)

Figure 2.2-3 The Representation of Cracks in the Discrete Crack Modelling Approach  
(a) One-directional Cracking, (b) Two-directional Cracking

### ***C. Comparing the Methods***

At the Smearred Crack Modelling Method, when a crack has occurred at even a small part of an element, the element is assumed as totally cracked. Therefore, during the analysis, a lower collapse load factor can be obtained in this method relative to the Discrete Crack Modelling Method. Moreover, no matter how deep the crack is or which part of the element has cracked, the crack is assumed as spread over the whole element. Therefore, no detailed information on the cracks is required to apply this method. This makes the analysis both faster and easier as compared to the Discrete Crack Modelling Method.

On the other hand, the Discrete Crack Modelling Method necessitates more detailed observation on the cracks, such as their location and depth. Since only cracked part of the finite element is taken into account in calculations, it is highly possible to obtain higher collapse load value in Discrete Crack Modelling Method relative to that in Smearred Crack Modelling Method. Additionally, since cracked elements have been removed from the model, crack propagation through the rest of the elements can be followed easily in this method.

Despite these differences between the methods, the similar crack propagation is observed in the results of the analyses performed applying both methods. In this respect, since progresses faster, generally the Smearred Crack Modelling Method is used in this study. The main difference may be seen at the collapse load value, despite the fact that the same results are obtained in the beam example performed in this Section. If the complexity of the structure (such as for example Hagia Sophia) increases, this difference can be seen explicitly.

### ***D. An Example for the Smearred and Discrete Crack Modelling Methods***

A simple beam, which is shown in Figure 2.2-4, is taken as an example to observe the process followed in the Smearred and Discrete Crack Modelling

Methods. The material of the beam is selected as masonry and, its modulus of elasticity is taken as 3000 MPa, the unit weight 18 kN, and the Poisson ratio 0.2.

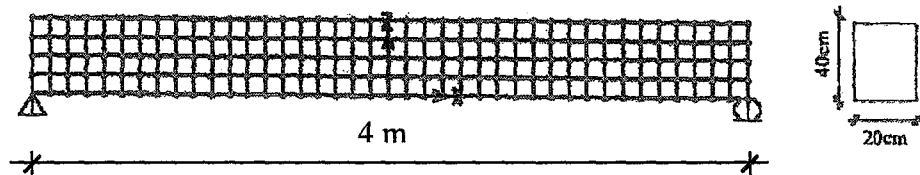


Figure 2.2-4 Simple Beam Example

The crack propagation through the beam in Figure 2.2-4 is investigated utilising the Load Increment Method. Cracks are taken into account by using the Crack Modelling Methods introduced in Sections 2.2.2.A and 2.2.2.B. To begin with, the beam is analysed under its self-weight and this analysis is progressed by increasing the self-weight of the beam with a constant ratio, higher than 1. For each step, the principal stresses for all finite elements are calculated. When the principal stress of an element exceeds the crack strength limit, the element is considered as cracked. The crack strength limit is taken as 75% of the strength limit in either compression or tension (Chen, 1994). Accordingly, the crack compression strength limit is 11.25 MPa and the crack tension strength limit is 1.05 MPa.

Cracks are introduced in the finite element model by using one of the Crack Modelling Methods, and the structure is analysed again with the same load until no crack occur for that loading. Proceeding in this way, it is possible to follow the propagation of cracks.

In this example, the beam is considered as collapsed when all neighbouring elements at the axis of symmetry according to the Z-direction, which is the most critical region in the beam, are cracked. This is defined as “collapse condition” for this example. Since the material is masonry and the compression strength of masonry is almost 10 times of the tension strength, no compression crack is observed during the analysis.

The above procedure, so called as Load Increment Method, is used for both Crack Modelling Methods. The Smeared and Discrete Crack Modelling Methods used in modelling of cracks are explained in following.

*Smeared Crack Modelling Method:*

When a crack occurs at an element, modulus of elasticity of the element is decreased to 0.1. If cracks continue, which means new cracks occur at other elements, for the same loading, the elasticity moduli of the new cracked elements are decreased as well. When the propagation of cracks stops, the load that affects the structure is increased. This procedure is continued until the collapse condition is reached. Stress distributions for the Smeared Crack Modelling Method are given in Figure 2.2-5.

*Discrete Crack Modelling Method:*

When a crack occurs at a node of an element, initially, a second node is defined for the cracked element with the identical coordinates to release the displacements of the cracked node from the beam. If the propagation of crack continues at further steps, cracked part of the finite element is removed from the beam (Figure 2.2-6). Finally, when the crack covers almost the whole finite element, the complete finite element is removed from the beam.

Once a crack develops, the load is not increased and the beam is analysed with the same load to let the crack to propagate. Although the load is not changed, new cracks may develop because of redistribution of the stresses through the structure. This procedure is carried out until the collapse condition is obtained. Stress distributions are given for the Discrete Crack Modelling Method in Figure 2.2-6.

For both methods, no crack is observed through the beam until the load reaches to 1.95 times its self-weight. At this load value, cracks occur at the middle part of the beam, and then, they start to propagate to the neighbouring elements for following steps. Despite that the load factor is the same, cracks progress by introducing them according to the procedure of the method used

because of stress redistribution. The cracks propagate very fast at this load factor and finally, the collapse condition is reached. As it can be seen in Figures 2.2-5 and 2.2-6, there are tension stresses at the bottom part of the beam for both methods. While there is no crack in the beginning, increasing the load value, these tension stresses exceed the crack strength limit. Introducing the cracks caused by the tension stresses into the model, the tension regions spread through the top section of the beam. Finally, the whole neighbouring elements at the axis of symmetry of the beam are cracked and the collapse condition is reached at the load of 1.95 times self-weight of the beam. This value can be also determined by considering the bending effect on a simple beam. In this case, the stress of the beam is calculated by using following equation

$$\sigma = \frac{M}{W} \leq \sigma_{\text{climit}} \quad (2.2.7)$$

In this equation,  $\sigma_{\text{climit}}$  denotes the crack strength limit, while  $\sigma$  is the stress,  $M$  is the bending moment and  $W$  is the section modulus.

For a simple beam under uniform loading, the maximum bending moment occurs at the axis of symmetry and it is calculated by Equation 2.2.8.

$$M = qL^2/8 \quad (2.2.8)$$

where  $q$  is the equivalent distributed load and  $L$  is the span of the beam.  $q_c$  denotes the collapse load value and equals  $\lambda_c$  times the self-weight of the beam.

$$q_c = \lambda_c q \quad (2.2.9)$$

Equations 2.2.8 and 2.2.9 are substituted in Equation 2.2.7 and rearranged in following equation

$$\sigma = \frac{q_c L^2/8}{W} \leq \sigma_{\text{climit}} \quad (2.2.10)$$

Moreover, the value of the section modulus is calculated as

$$W = bh^2/6 \quad (2.2.11)$$

$$W = 0.2 \times 0.4^2 / 6 = 0.0053 \text{ m}^3$$

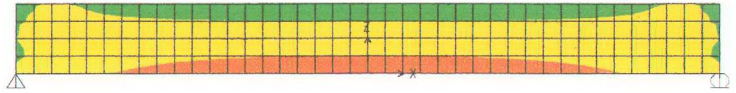
and crack strength limit,  $\sigma_{\text{limit}} = 1.05 \text{ MPa} = 1050 \text{ kN/m}^2$ . Moreover, the self-weight of the beam per meter

$$q = 0.2 \times 0.4 \times 18 = 1.44 \text{ kN/m.}$$

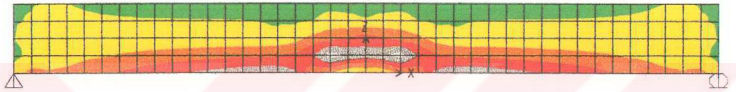
After substituting the known entities into Equation 2.2.10, the unknown value,  $\lambda_c$ , is calculated as

$$\sigma = \frac{\lambda_c \times 1.44 \times 4^2}{8 \times 0.0053} \leq 1050 \quad (2.2.12)$$

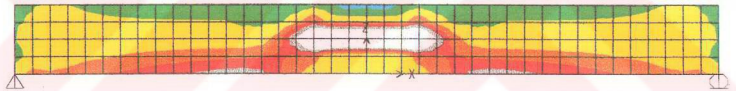
$$\lambda_c = 1.94$$



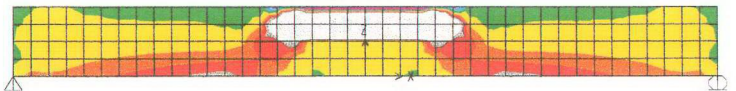
Load Factor = 1



Load Factor = 1.95



Load Factor = 1.95

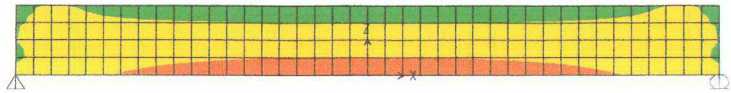


Load Factor = 1.95



Figure 2.2-5 Maximum Principal Stress Distribution through the Beam for the Smearred Crack Modelling Method (MPa)

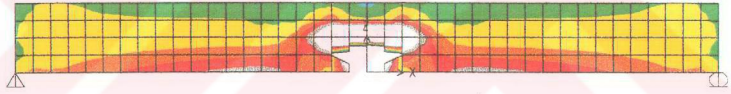




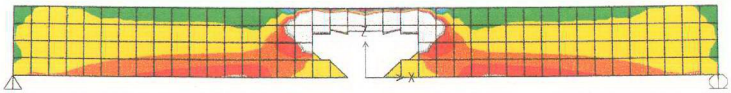
Load Factor = 1



Load Factor = 1.95



Load Factor = 1.95



Load Factor = 1.95

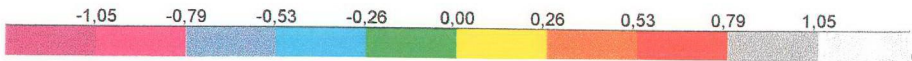


Figure 2.2-6 Maximum Principal Stress Distribution through the Beam for the Discrete Crack Modelling Method (MPa)

# CHAPTER 3

## STRUCTURAL PROPERTIES OF HAGIA SOPHIA

Hagia Sophia was built with the orders of the Emperor Justinian between 532 and 537, and it has stood up as an inspiring architectural and engineering marvel throughout 15 centuries. The Anatolian scientists, Anthemius of Tralles and Isidorus of Miletus created it that remained as the largest vaulted structure in the world for some 800 years. Its central space, vaulted in one continuous sweep from west to east, remained unequalled to this day. For the first nine centuries it remained the principal church of the Byzantine Empire, and then, for another five it served as the principal Ottoman Mosque (Mainstone, 1993; Erdik, 1993).

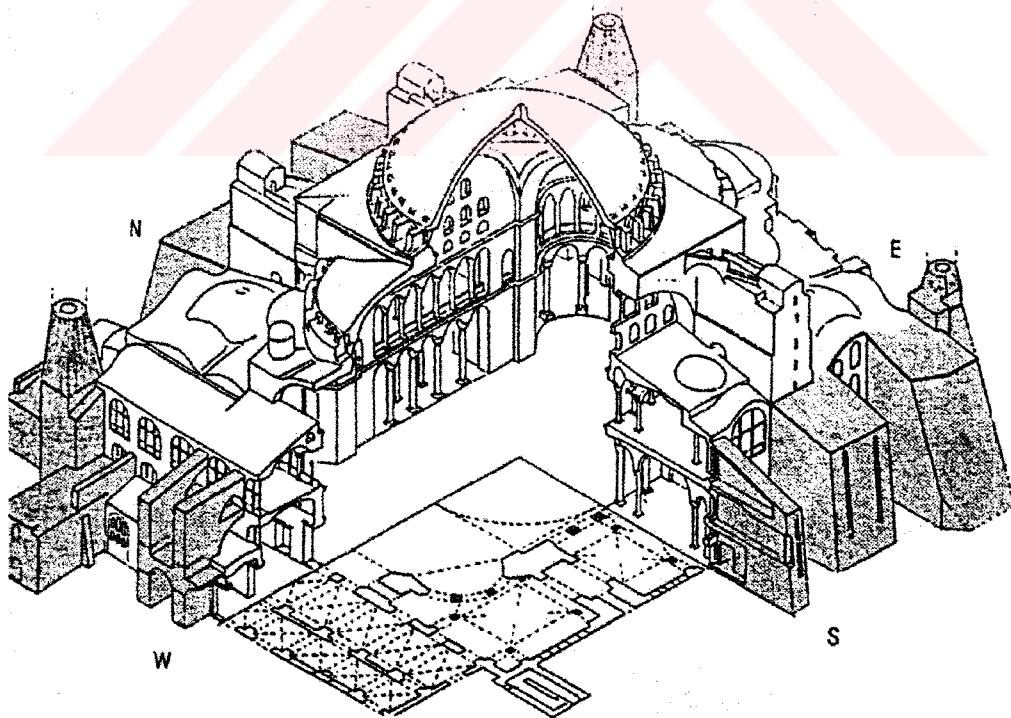


Figure 3.1 The Structure today showing, except at the South West, the Principal External Additions (Mainstone, 1993)

Because of the universal importance of Hagia Sophia, some campaigns of its restoration have been conducted for years with a big attention. In fact, the methods of renovation, restoration and strengthening of historical structures are relatively new and these methods are mostly different from the conventional reinforced concrete structures and even, they differ from one structure to the other. This is because, each historical structure has its own architectural and structural features, and every structure has to be observed considering its own load carrying system. Consequently, this requires detailed knowledge about the structure, and its history. In this section a detailed information about Hagia Sophia is given to understand its structure better.

### **3.1. Architectural Features of Hagia Sophia**

The structure has a free internal space 30m wide, 80m long and 55m high and its plan is almost symmetrical in both axes (Figure 3.1-1). The central dome, with two diameters averaging 30.98m measured between the skirtings, is carried by the arches and pendentives spanning between four rectangular main piers. The arches on the east and west are braced by semidomes of the same diameter as the central dome and huge pendentives have the general form of equilateral triangles, segments of a common, great sphere whose equator adjoins the lower angles of the pendentive surfaces. At the north and south there are double arches. The upper arch on each side, which is the only one visible in the interior, corresponds in span to the single main arches at east and west, though its width, is purely conjectural (Mark, 1988; Meyer, 1988; Mainstone, 1965).

The previous form of Hagia Sophia was an aisled basilica of the type then usual in the eastern Roman Empire. When this Theodosian church was rebuilt after a fire in 532, Justinian apparently wanted both to avoid the risk of a future similar fire, which called for vaulted masonry rather than trussed timber roofs, and to give the new church a more imposing form that would stand comparison with and even surpass a number of existing domed churches and domed palace audience halls (Mainstone, 1988).

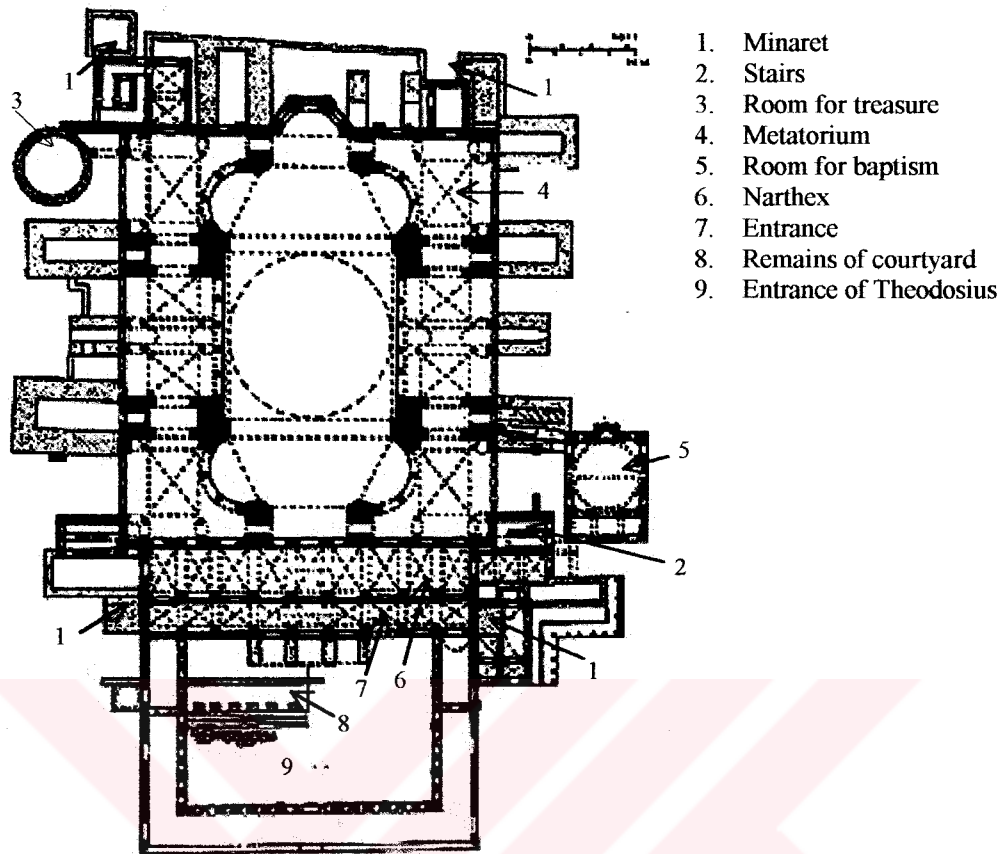


Figure 3.1-1 The Plan of the Entrance Floor of Hagia Sophia (Gezi, 1998)

The plan, as set out when rebuilding began, shows clear evidence of the desire not to depart more than was necessary from the central nave and flanking aisles of the earlier plan. At the same time it shows how Anthemius and Isidorus incorporated features from earlier domed centralised structures and from vaulted structures with longitudinal plans like the Roman Basilica Nova. Their intention was clear. It was to vault the entire nave with a daring and unprecedented combination of a central dome carried on pendentives and two semidomes of the same diameter, each opening below into smaller semidomes. In a typically Roman manner, these smaller semidomes were to rise directly over semicircular exedra, which were open, through colonnades, to the aisles. Similar, but straight, colonnades would divide the central parts of the aisles from the nave. From the dome down to the springing levels of the pendentives and large and smaller semidomes, all the vaults could have part-spherical surfaces, which would meet naturally in perfect part-circular arches (Mainstone, 1988).

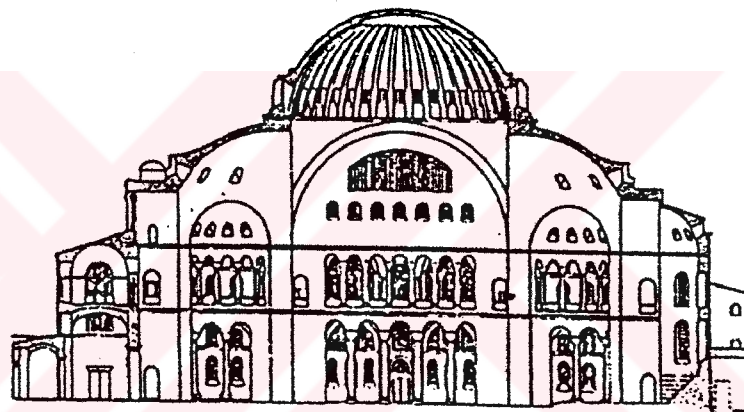
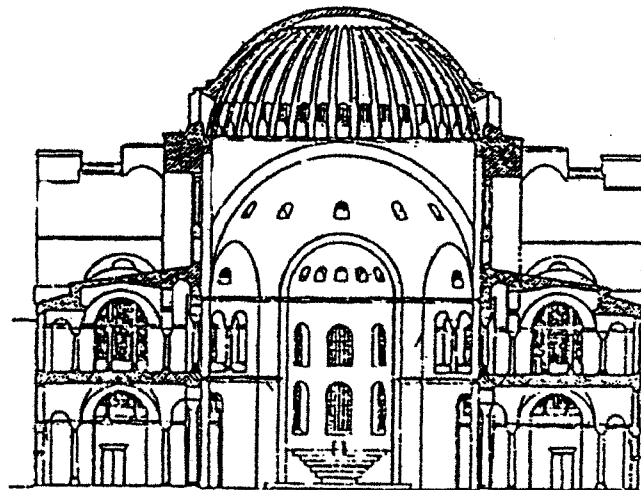


Figure 3.1-2 The North-South (upper one) and East-West Elevations of Hagia Sophia (Mainstone, 1988)

The array of the windows around the base of the main dome that yield a diffuse light and create the illusion of the dome suspended above the vast interior space is assumed as originated solely for visual effect (Figure 3.1-2). Moreover, the placement of these windows in a place where, tensile hoop forces would be expected to be critical seems audacious. But now, it is clear that the base of the dome had remained solid, it would have been meridional cracked. The window openings were thus a prudent expedient to ward off cracking. Although there is no way of knowing the details of the original openings, it may be hypothesised that it was similar to the present window configuration.

The openings were likely carried to an angle exceeding 50 degrees above the horizontal equatorial plane, which implies that designers had knowledge of earlier dome fractures. Evidently, the window treatment derived from structural rather than stylistic concerns (Mark, 1988).

In the aisles and galleries, there must originally have been an equal feeling of continuity from west to east. However, here the projections that were added to the piers and staircase towers to carry underpinning arches and reinforce their interconnections meant that the widths were reduced by a third alongside the piers. They thus virtually became sequences of separate bays. Externally, the raising of the staircase towers and the walls linking them, above the gallery roofs, to the backs of the main piers gave to the buttressing arms at the north and south their present prominence in place of what would otherwise have been a more pyramidal rise towards the dome from all directions (Mainstone, 1988).

A further important contribution was made to the overall character of the interior by the clothing of all visible surfaces by thin skins of marble or gold ground mosaic. This treatment had the effect of dematerialising the solid structure of the piers and arches and hiding their great masses. Since, also, the vaults, arches and walls everywhere merged smoothly into one another, it created an effect of insubstantial continuously flowing surfaces articulated only by the horizontal cornices. The windows and the openings in the colonnades did little to interrupt the continuity. Glimpses through the colonnades of partly revealed outer space gave, rather, a certain ambiguity to the spatial boundaries, reinforcing the effect produced by their tendency to disappear briefly from sight where they turned away towards one of the exedra (Mainstone, 1988).

### **3.2. Materials used in the Structural System of Hagia Sophia**

While the main materials used in the structure are stone, brick and mortar, iron as 'clamps', and 'ties', and wood and also with lesser extent lead was used. The most part of the structure was built by brick masonry, of which mortar joints are very



thick, while the main piers and the lower part of the external buttresses are made by stone block masonry.

Brick is the main structural material of all domes, arches, external walls, and most of the piers. Stone was used especially in columns and at main piers up to the springing levels of arches. The piers made out of block stones are tender limestones or locally green granites and these different materials were used together without a defined order. The cornice at the base of the dome, the other cornices at the lower levels and the monolithic columns were made of stone as well. Marble has been used in the nave, the aisles and the colonnades of the galleries (Crocì, 1997; Yorulmaz, 1993).

Most interior surfaces of Hagia Sophia were covered by a thick layer of plaster on top of which were frescoes or mosaics. Brick and mortar are accessible in the interior passages of buttresses, but it is not always clear whether materials date from the original construction or from later restoration (Mark, 1993b).

Structural studies to determine the earthquake worthiness of Hagia Sophia have shown that the static and dynamic behaviour of the monument depends very strongly on the mechanical and chemical properties of the mortar and bricks used in masonry (Moropoulou, 1998a). Brick is one of the main load carrying structural material used in the building with the dimension of 35~40 cm square and a thickness of 4 to 5 cm. Mortar was used as a conjunction material of stone blocks and bricks. The typical thickness of mortar joints is 5 to 6 cm; therefore their volume is almost equal to that of bricks (Crocì, 1997; Yorulmaz, 1993).

The conventional civil engineering approaches for determining mechanical properties of materials are essentially ruled out because of the lack of large specimens. Although, methods such as quantitative X-ray diffraction, thermal analysis, and automated image analysis of polished sections under scanning electron microscopy can be used to derive both chemical composition and physical properties. These non-destructive methods were supplemented by Bosphorus University/Turkey, and Princeton University/USA. The results of the test showed that the mortar of

Hagia Sophia displayed considerable mechanical strength along with longevity and were considered as early examples of concrete. The test results to date are consistent with pozzolanic mortar. These phenomena were studied in relation either to hydraulic lime as a binder or to the crushed brick, and it was also seen that pozzolan physically and chemically active aggregates, which were added in order to improve the mortar's performance (Mark, 1993b; Livingston, 1992). Mortar was made by gravel and brick particles except for lime ground in such a way to obtain fragments and dust, in order to give to the mortar nearly pozzolanic characteristics. This kind of mortar has been named as "Horasan Mortar" (Crocì, 1997; Yorulmaz, 1993). The most important structural characteristic of pozzolanic material is that it increases the tension capacity of the structural elements. Because of these properties of the mortar, it can be said that the mortar used in the structure is not only a conjunction element, but also it is a structural element as concrete consisting of a cementitious matrix and crushed brick fragments as aggregate. The brick elements in the structure may be thought of as providing stiffness rather than strength as it is in the case of present day construction, while the mass density of the composite is less than of bricks (Livingstone, 1992; Çakmak, 1998).

### **3.3. Structural System of Hagia Sophia**

Hagia Sophia can be considered as a sample of rather different structural approach. Imagined as a piece of historic heritage reflecting the power and superiority of the Eastern Roman Empire, Hagia Sophia was foreseen to overpass all existing monumental buildings in majesty. The primary structural support system of Hagia Sophia can be described as follows: The spherical main dome rests on a square dome base. It, stiffened by ribs, has a nearly constant thickness of around 0.7m (increasing to about 0.9 m down through the ribs), (Figure 3.3-1), (Crocì, 1997).

In the dome of Hagia Sophia, the most important aspects in definition of structural behaviour are the reduction of the thickness, the dome configuration with a lower sweep and the structural support system (semidomes, buttresses, etc.), which is discontinuous and placed in order to grant a radial rather than an annular counteraction (Crocì, 1997).



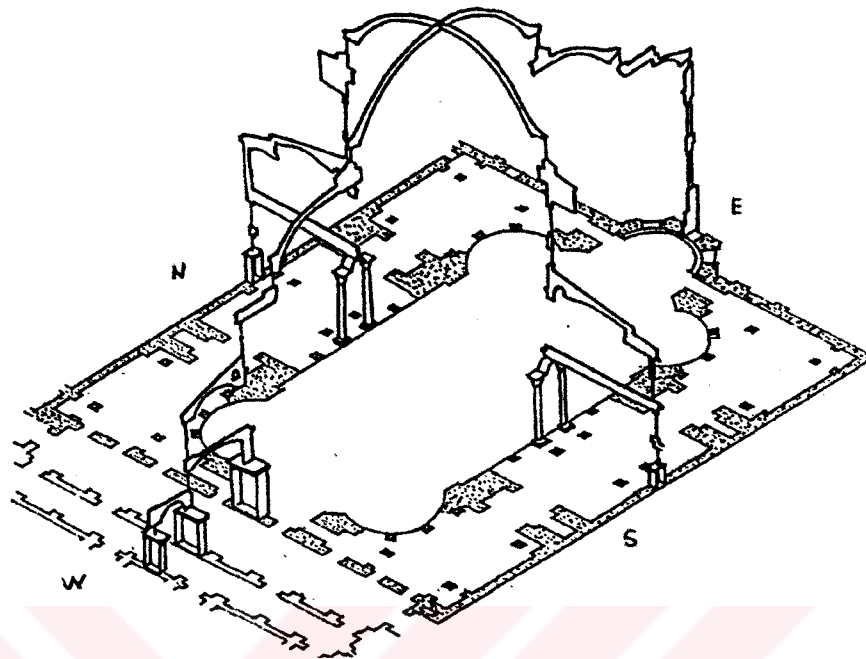


Figure 3.3-1 Isometric Plan, Longitudinal Section and Cross Section of Hagia Sophia (Mainstone, 1965)

In the N-S direction the four buttress piers, two at the north and two at the south, provide lateral support to the main piers (Figures 3.3-1 to 3.3-3). Each semidome at the east and west is supported by these buttress piers connected with a barrel vault, by two exedra semidomes and the colonnade system beneath them (Durukal, 1997). The exedra semidomes are carried partly by the colonnades and abut the diagonally aligned smaller principal arches (Mainstone, 1990). Such a daring architectural concept was not allied by sound structural solutions. The original solution was readily affected by some conceptual weaknesses and partial collapses had happened during the erection of the building (Karaesmen, 1993).

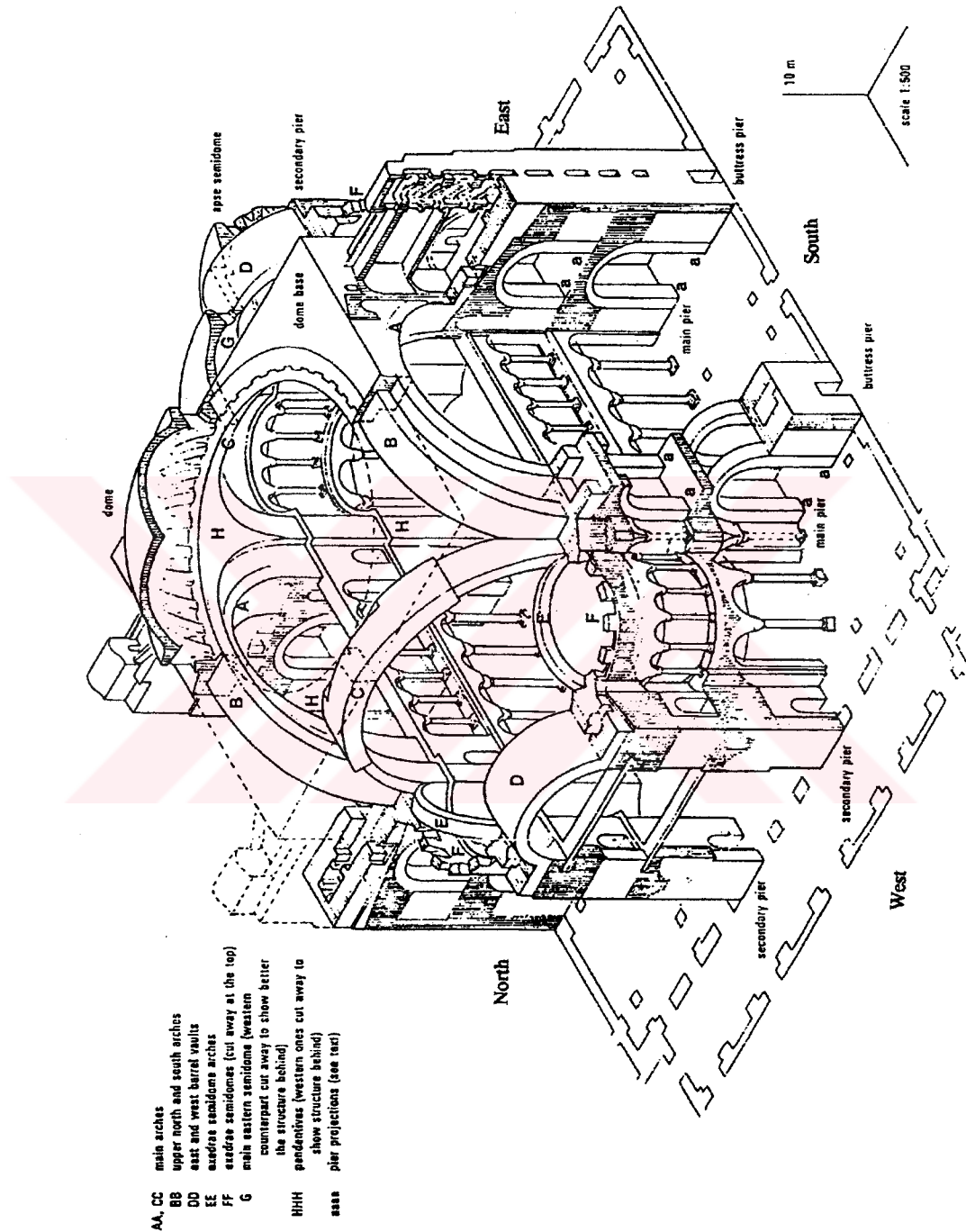


Figure 3.3-2 The Main Structural System with the Secondary Systems Cut Away and with Further Cuts at the West and South to Show More Clearly the Forms of the Arches, the Buttress Piers, and the Connections Between These Piers and the Main Piers (Mainstone, 1988).

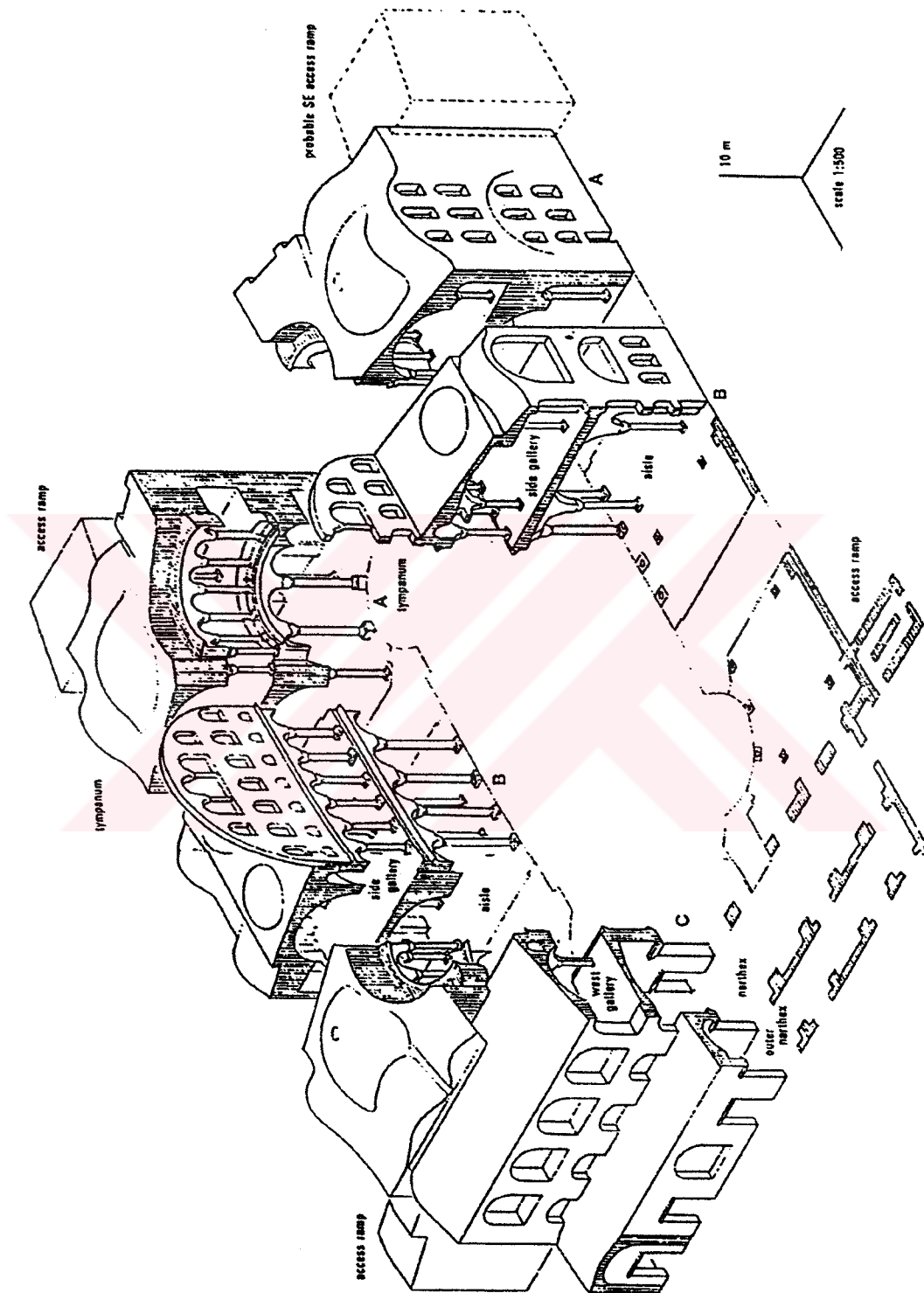


Figure 3.3-3 The Five Secondary Structural Systems, A, A, B, B, C. Cut Free from the Piers of the Main System and with Parts of B and C at the South West Drawn only in Plan to Show More Clearly the Remaining Forms (Mainstone, 1988).

At north and south, with no galleries, the main piers could be very substantially connected to the buttress piers alongside them across the aisles and these piers are similarly proportioned at ground level. But only very shallow interconnections are possible over the aisles without unduly interrupting their continuity or unduly raising the gallery floor and, above the gallery roof, there are initially only parallel pairs of arches carrying low walls spanned by a barrel vault. These interconnections are all weak. Because they were constructed of brickwork with wide mortar joints and were subjected to heavy load before the mortar had reached full strength. A further weakness was introduced by a considerable reduction in the cross sections of the main piers at gallery level from that at ground level (Mainstone, 1993).

The use of mortar with reduced hydraulic properties (which reach full stiffness and strength in a very long period of time) and the exceptional speed of construction (18 months until the completion of the arches) has magnified the deformations of the piers during the construction of the arches and the first dome; that very likely has been the cause of the collapses occurred two decades after the construction was finished (Aoki, 1993). Due to earthquakes in 558 the eastern arch and the first dome, in 989 the western arch, and in 1346 again the eastern arch collapsed together with portions of the main dome and the semidomes. However the main structure remained intact. The collapse of the first roof was mainly caused by the shallow profile of the main dome, which was not resistant against seismic forces. The earthquakes above are believed to originate from the North Anatolian Fault zone passing from about 20km south of the Hagia Sophia. All the permanent deformations have influenced the geometry of the present dome and of the structural reinforcements added to balance the thrusts, but their progressive increase has influenced the stress distribution and therefore the seismic behaviour and damages occurred in the following times (Erdik, 1993; Croci, 1997).

The broad pattern of cracks in the primary structure can be inferred from proven deformations. Most cracks were hidden. If the cracks were known the transmission of outward thrusts could be understood (Mainstone, 1990). Cracking in the structure as a whole even has one beneficial effect. As amplitudes increase during an earthquake

it leads to reductions in natural frequencies, which make damaging resonance with a predominant ground motion highly unlikely (Mainstone, 1993).

The full present state of the main piers is not known. However, the earlier exposures of the masonry of the southern main pier at gallery part revealed instances of the splitting under the high local compression due to reduced cross section and imperfect bearing between blocks. Also, the deformations in the main transverse arches are to be expected as a result of hinging deformations.

In the original form, thrusts of the dome along the longitudinal axis are carried down fairly directly through the large and smaller semidomes to their supports, while transverse thrusts reach the main piers only indirectly via the pairs of arches at north and south (Figure 3.3-4). These arches are thus required to arch horizontally as well as vertically, which adds to the thrusts they exert on the piers in the longitudinal direction (Mainstone, 1990).

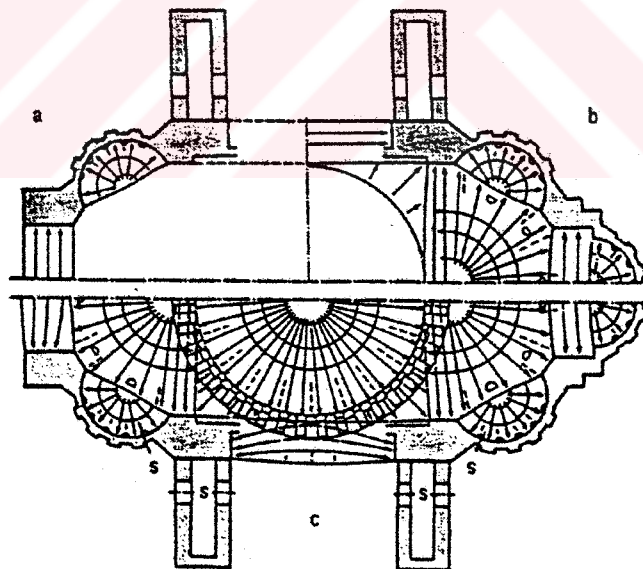


Figure 3.3-4 Thrust Lines (arrowed) in the Main Vaulting System and the General Pattern of Associated Cracking (broken line) (Mainstone, 1990)

- a. After completion of the small semidomes (assuming that they were completed before the large semidomes)
- b. After completion of the large semidomes and pendentives;
- c. After completion of the dome

Evidence of the action of the thrusts is clearly visible in outward leans of all the piers, most notably in outward leans of upper stages of the main piers in the transverse direction, and in lateral bowing of the main arches. There is also widespread cracking of the type to be expected in these circumstances. Though it is mostly hidden behind the present surface renderings, its presence has been confirmed by exploratory probes. It includes both radial cracking of the vaults and cracks extending into the piers and associated with major shear displacements (Mainstone, 1990).

The lack of circumferential continuity involves larger radial deformations at the springs of the dome reaching the highest value in the transversal direction. The different stiffness in the two main directions has contributed to amplify the seismic effects. The global structure is initially stiffer in the transversal direction because of the external buttresses and the collaboration assured by the semidomes to the transversal main arches; however stiffness seriously decreased when the buttresses and the transversal arches cracked. The longitudinal stiffness was reduced by the cracks in the wall under the longitudinal main arches (Croci, 1997).

The longitudinal seismic component in one of the earthquakes mentioned above caused the partial collapse of the semidomes detached producing hammering effects between the main transversal arches and the semidomes themselves. This partial collapse of the semidomes reduced the stiffening of the main arches and their lateral counteraction. The transversal global stiffness is then reduced and the stresses and the damage in the main piers and in the buttresses increased; the transversal arches are affected by large deformations in their own vertical plane and out of this plane because of the torsional deformations of the main piers. The residual deformations and curvature reductions caused the collapse of a transversal arch with the respective portion of the dome. The other transversal arch survived because of the thrust reduction, while the walls under the longitudinal main arches, although damaged, allowed a small deformation of the corresponding arch, preventing larger collapses (Croci, 1997).



### **3.4. Previous Restorations and Renovations on Hagia Sophia**

The conservation of a historical masonry building presents many different problems from the design of a conventional reinforced concrete structure. It carries its loads largely by compression. The masonry usually exhibits extensive cracks where primary tensions arise or where high local primary compressions lead to high orthogonal tensions. Hagia Sophia exemplifies these differences to the full (Mainstone, 1993).

Hagia Sophia was destroyed partially by earthquakes and restored several times after construction. However, the history of the restoration, especially of the restored parts, is not clearly known, and various researchers have worked on this matter.

To find out that either the present strength of the structure is adequate or there are weaknesses in the structure, the construction history and the changes undergone must be investigated in detail. However, the scale, complexity and inaccessibility of most of the working masonry behind facings of marble, mosaics or rendering make it difficult to determine the load distribution and the load bearing capacity of the structure (Mainstone, 1993).

Working from both existing survey, data and observation, on measurement and concentrating on the main arches and their supporting piers, it is possible to trace out the growth of their deformations, the reasons for the recorded collapses and the limits of the recorded partial reconstruction.

#### *Main dome, arches and pendentives:*

During construction itself, because of the scale of the enterprise and Justinian's impatience to see it, some difficulties arose soon after construction of the main arches began as known from the 6<sup>th</sup> century accounts. As a result of the weakness determined, the supports began to yield alarmingly even before the main east and west arches had been completed. Bracing arches of cut stone carried on projections from the piers were hurriedly constructed across both aisles and galleries and the walls above were extended upwards with further barrel vaults spanning between them to slow down this yielding (Figures 3.3-2 and 3.3-3). The dome had been

intended to set on a circular base that was not so longer like that and on arches that were already deformed, particularly the eastern one. The builders were disquieted by exceedingly large outward deformation of the main piers, and the original design needed to be modified. Later, the first partial collapse observed was primarily a collapse of the central part of the main eastern arch. The part of the main dome, which rested on the collapsed section, also fell, but the rest remained standing. Finally, the main dome fell after being subjected to earthquakes that occurred in 553 and 557. And the entire main dome was rebuilt to a higher profile after reconstruction of the fallen part of the arch and some additions to the faces of the main north and south arches to reduce the excess over the east-west diameter. The second main dome with a six-meter higher profile than its predecessor was erected in 558-562. The new main dome was similar to the collapsed one except it had a higher profile, so thrusts would have been about half as great (Mainstone, 1993; Mark, 1993b).

The second and third collapses were seen primarily in the arches; first, the main western arches then, the second time, the main eastern arch. Again they led to the fall of that part of the main dome thereby deprived of support. The third collapse occurred at north during an earthquake in the thirteenth century. Both reconstructions were limited to the replacement of fallen parts, so the 6<sup>th</sup> century sections of the main dome remained standing. Reconstruction of the eastern arch, the upper part of the eastern semidome, and the adjacent parts of the eastern pendentives were intended to reinstate them to the original form, though the work was performed less precisely, so there is a particularly clumsy join between the 6<sup>th</sup> century and 14<sup>th</sup> century portions of the northern pendentive (Figure 3.4-1) (Mainstone, 1993).

Reconstruction at west was more cautious. Since the west main arch and the adjacent part of the main dome have collapsed in the 989 earthquake, a restoration campaign has started. The 15 ribs at this part of the main dome have been renewed and strengthened, and the west main arch has been rebuilt (Altan, 1935; Wiener, 1998). There was a significant change in longitudinal profile of the west semidome above the level of the windows (Figure 3.4-2), a considerable increase in depth and width of the reconstructed part of the arch, and several additions including the blocking of two windows at each end of the dome reconstruction (Mainstone, 1993).



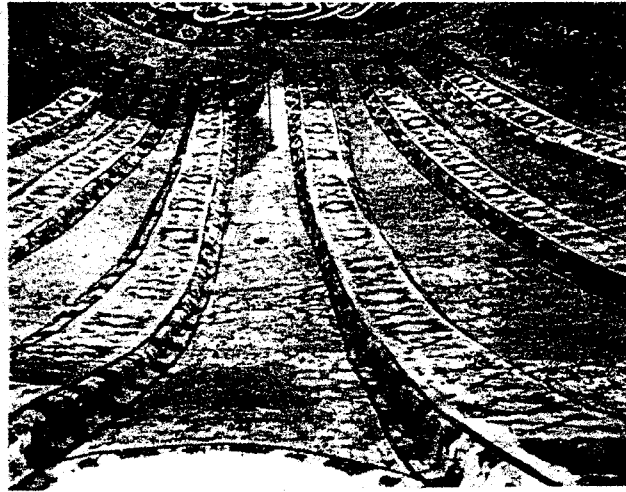


Figure 3.4-1 The Join between the Fourteenth-Century Reconstruction of the Dome (on the left) and the Surviving Sixth-Century Work (on the right), above the West tip of the South East Pendentive. Compare the Lines of the Ribs in the Two Sections and note the Pronounced Irregularity of the Fourteenth Century Work at the Top (Mainstone, 1988)

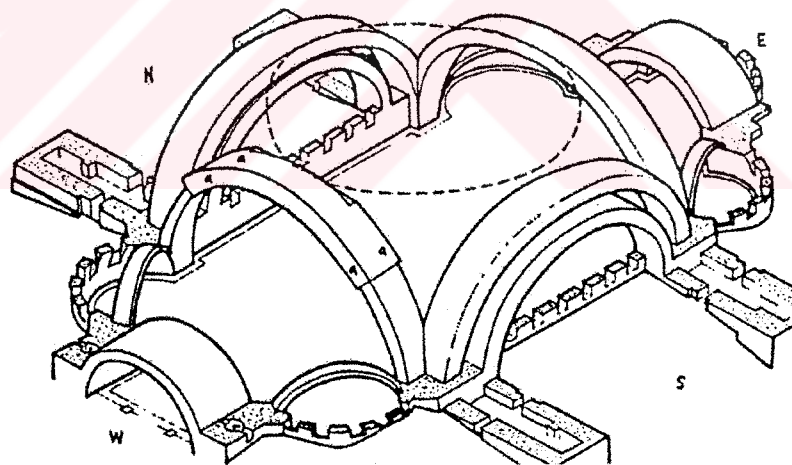


Figure 3.4-2 Isometric View of the Arches that Carry the Semidomes, Pendentive and the Central Dome (Mainstone, 1965). The Increased Section of the Main Western Arch is Part of the Tenth Century Reconstructions. (The upward extensions of the buttress piers removed for clarity)

Because of the campaigns of consolidation and repair performed, the outward appearance of the structure has changed with the rising of the main dome after the first collapse. Despite partial collapses after earthquakes in the tenth century, and again in the fourteenth, the general form of the second dome remains unchanged

today. But structural repairs associated with these incidents as well as other adversities have involved the placement of additional buttressing throughout the structure (Mark, 1993b). But the reconstruction and other works have preserved most of the original structure intact to this day.

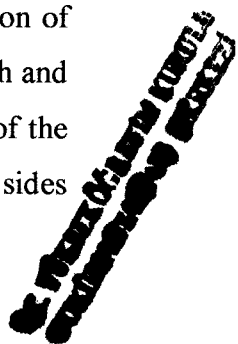
Three main phases of structural repair and strengthening are recorded, apart from works associated with the major reconstructions. The first phase was initiated in 1317 in the reign of the Andronicus Palaeologus', the second in 1573 under the architect Sinan; and the third in 1847 under the Swiss architect Gaspare Fossati, assisted by his brother Giuseppe.

The principal work undertaken in 1317 was the construction of new buttresses. In 1573, the mandate to Sinan was a general one to undertake all repairs that seemed necessary. In 1847, the mandate was again in fairly wide in scope (Mainstone, 1988). Sinan's and Fossati's works are discussed in details later on in this Section.

The upward continuations of the buttress piers (Figure 3.3-2) and their connections with the main piers date back to the original construction. They have, to an extent varying from buttress to buttress, been repaired and consolidated subsequently in various ways. The principal repairs have been renewals of the barrel vaults that span between the connection walls. The principal consolidations have taken the form of stone pilasters built against the walls, iron ties inserted between the connection walls, and narrowings of the arched openings that give passage through these walls at gallery-roof level. The major work appears to have been done under Sinan. But there is also evidence of earlier work in about the tenth century; and some further works, including the remodelling of the aedicules at the heads of the internal stairs, was done by Fossati.

#### *Buttresses:*

The identification of the buttresses due to Andronicus and the identification of possible earlier forms of some of them, are all more difficult. However, the south and east buttresses (Figures 3.4-3 to 3.4-5) are attributed to Andronicus the dating of the remainder, Gregoras. He did not state that buttresses were built on these sides



only. Some of the other masses, including, perhaps, some of those on the north but excluding that against the original south-west buttress pier and those against the central bays of the aisles on both north and south, may well also be due partly or wholly to Andronicus (Figure 3.4-6) (Mainstone, 1988).

The flying buttresses at the west are almost certainly of earlier date. They were most probably constructed during the Latin occupation in the early or mid-thirteenth century (Figure 3.4-7) (Mainstone, 1988).



Figure 3.4-3 The Buttresses at the South

The pair of flying buttresses at the east suggests that they are later (Figure 3.4-5). These buttresses look Ottoman, but they could all date originally from work undertaken by Andronicus (Mainstone, 1988).

The four buttress piers in front of the external narthex is built most probably in the 9<sup>th</sup> century (Wiener, 1998) (Figure 3.4-7).





Figure 3.4-4 The Buttresses at the East



Figure 3.4-5 The Flying Buttresses at the East



Figure 3.4-6 The Buttresses at the North



Figure 3.4-7 The Flying Buttresses at the West



*Fillings, ties and cramps:*

Most of the fillings are to be found in the buttress piers across the aisles from the main piers. More important probably are the fillings to the main piers at gallery level. The total number of added ties and cramps is unknown. There are ties spanning between column heads or across the springing of vaults in both aisles and galleries. And also there are circumferential ties set around the base of the dome in 1848 and again in 1926. The intention behind these works in most cases is to halt outward movements, either of the primary structure or of the secondary structure of the aisle and gallery vaults. Both ties and buttresses were used for this purpose. Also the fillings in the buttress piers serve for this aim, while the fillings to the main piers at gallery level were intended to reduce the vertical load. The purpose of the long horizontal cramps on the south-west that were exposed in the 1930s on its east face restraint the splitting of the masonry (Mainstone, 1993).

*Minarets:*

One of the most important additions to Hagia Sophia made by Mehmed the Conqueror was the minaret in the south-east corner (Figure 3.4-8). Documents published by Ahmed Refik indicate that Mehmed the Conqueror's minaret was constructed of wood and that this was replaced by a brick minaret during the reign of Selim II (1566-1574) (Yücel, 1986).



Figure 3.4-8 The Structure from the South (Mainstone, 1988)

In the oldest known engraving of Hagia Sophia, published by Harman Shedel, only one minaret is to be seen. In the landscape drawn by Jerome Maurand in 1544 two minarets can be distinguished. In the great panorama of Istanbul drawn by Melchior Lorich, who visited Istanbul in 1599, there are two minarets, one over the half dome and the other in the south-east corner. Sultan Selim II had a new minaret constructed by Sinan. This is typical of the minarets constructed by this architect, with a monumental base from which rises a round, slender, grooved column with a parapet adorned with stalactite decoration. Sultan Murad III (1574-1595) had two very simple minarets of identical form built at the western end of the building.

*Sinan's works:*

In the time of Sultan Selim II, Architect Sinan has been charged of repairing the structure. He strengthened the structure by placing arches in the empty spaces between the main piers supporting the main dome and the sidewalls. Also, major work of renewing of the barrel vaults that span between the connecting walls, building stone plasters against the walls, and inserting iron ties between the connecting walls has been done under his directions (Mainstone, 1988). In 1573, so many houses surrounding the structure and the depot belonging to the government have been demolished. Also, it has been ruled out that any new structure around Hagia Sophia would be at least 24m distance. The buttresses had been built in 1317 were strengthened and the top of them was covered by Sinan (Wiener, 1998). Moreover, in some references it was reported that he has built new buttresses to support the inner piers to prevent the main dome extend outward. However, which buttresses are built by Sinan is not clear (Altan, 1935; Yücel, 1986; İpşirli, 1989).

*Fossati's works:*

In Sultan's Abdülmecid's time, Fossati Brothers had conducted a huge restoration work in the structure. 13 piers declined from the straight vertical line were straighten by using stretchers; the dome was circled with stretchers from the outside, retrofitted; the leads were renewed; the mosaics were cleaned, repaired and covered with paint. Also the emperor mahfil (the upper floor) was constructed, and a madrasa and muvakkithane (timing building) were built outside of the structure (Koyunlu,

1990). In addition, small flying buttresses erected at an indeterminate date over the squint-like arches between the buttress arms and the dome base were removed by Fossati during the erection of the new steel hoops both in the dome and the drum (Figure 3.4-9). He thought that since the steel hoops were erected at the dome base, there would be no need to the flying buttresses. However, a widely spread group of lesions present in a regular, repetitive way all over the ribs can be examined at the windows at the dome base. These lesions certainly appeared after Fossati's restoration (Mainstone, 1988; Blasi, 2001).



Figure 3.4-9 The Structure from the South-West in 1847 (Mainstone, 1988). The flying buttress piers, one of them is circled, between the buttress arms and the dome base are seen.

The 1894 Earthquake has affected many historical structures in Istanbul like Hagia Sophia. After this earthquake, an investigation has been carried out to repair the structure and to renew the plasters. Some parts of the structure, where the plasters had been opened, were renewed with Horasan mortar. Because there were openings in the face of the pier across the türbe (tomb), the old plasters here were removed, cleaned, and these openings were stretched with steel ties, and finally they were filled with Horasan mortar. Although the structure had structural damages, i.e. the deformation in the main dome, the derivation in one of the semidomes, some partial collapses in the side walls, settlements in the main piers, the deformations in Hagia Sophia has been ignored, and recommended only decorative repairs after the earthquake (Batur, 1993).



# CHAPTER 4

## ANALYSIS OF THE STRUCTURAL SYSTEM OF HAGIA SOPHIA

The analyses performed in this study are categorised into two parts. At the first part, the Load Increment Method is used and the crack propagation through the structure is obtained. The Smeared Crack Modelling Method is used in modelling of cracks. Additionally, the Discrete Crack Modelling Method is also considered at the first part of the analyses. The main objective of the study is not to find out the collapse load of the structure, but to follow the crack propagation through and its effect on the structural system. To do so, the Smeared Crack Modelling Method is chosen in the analyses. This method is found sufficient enough to obtain the approximate collapse load of the structural system as discussed in Section 2.2.2.

At the second part of the study, the dynamic vulnerability of the structure is considered. The propagation of cracks is observed by combining the Load Increment and the Spectral Analysis Methods. In order to model the cracks, the Smeared Crack Modelling Method is used for different assumptions in this case. Furthermore, the reduction of the thickness of the element due to crack is taken into account by decreasing the elasticity modulus of cracked elements. The methods and procedures used in the analyses are explained in Section 4.3.

The structure is considered as collapsed, when cracks cover almost one third of the surface of one of the main load bearing elements, and the analysis stops at this condition. This is defined as “Collapse Condition” for both parts of the analyses.

### 4.1. Finite Element Models used in the Analyses

Four different models are used in the analyses. The First Model, which is denoted as M1, is taken from the Kandilli Earthquake Observatory and Research

Institute (Figure 4.1-1). This model was developed by K. E. Hill in Civil Engineering Department of Princeton University in 1991, and revised by adding some structural elements and changing some of the structural properties by Durukal in 1992. The model is developed for Structural Analysis Program, namely SAP90. In this study, the data are converted to the new version of this program, namely SAP2000.

The structural elements included in the First Model can be summarised as follows (Figures 4.1-1 and 3.3-2):

Primary load bearing elements:

- The main dome,
- two semidomes,
- four main arches,
- four pendentives and
- four main piers.

Secondary load bearing elements:

- Four secondary semidomes attached to the main semidomes,
- the apse semidome,
- two tympanum walls,
- six secondary arches,
- four secondary piers,
- four buttress piers and
- the columns under the secondary semidomes and tympanum walls.

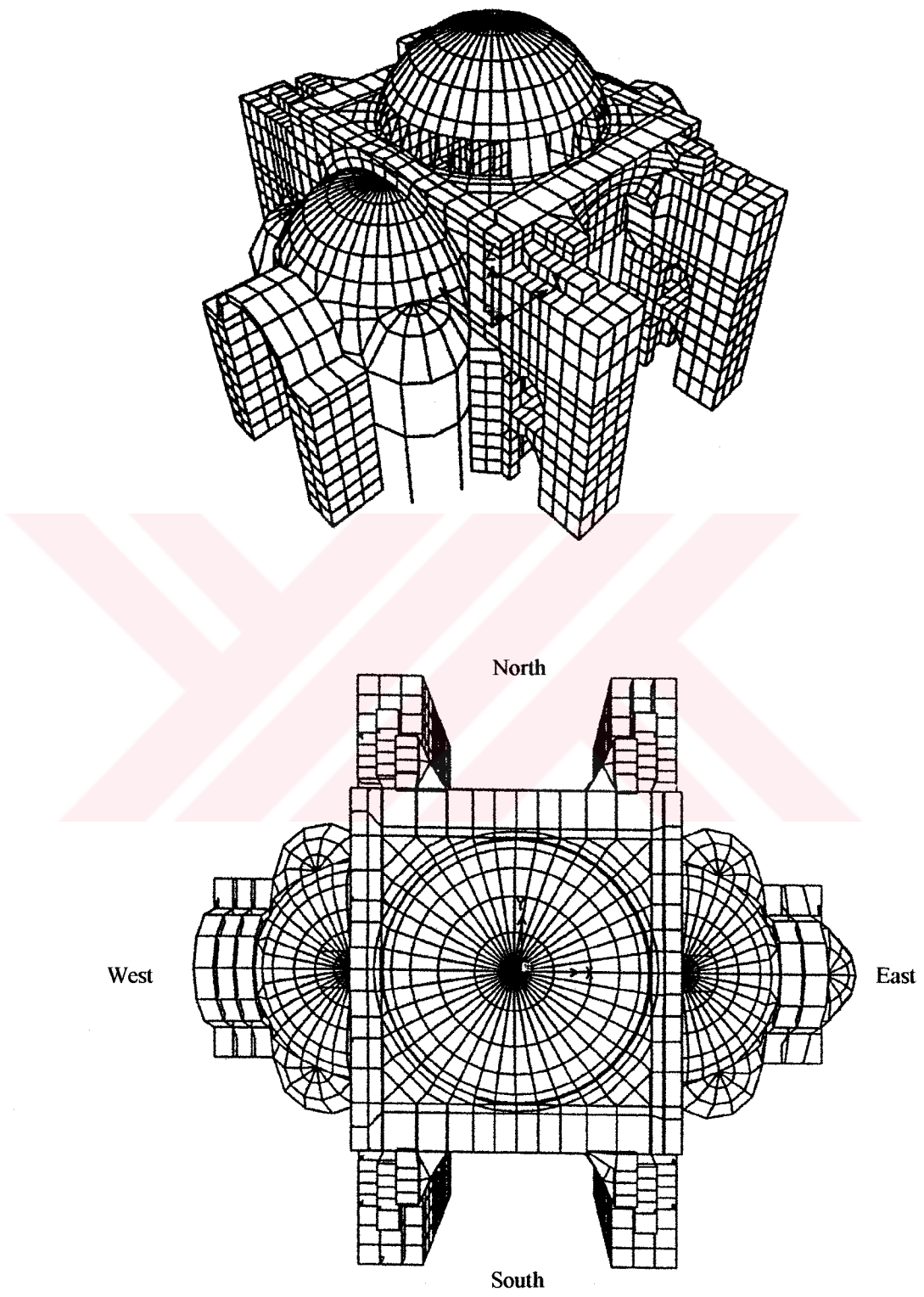


Figure 4.1-1 The 3-Dimensional and Top Views of M1

Since cracks start at the connection region between the secondary semidomes and the main semidomes, the crack propagation through the main structural elements cannot be detected. Because the aim is to investigate the crack propagation through the main structural elements, the Second Model, namely M2, consisting of only the main load bearing elements, is also considered in the first part of the analyses. The Second Model is derived from the First Model by leaving the secondary elements out of consideration. By doing so, the crack propagation through the main structural elements is followed with less computing effort.

The structural elements included in the Second Model can be summarised as follows (Figure 4.1-2):

- The main dome,
- two semidomes,
- four main arches,
- four pendentives and
- four main piers.

The effect of the buttress piers is taken into consideration in the Second Model by springs at the regions where they are connected to the main piers. Moreover, springs are placed at the inner surface of the north and south main arches to take the supporting effect of the tympanum walls into consideration. Locations and directions of the springs are shown in Figures 4.1-2 and 4.1-7, respectively. The spring coefficients are chosen to match the numerical frequencies of the model to those obtained from the ambient vibration survey performed by Durukal, 1992. According to the results of ambient vibration survey, the first three frequencies of the structure are 1.9, 2.1 and 2.7, while the first three mode shapes being E-W lateral, N-S lateral and torsional, respectively (Durukal, 1992). The Second Model considered here has the computational frequencies 1.94, 1.99 and 2.35, and the same mode shapes as of the structure itself.

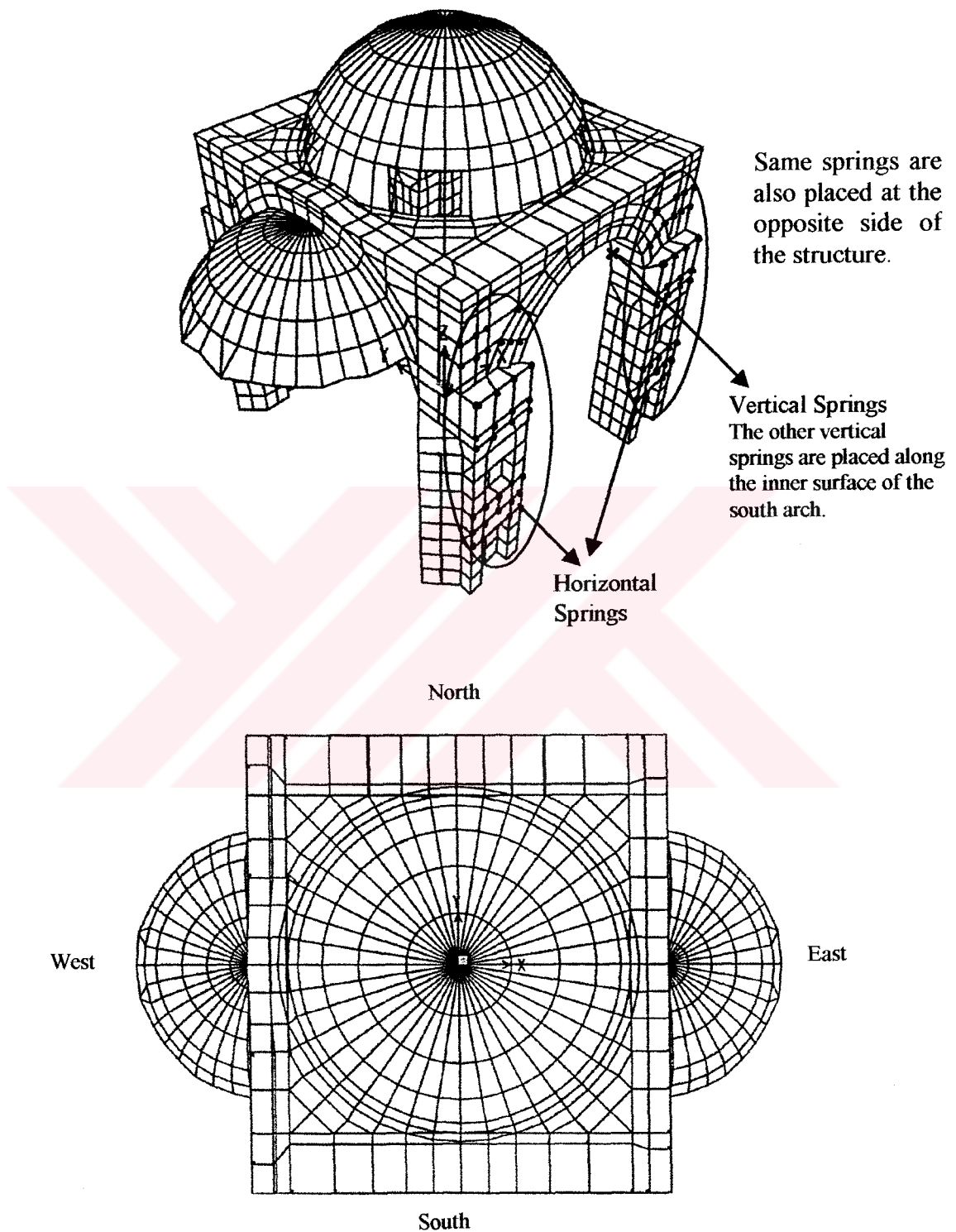


Figure 4.1-2 The 3-Dimensional and Top Views of M2

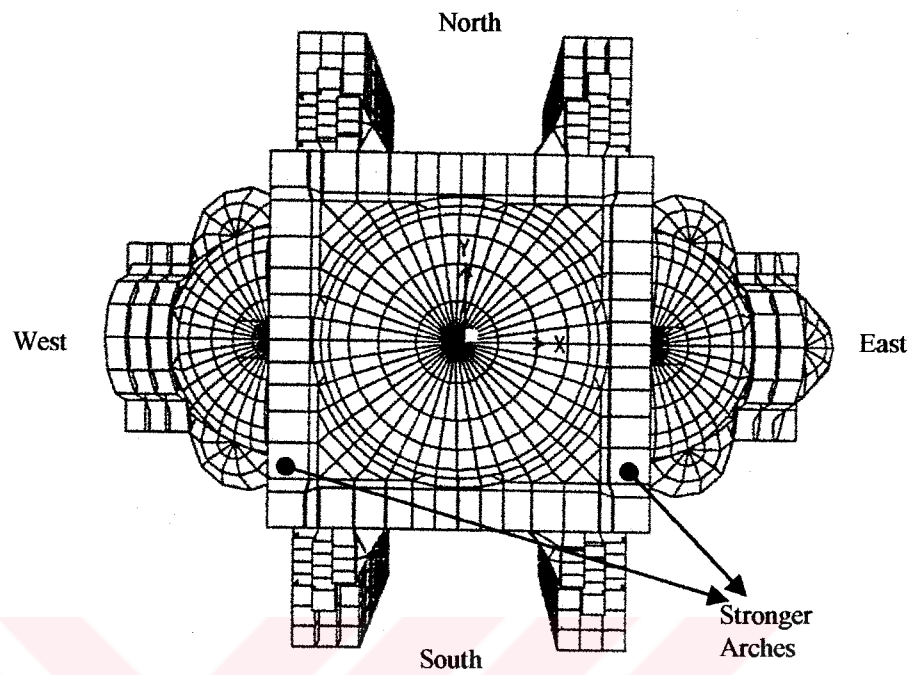
- Springs in the North-South Direction, on the South Surface of the South Main Piers and on the North Surface of the North Main Piers.
- x Springs in the Vertical Direction, on the Inner Surface of the North and South Main Arches.

As an alternative to the First Model, the size of the east and west arches is increased to be equal to the size of the north and south arches in order to study the effect of the arch stiffness on crack propagation. The Smeared Crack Modelling Method is used in this analysis. This model, namely M3, can be seen in Figures 4.1-3 (a) and 4.1-5.

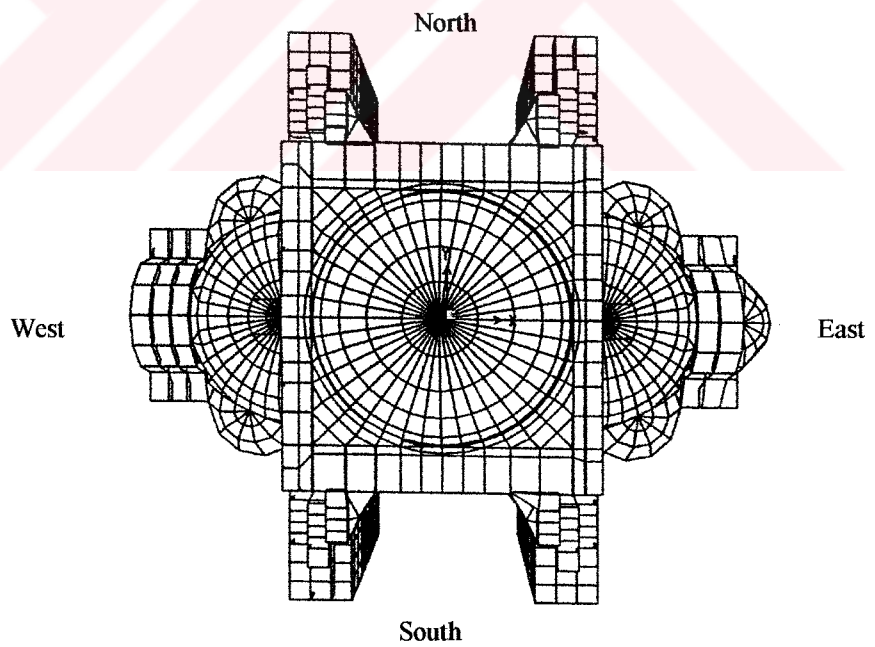
Furthermore, as another alternative to the First Model, a steel ring of 9cm diameter is considered between the top of the windows and the main dome to find out its effect on crack propagation, again by using the Smeared Crack Modelling Method. This model, denoted by M4, can be seen in Figures 4.1-4 and 4.1-5.

Although the structure is actually located in the south-east direction, for convenience, the apse side (Figure 3.3-2) is considered to be nominally in the east direction. The coordinate system is based on this assumption, the apse being in the +X direction, the entrance or the narthex (Figure 3.3-3) on the western side showing -X direction. The positive and negative directions for Y and Z-axes are defined accordingly. The individual structural elements are named depending on their positions in this coordinate system: like east and west semidomes, north, south, east, and west arches, south-east main pier, north-west buttress pier, etc. as given by Mainstone (Figures 3.3-2 and 3.3-3), (Durukal, 1992).

As a result of numerous repairs, changes and alterations, the structure, as it is today, is hardly regular. However, in modelling for computation, an idealised geometry is adopted. Hence, the radii of the main dome and the semidomes are taken as 15.5 m in each model. The main dome rests on a square base and has the thickness of around 0.7 m. On the other hand, the thickness of the main semidomes is 0.8 m, while it is only 0.375 m for the secondary semidomes. Moreover, the main dome is stiffened by ribs. The base of the windows under the main dome is at the elevation 41m from the ground, the height of the structure from ground to the top of the main dome being 55 m.



(a)



(b)

Figure 4.1-3 The Top Views of M3 (a) and M1 (b)

To compare the size of the stronger east and west arches with those at the First Model easily, the plan of the First Model is drawn again.



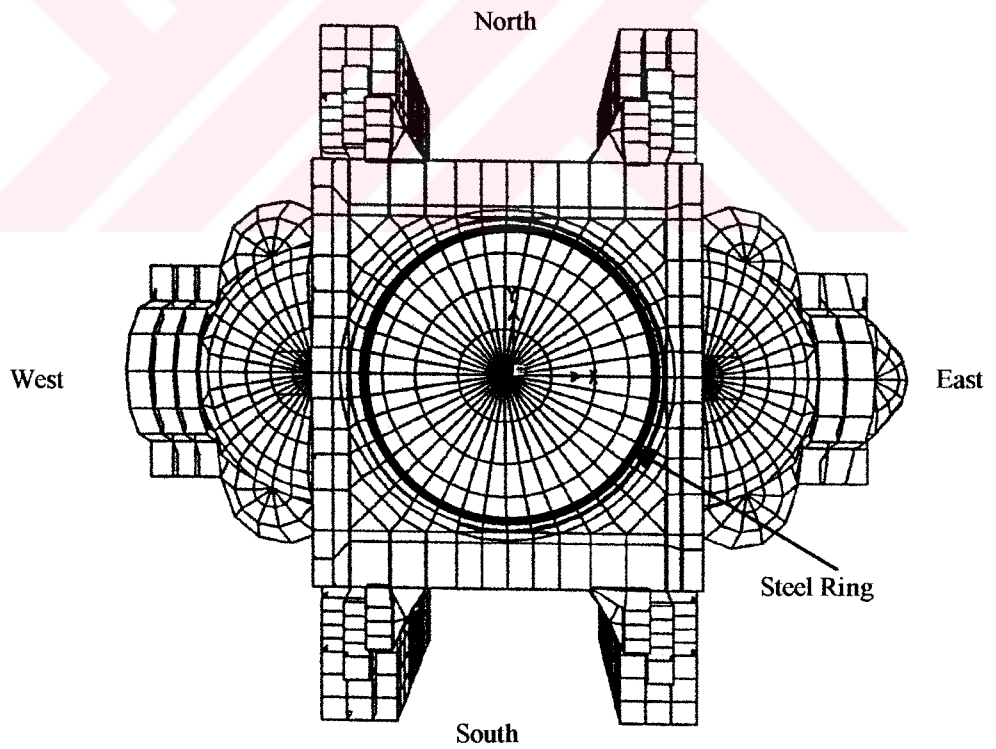
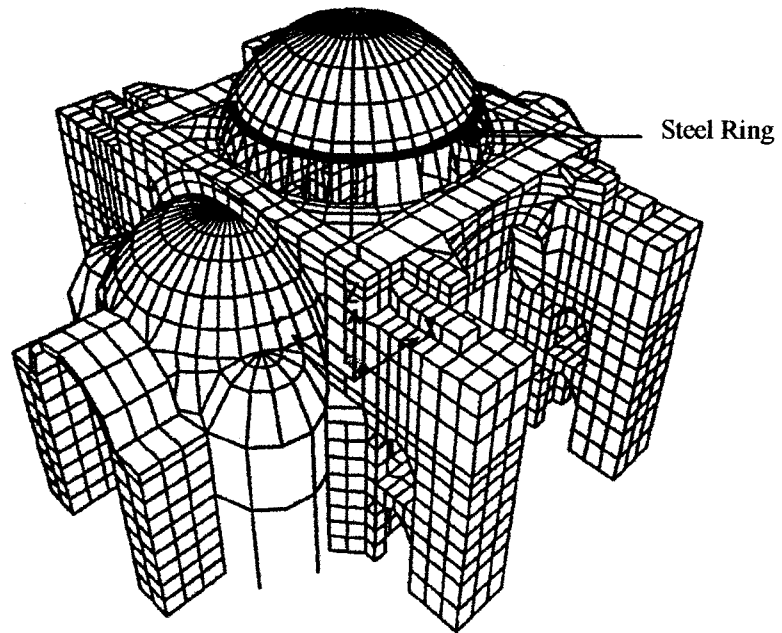
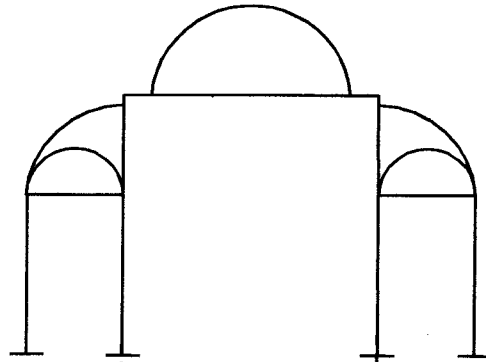


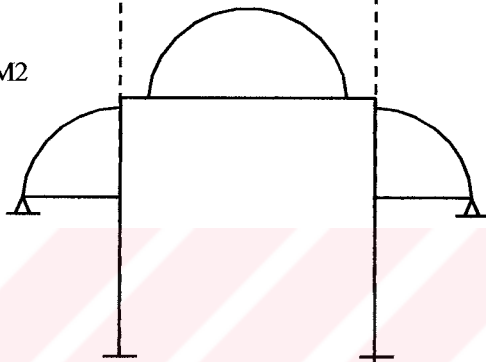
Figure 4.1-4 The 3-Dimensional and Top Views of M4

The steel ring is not drawn in scale consciously to show it clearly.

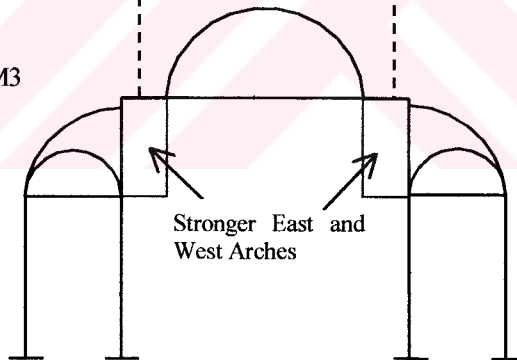
The "First Model" – M1



The "Second Model" – M2



The "Third Model" – M3



The "Fourth Model" – M4

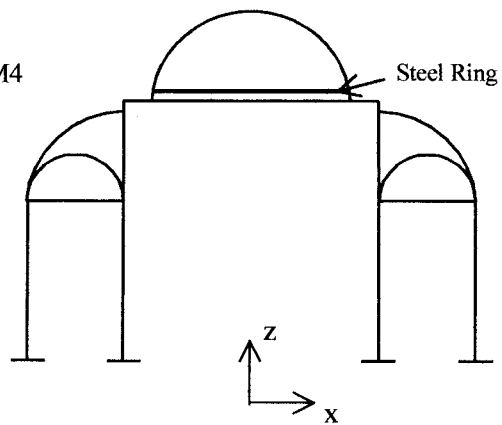


Figure 4.1-5 Four Models used in the Analyses: M1, M2, M3 and M4

#### 4.1.1. Material Properties

Material properties of some structural elements of the model, which is developed by Hill, have also been modified according to the recent researches. The structure is mainly made out of stone, brick and mortar. The main piers are stone masonry up to the springing levels of the arches. The upper part of these piers, the pendentives, all arches and all domes are made of brick masonry with mortar. To represent the double arches at north and south, modulus of elasticity of the solid elements between the top and bottom double arches has taken as one third of that of the arches. They are seen in Figure 4.1-6 (a).

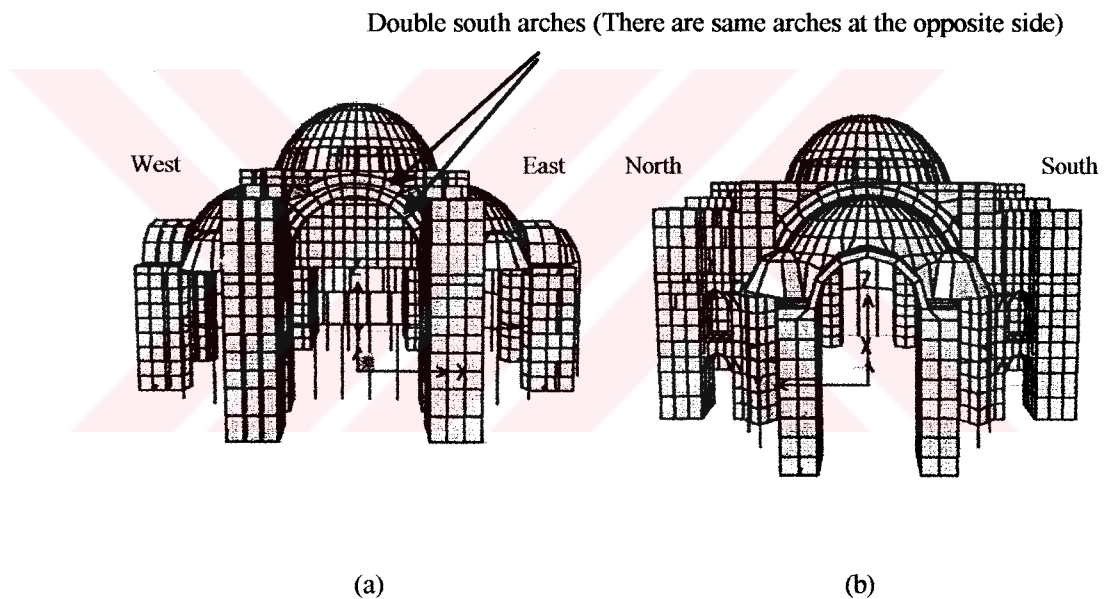


Figure 4.1-6 The Views of M1 from the South (a) and West (b)

Strength limit values for the material in compression and tension are taken as 15 MPa and 1.4 MPa, respectively (Smith, 1996).

Table 4.1-1 The Characteristic Values of the Materials used in the Analyses  
(Durukal, 1992; Spektra, 1998)

Structural Element	Modulus of Elasticity (MPa)	Poisson Ratio	Unit Weight (kN/m <sup>3</sup> )	Thickness (m)
The Main Dome	3,000	0.20	18	0.7
Two Primary Semidomes	3,000	0.18	17	0.8
Four Main Arches -The East and West Arches, -The North and South Arches.	4,000 3,000	0.18 0.20	18 17	
The Pendentives	3,000	0.17	12.5	
The Main Piers From the springing level to the top From the ground to the springing level	3,000 8,500	0.17 0.20	17 20	
The Small Piers	100,000	0.2	20	
The Secondary Semidomes	3,000	0.18	18	0.375
Beams and Columns	10,000	0.2	20	

The material behaviour in both static and dynamic analyses is taken as linear in order to be able to use the superposition rule in the spectral analysis. More explanation about the linear analysis is given in Section 4.2.

#### 4.1.2. Supports

Fixed connection with the foundation is assumed in all models considered in this study. Since solid elements have 3 translational degrees of freedom in three global axes (X, Y, Z), they are fixed only for translation in these axes for the main piers, the buttress piers and the secondary piers, which are modelled by solid elements. On the other hand, frame elements have 6 degrees of freedom at each point, 3 of them being translational and the other 3 rotational. The supports of the structure are shown in Figure 4.1-8. The support conditions are assumed to be almost the same for all models considered in this study. However, the secondary semidomes are simply supported in 3 global axes (X, Y, Z) in the Second Model (Figure 4.1-5). The springs placed in the Second Model are shown in Figure 4.1-7.

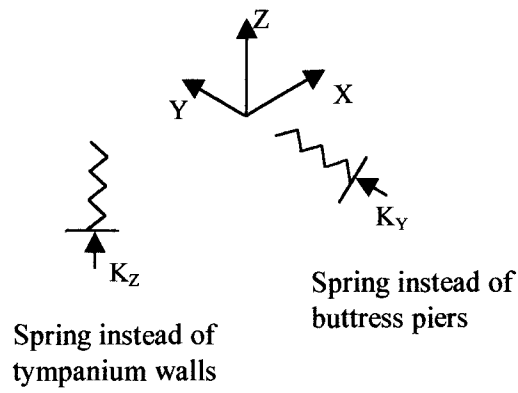


Figure 4.1-7 The Directions of the Springs used in M2

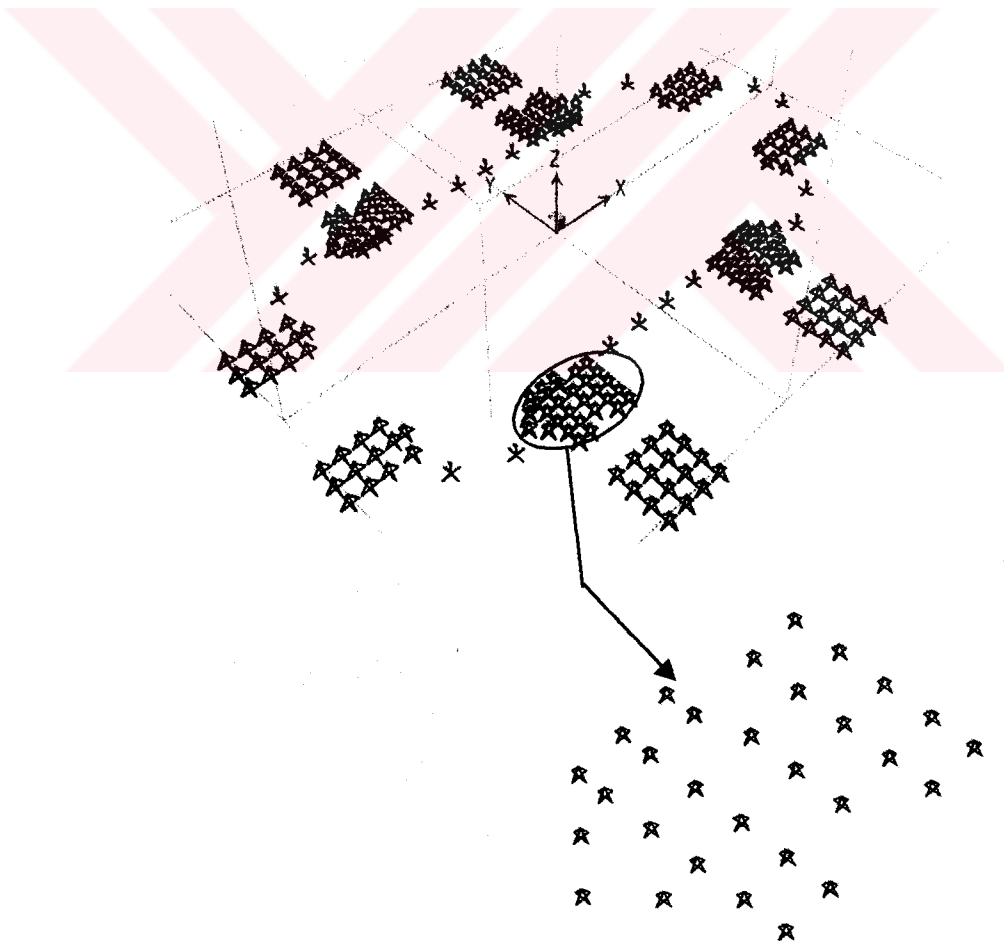


Figure 4.1-8 The Position of the Supports

Pier supports are fixed in X, Y, Z (Translation only)

Column supports are fixed in X, Y, Z,  $R_x$ ,  $R_y$ ,  $R_z$  (Translation and Rotation)

#### 4.1.3. Types and Properties of the Elements chosen in the Models

Whole arches, pendentives and piers are modelled by solid elements to represent the geometry and the material properties of the existing structure. The main dome, the semidomes and the tympanum walls are represented by shell elements. Frame elements are used in modelling of the ribs of the main dome and the columns under either the tympanum walls or secondary arches. Moreover, frame elements are used in modelling of the ring placed between the top of the windows and the main dome in the Fourth Model. The First Model consists of 369 frame elements, 720 shell elements and 2610 solid elements, whereas the Second Model consists of 212 frame elements, 444 shell elements and 1432 solid elements. The properties of the elements used in the models are briefly explained below.

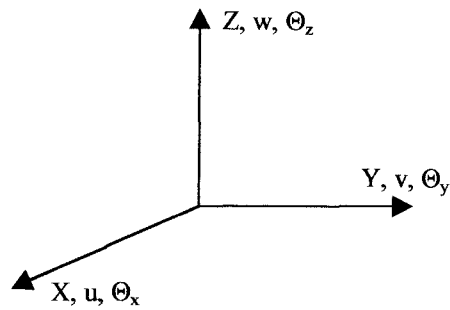
##### *Frame Elements*

The Frame Element uses a general, three-dimensional, beam-column formulation including the effects of biaxial bending, torsion, axial deformation, and biaxial shear deformations (Bathe and Wilson, 1976).

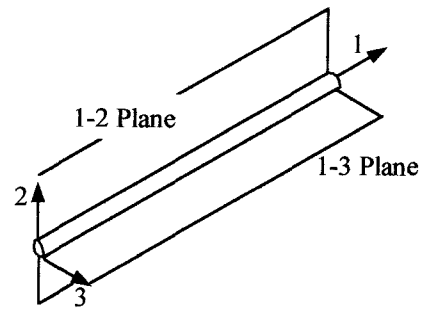
The Frame Element is modelled as a straight line connecting two joints. Each element has its own local coordinate system for defining section properties and loads, and for interpreting the output.

The Frame Element normally activates all six degrees of freedom at both of its connected joints, being 3 of them in translation and 3 of them in rotation. The axes and the positive directions of the forces and moments at the frame elements are seen in Figure 4.1-9. The forces and the moments at the joints of the frame elements are shown below.

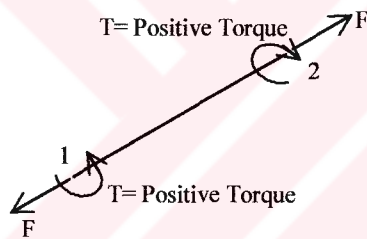
F:	Axial Force
V <sub>2</sub> :	Shear Force in the 1-2 Plane
V <sub>3</sub> :	Shear Force in the 1-3 Plane
T:	Torsion
M <sub>2</sub> :	Bending Moment in the 2-Direction
M <sub>3</sub> :	Bending Moment in the 3-Direction



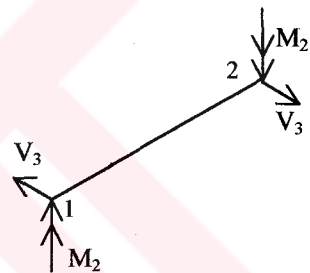
Global Axes



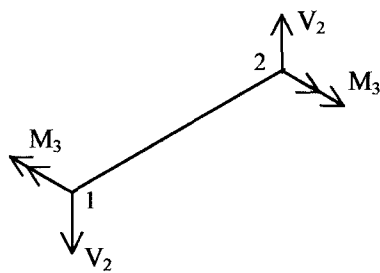
Frame Element Local Axes



Axial Force and Torque



Positive Moment in the 2-Direction and Shear in the 1-3 Plane



Positive Moment in the 3-Direction and Shear in the 1-2 Plane

Figure 4.1-9 The Positive Axes, Forces, and Moments of Frame Elements



### *Shell Elements*

Shell elements used for modelling of domes have a three or four-node formulation that combines separate membrane and plate-bending behaviours. It activates all six degrees of freedom at each of its connected joints, 3 of them being in translation and the other 3 in rotation. The forces, moments and stresses at nodes are shown below (Spektra, 1998; SAP2000 Manual, 2000).

$F_{11}$ :	Axial Plane Force in the 1-Direction
$F_{12}$ :	Shear Force in the 1-2 Plane
$F_{22}$ :	Axial Plane Force in the 2-Direction
$F_{MIN}$ :	Minimum Principal Force
$F_{MIN}$ :	Minimum Principal Force
$F_{MIN}$ :	Minimum Principal Force
$F_{MAX}$ :	Maximum Principal Force
$M_{11}$ :	Bending Moment in the 2-Direction
$M_{12}$ :	Twisting Moment in the 1-2 Plane
$M_{22}$ :	Bending Moment in the 1-Direction
$M_{MIN}$ :	Minimum Principal Moment
$M_{MAX}$ :	Maximum Principal Moment
$S_{11}$ :	Stress in the Local 1-Axis in the 2-3 Plane, hoop stress for domes
$S_{22}$ :	Stress in the Local 2-Axis in the 1-3 Plane, radial stress for domes
$S_{MIN}$ :	Minimum Principal Stress
$S_{MAX}$ :	Maximum Principal Stress

Maximum principal stress ( $S_{MAX}$ ) shows generally tensile regions, i.e. positive. On the other hand, minimum principal stress ( $S_{MIN}$ ) shows generally compressive regions being negative. Directions of the maximum and minimum principal stresses do not depend on directions in either global or local axes (SAP2000 Manual, 2000).

Each Shell Element can be quadrilateral or triangular as shown in Figure 4.1-10. The positive forces and the moments are seen in Figure 4.1-11.

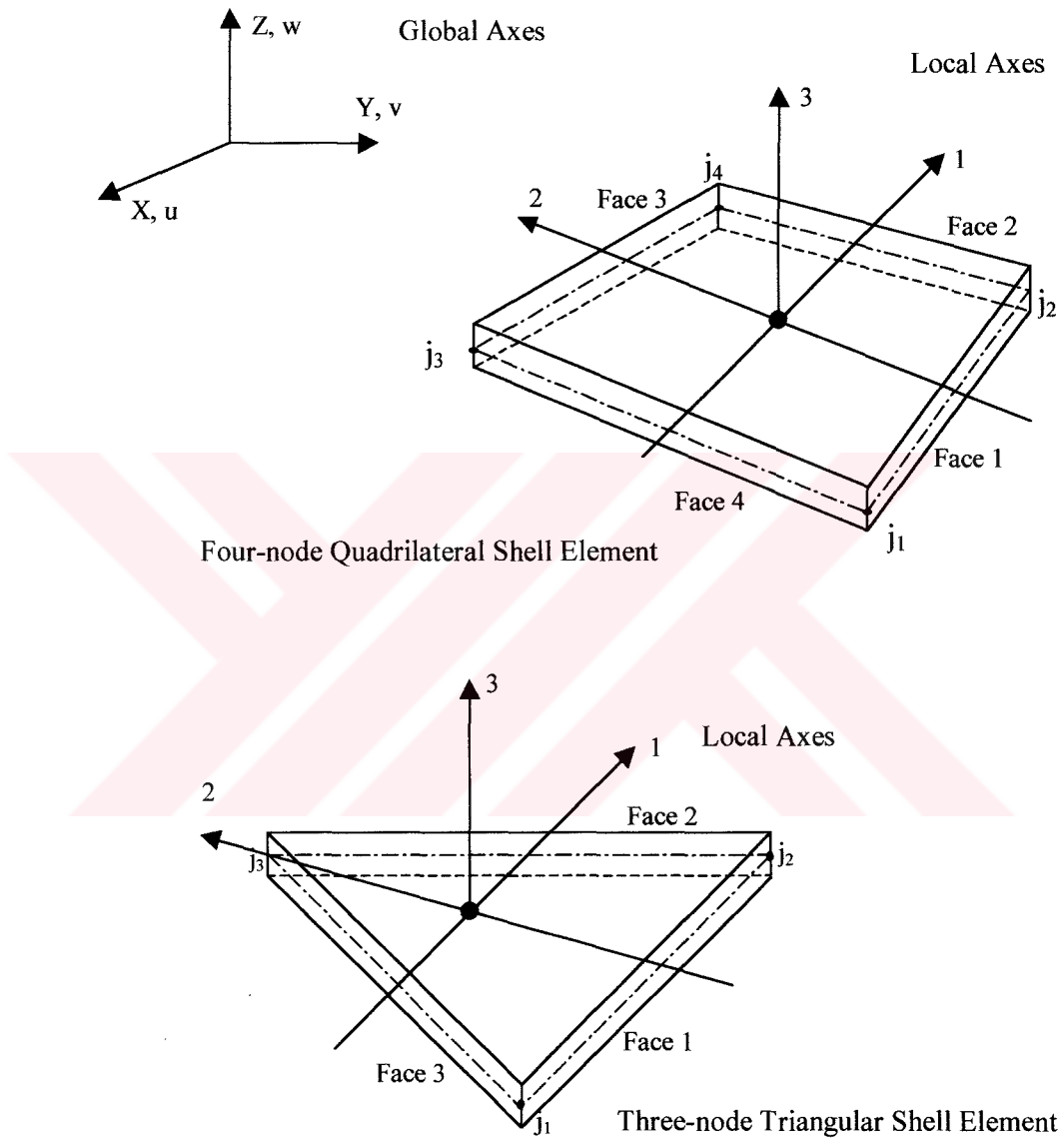
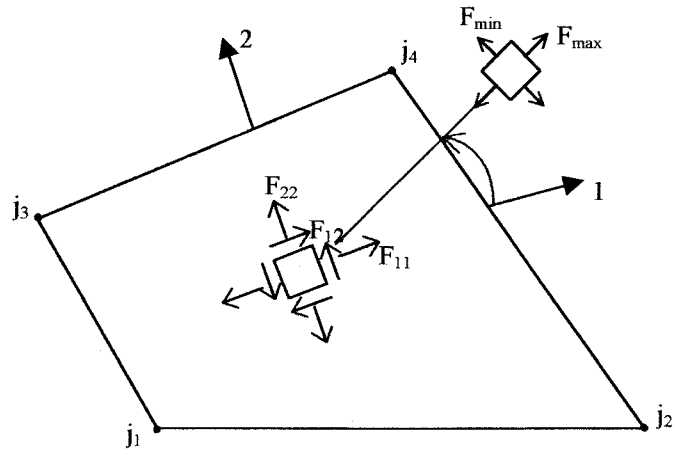


Figure 4.1-10 General Types of Shell Elements (SAP2000 Manual, 2000)



Membrane Forces

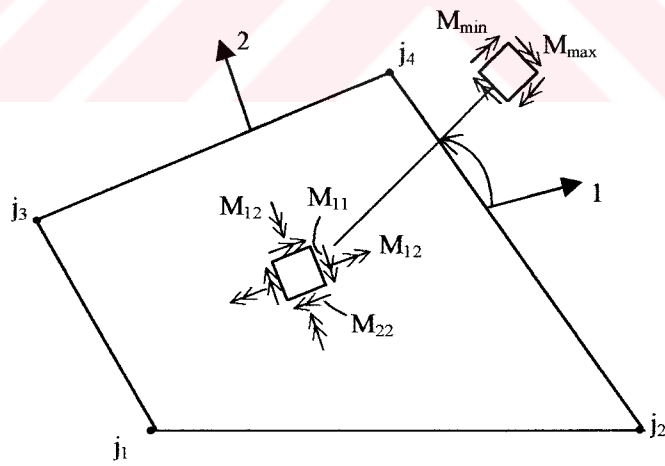


Plate Bending and Twisting Moments

Figure 4.1-11 Forces and Moments in Shell Elements (SAP2000 Manual, 2000)

### ***Solid Elements***

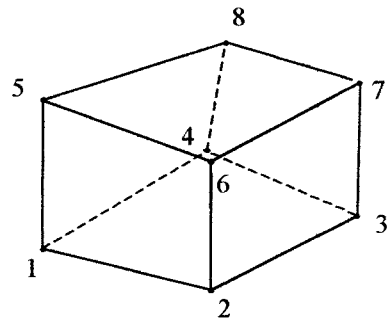
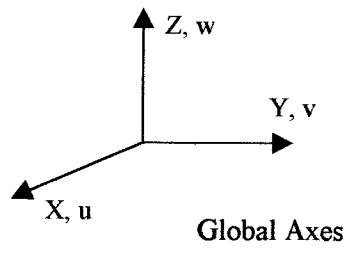
The Solid Element is an eight-node element for modelling of three-dimensional structures and solids. Solid elements are used in the case that frame or shell elements cannot represent the structural elements because of either the geometry of the structure or the location of the material. They are called according to their node numbers; hexahedral having 8 nodes, pentahedral having 6 nodes and tetrahedral having 4 nodes (Figure 4.1-12).

Generally hexahedral solid elements are used in modelling of the structure in this study, while pentahedral elements are chosen in modelling of the pendentives. Tetrahedral elements are not used in the models considered in the study (Spektra, 1998).

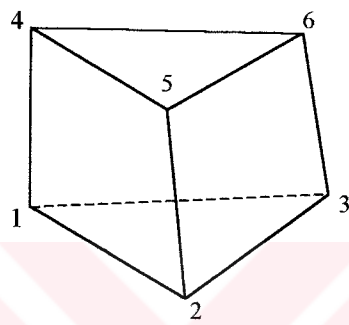
The local coordinate system for each Solid element is identical to the global system. The local coordinate system is used for defining material properties and loads, and for interpreting output.

The Solid Element models a general state of stress and strain in a three-dimensional solid. All six stress and strain components are active for this element (SAP2000 Manual, 2000). The forces, moments and stresses at nodes are shown below (Figure 4.1-12):

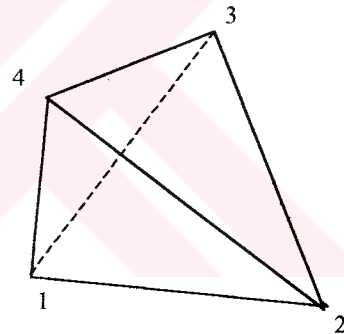
$S_{11}$ :	Stress in the Local 1-Axis in the 2-3 Plane
$S_{22}$ :	Stress in the Local 2-Axis in the 1-3 Plane
$S_{33}$ :	Stress in the Local 3-Axis in the 1-2 Plane
$S_{12}$ :	Stress in the Local 2-Axis in the 2-3 Plane
$S_{21}$ :	Stress in the Local 1-Axis in the 1-3 Plane
$S_{13}$ :	Stress in the Local 3-Axis in the 2-3 Plane
$S_{31}$ :	Stress in the Local 1-Axis in the 1-2 Plane
$S_{23}$ :	Stress in the Local 3-Axis in the 1-3 Plane
$S_{32}$ :	Stress in the Local 2-Axis in the 1-2 Plane
$S_{MIN}$ :	Min Principal Stress
$S_{MAX}$ :	Max Principal Stress



Hexahedral Solid Element



Pentahedral Solid Element



Tetrahedral Solid Element

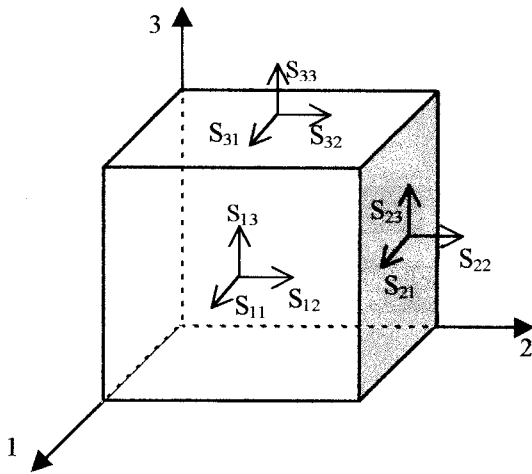


Figure 4.1-12 Solid Elements

## 4.2. Assumptions of SAP2000

The fundamental equations of structural mechanics can be placed in three categories. First; the stress-strain relationship contains the material property information which must be evaluated by laboratory or field experiments. Second; the total structure, each element, and each infinitesimal particle within each element must be in force equilibrium in their deformed position. Third; displacement compatibility conditions must be satisfied.

If all three equations are satisfied at all points in a time, all other conditions will automatically be satisfied. For example, at any point in a time the total work done by the external loads must be equal the kinetic and strain energy stored within the structural system plus any energy which has been dissipated by the system. Virtual work and variational principles are of significant value in the mathematical derivation of certain equations; however, they are not fundamental equations of mechanics (SAP2000 Manual, 2000).

### 4.2.1. Force-Deformation Relationships

The stress-strain equation is the fundamental constitutive law for materials. However, for one-dimensional elements in structural engineering, these equations can be rewritten in terms of forces and deformations.

$$\Delta = L\varepsilon, \text{ and} \tag{4.2.1}$$

$$N = A \sigma \tag{4.2.2}$$

These equations express the relation among the total deformation  $\Delta$ ; the applied load  $N$ ; the length  $L$ ; the cross-sectional area  $A$ ; and the modulus of elasticity  $E$ . The unit of deformation,  $\Delta$ , has the same unit as length  $L$ , since the units of  $\sigma$  and  $E$ , are equivalent, cancel out the equation (Singer, 1962). This equation represents Hooke's law. Originally, Hooke's law specified merely that stress was proportional to strain. Since

$$\sigma = E \varepsilon, \quad (4.2.3)$$

the force deformation relationship is

$$N = k_a \Delta \quad (4.2.4)$$

where  $k_a = AE/L$  and is defined as the ‘axial stiffness’ of the member. Moreover, equation 4.2.1 can be written in the following form:

$$\Delta = f_a N \quad (4.2.5)$$

where  $f_a = L/AE$  and is defined as the ‘axial flexibility’ of the member. It is important to note that the stiffness and flexibility terms are not a function of the load and are only the material and geometric properties of the member. Deformations are equal under the loads either tension or compression and stresses occurred by loads acting on the material do not reach the yielding limit. These force-deformation relationships are considered fundamental in the traditional field of strength of materials and structural design.

In the static analysis, SAP2000 uses the linear equation system shown below:

$$[K] \{u\} = \{R\} \quad (4.2.6)$$

where  $[K]$  is the stiffness matrix;  $\{u\}$  is the displacement vector; and  $\{R\}$  is the force vector. Equilibrium and compatibility equations can be used to calculate the global stiffness matrix (SAP2000 Manual, 2000).

#### 4.2.2. Anisotropic Materials

The linear stress-strain relationships contain the material property constants, which can only be evaluated by laboratory and field experiments. The mechanical material properties for material are defined in terms of three numbers: modulus of elasticity  $E$ , Poisson’s ratio  $\nu$  and coefficient of thermal expansion  $\alpha$ . In addition, the unit weight  $\omega$  and the unit mass  $\rho$  are considered to be fundamental material properties.



The positive definition of stresses, in reference to an orthogonal 1-2-3 system, is shown in Figure 4.2-1. In matrix notation the six independent stresses can be defined by

$$\{f\}^T = [ \sigma_1 \ \sigma_2 \ \sigma_3 \ \tau_{21} \ \tau_{31} \ \tau_{23} ] \quad (4.2.7)$$

From equilibrium,  $\tau_{12} = \tau_{21}$ ,  $\tau_{31} = \tau_{13}$ , and  $\tau_{32} = \tau_{23}$ . The six corresponding engineering strains are

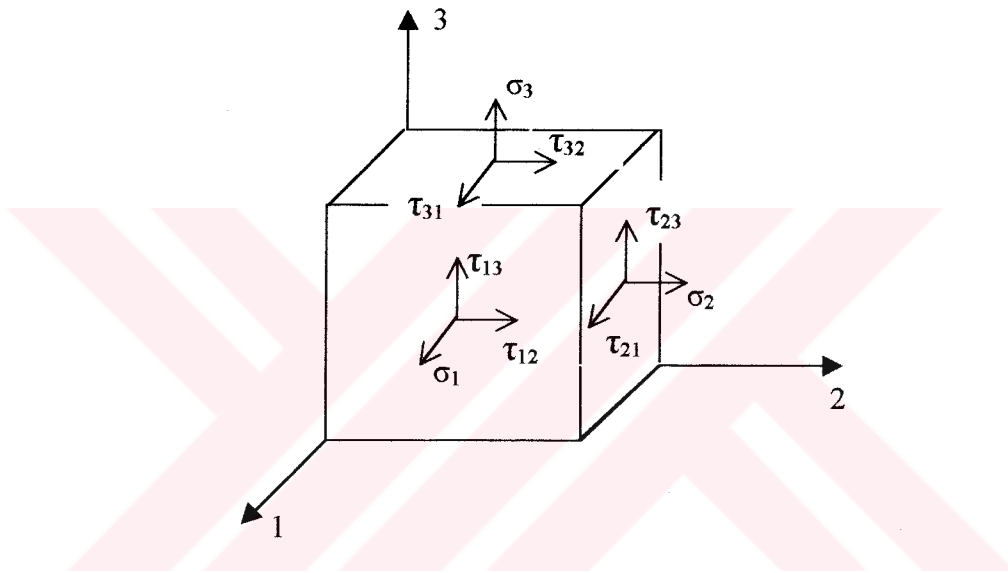


Figure 4.2-1 Definition of Positive Stresses

$$\{d\}^T = [ \epsilon_1 \ \epsilon_2 \ \epsilon_3 \ \gamma_{21} \ \gamma_{31} \ \gamma_{23} ] \quad (4.2.8)$$

The most general form of three dimensional strain-stress relationships, for linear structural materials subjected to both mechanical stresses and temperature change, can be written in the following matrix form:

$$\begin{bmatrix} \epsilon_1 \\ \epsilon_2 \\ \epsilon_3 \\ \gamma_{21} \\ \gamma_{31} \\ \gamma_{23} \end{bmatrix} = \begin{bmatrix} 1/E & -\nu_{12}/E & -\nu_{13}/E & -\nu_{14}/E & -\nu_{15}/E & -\nu_{16}/E \\ -\nu_{21}/E & 1/E & -\nu_{23}/E & -\nu_{24}/E & -\nu_{25}/E & -\nu_{26}/E \\ -\nu_{31}/E & -\nu_{32}/E & 1/E & -\nu_{34}/E & -\nu_{35}/E & -\nu_{36}/E \\ -\nu_{41}/E & -\nu_{42}/E & -\nu_{43}/E & 1/E & -\nu_{45}/E & -\nu_{46}/E \\ -\nu_{51}/E & -\nu_{52}/E & -\nu_{53}/E & -\nu_{54}/E & 1/E & -\nu_{56}/E \\ -\nu_{61}/E & -\nu_{62}/E & -\nu_{63}/E & -\nu_{64}/E & -\nu_{65}/E & 1/E \end{bmatrix} \begin{bmatrix} \sigma_1 \\ \sigma_2 \\ \sigma_3 \\ \tau_{21} \\ \tau_{31} \\ \tau_{23} \end{bmatrix} + \Delta T \begin{bmatrix} \alpha_1 \\ \alpha_2 \\ \alpha_3 \\ \alpha_{21} \\ \alpha_{31} \\ \alpha_{23} \end{bmatrix} \quad (4.2.9)$$

or in the symbolic matrix form

$$\{d\}=[\acute{C}]\{f\} + \Delta T\{a\} \quad (4.2.10)$$

The  $\acute{C}$  matrix is known as the compliance matrix and can be considered to be the most fundamental definition of the material properties since all terms can be evaluated directly from simple laboratory experiments. Each column of the  $[\acute{C}]$  represents the strains due to the application of a unit stress. The temperature increase  $\Delta T$  is in reference to the temperature at zero stress. The vector  $\{a\}$  indicates the strains due to a unit temperature increment.

For finite element analysis SAP2000 requires that the stresses be expressed in terms of the strains and temperature change. Therefore, within the program an equation of the following form is required:

$$\{f\}=E\{d\} + \{f_0\} \quad (4.2.11)$$

in which  $E=[\acute{C}]^{-1}$  (SAP2000 Manual, 2000).

### 4.2.3. Dynamic Analysis

#### A. Eigen-value Analysis

The frequencies and mode shapes can be obtained performing the Eigen-value analysis. In the Eigen-value analysis, the equation system shown below is used

$$[M] \{\ddot{u}\} + [K]\{u\} =\{0\} \quad (4.2.12)$$

where  $[M]$  is the mass matrix;  $[K]$  is the stiffness matrix;  $\{\ddot{u}\}$  is the acceleration vector and;  $\{u\}$  is the displacement vector.

The equation system 4.2.12 can be solved with the equation shown below:

$$[K]\{\emptyset\} = [M] \{\emptyset\} [\Omega^2] \quad (4.2.13)$$

where  $[\Omega^2]$  is the diagonal matrix giving Eigen-values (modal frequencies) and  $\{\mathcal{O}\}$  is the vector of mode shapes corresponding with the modal frequencies.

### ***B. Definition of Response Spectrum***

For three-dimensional seismic motion, analysis is performed using the modal equation below:

$$[M] \{\ddot{u}\} + [C] \{\dot{u}\} + [K] \{u\} = \{M\} \ddot{u}_{gx} + \{M\} \ddot{u}_{gy} + \{M\} \ddot{u}_{gz} \quad (4.2.14)$$

where  $[M]$  and  $[K]$  are the mass and stiffness matrices, respectively, while  $[C]$  is the damping matrix. Besides,  $\{u\}$ ,  $\{\dot{u}\}$  and  $\{\ddot{u}\}$  denote the relative displacement, velocity, and acceleration vectors with respect to the ground;  $\ddot{u}_{gx}$ ,  $\ddot{u}_{gy}$ , and  $\ddot{u}_{gz}$  are the components of uniform ground acceleration.

Response-spectrum analysis seeks the likely maximum response to these equations rather than the full time history. The earthquake ground acceleration is given as a digitised response-spectrum curve of pseudo-spectral acceleration response versus period of the structure.

Even though accelerations may be specified in three directions, only a single positive result is produced for each response quantity. The response quantities include displacements, forces, and stresses. Each computed result represents a statistical measure of the likely maximum magnitude for that response quantity. The actual response can be expected to vary within a range from this positive value to its negative. No correspondence between two different response quantities is available. No formation is available as to when this extreme value occurs during the seismic loading, or as to what the values of other response quantities are at that time.

Response-spectrum analysis is performed using load superposition (Wilson and Button, 1982). Modes may have been computed using Eigen-vector analysis or Ritz-vector analysis.

A scale factor is specified to multiply the ordinate, i.e. pseudo spectral acceleration response of the function. This is often needed to convert values given in terms of the acceleration due to gravity to units consistent with the rest of the model.

For a given direction of acceleration, the maximum displacements, forces and stresses are computed throughout the structure for each vibration mode. These modal values for a given response quantity are combined to produce a single, positive result for the given direction of acceleration. CQC (Complete Quadratic Combination) method is used in this study for combination. Obtaining the single, positive result for each direction of acceleration, these directional values are combined with SRSS (Square Root of the Sum of their Squares) method.

The CQC method takes into account the statistical coupling between closely spaced Modes caused by modal damping. Increasing the modal damping increases the coupling between closely spaced modes. If the damping is zero for all Modes, this method degenerates to the SRSS method. CQC combines the modal results by the Complete Quadratic Combination technique described by Wilson, Der Kiureghian, and Bayo (1981). SRSS method combines the modal results by taking the Square Root of the Sum of their Squares (SAP2000 Manual, 2000).

### **4.3. Methods of Analysis and Solution Techniques**

#### **4.3.1. Load Increment Method**

In the analyses, the structure is subjected to a load, which is incremented by multiplying its self-weight by a constant ratio, namely the load factor. The propagation of the cracks through the structural elements with the effect of the load increment is determined for each load factor. For the load increment, the interval is selected as 0.2.

The structure is subjected to the external vertical loading shown below;

$$P_v = \lambda W_s \quad (4.3.1)$$

where  $P_v$  is the vertical load;  $\lambda$  is the load factor; and  $W_s$  is the self-weight of the structure.

The First, Third and Fourth Models are analysed with the Smearred Crack Modelling Method. The steps of this analysis are given as a flow chart in Figure 4.3-1. As can be seen from the figure, the load acting on the structure is multiplied by the load factor  $\lambda$ , starting with  $\lambda=0.8$ , because cracks occur already at this load factor. The principal stresses for all elements and the displacement at the apex of the main dome are calculated. When the principal stress of any element exceeds 75% of the strength limit (11.25 MPa in compression and 1.05 MPa in tension), the element is assumed as cracked (Chen, 1994).

At each load factor, the elements whose principal stresses exceed the crack strength limit are determined, and the modulus of elasticity of these elements is reduced to 0.1. The model is analysed for the same load factor to let the cracks to propagate. When cracks stop occurring, the load factor is increased for the next step. Since the compression strength limit is almost 10 times higher than the tension strength limit, no compression crack is observed during the analyses. Hence, the tension strength limit, which is decisive, is used in the flow chart and not the compressive strength. The structure is considered as collapsed when cracks cover almost one third of the surface of one of the main load bearing elements. This case is called as "Collapse Condition".

The results of the analyses of the First, Third and Fourth Models are given for the maximum principal stress in Sections 5.1.1, 5.1.3 and 5.1.4.

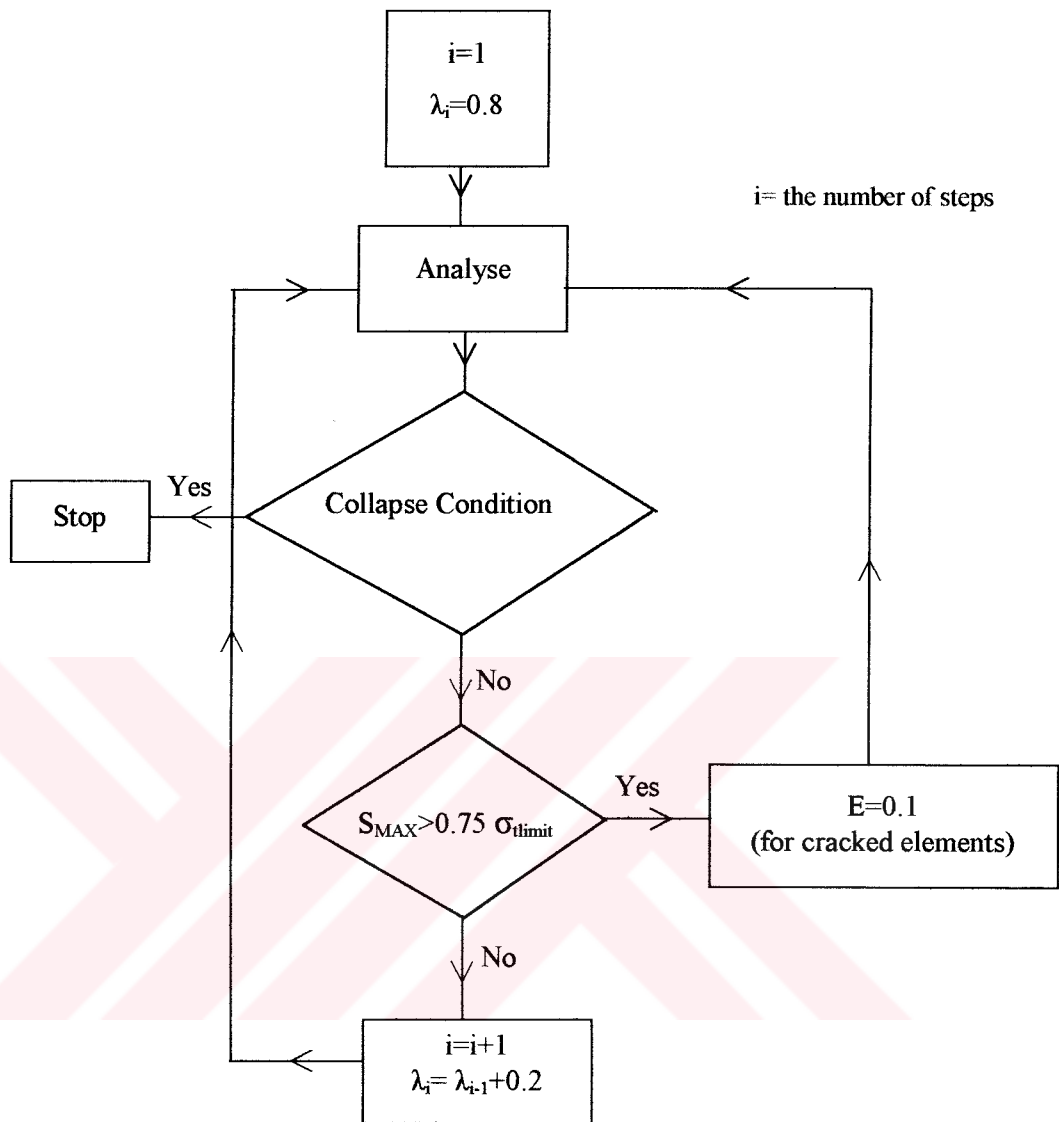


Figure 4.3-1 The Flow Chart of the Load Increment Method for the Smeared Crack Modelling

The Second Model is analysed by applying the Discrete Crack Modelling Method. Again, the model is loaded first with 0.8 times of the self-weight. As in the Smeared Crack Modelling Method, when principal tension (or compression) stress of an element exceeds 75% of the limit value (11.25 MPa in compression and 1.05 MPa in tension), the element is considered as cracked (Chen, 1994). Then, a second node is defined for the element with the same coordinates to release the displacements of the cracked parts from the model. After that, if the crack propagates, the cracked part of the element is disconnected from the model. Finally, when the crack covers almost the whole

element, this element is removed from the model. Once a crack has developed, the load factor is not increased. However, the new model is analysed once more in the next step. Although the load factor has not been changed, new cracks may develop because the stress distribution of the system is changed. Proceeding in this way, it is possible to follow the crack propagation through the structure. This procedure is carried out until the collapse condition is reached (see Section 4.3.1). The flow chart of this procedure is given in Figure 4.3-2.

The results of the static analysis of the Second Model for the maximum principal stress are given in Section 5.1.2.

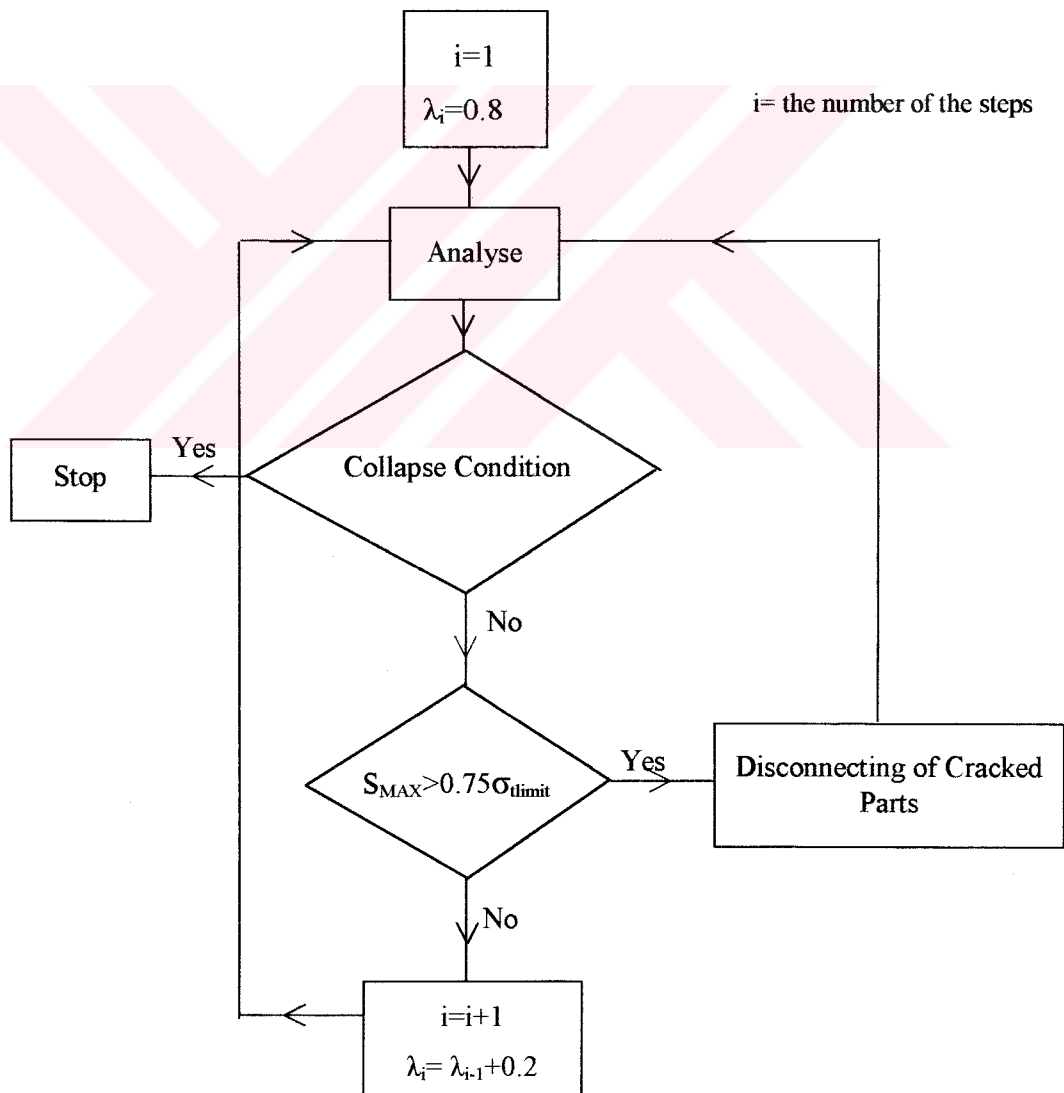


Figure 4.3-2 The Flow Chart of the Load Increment Method for the Discrete Crack Modelling



### 4.3.2. Spectral Analysis

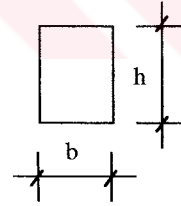
The aim of this part of the study is to find out the approximate dynamic vulnerability of the structure under the earthquake acceleration 0.4g by using the model including cracks under its self-weight ( $\lambda=1$ ).

At the first stage, the First Model, M1, is loaded starting with the load factor of 0.8 and then, the cracked regions are determined. When the propagation of cracks stops at  $\lambda = 0.8$ , the load factor increases and then, new cracks are introduced to the model until propagation of the cracks stops. The Smeared Crack Modelling Method is used to follow the propagation of cracks as seen in Figure 4.3-4. However, as can be seen in the figure, different from the static analysis part, the new values of modulus of elasticity for the cracked elements are calculated proportional to  $h^{1.5}$ , while  $h$  is the thickness of the element. This assumption is made knowing that the stresses depend on the thickness of the element for axial forces and square of the thickness in a cracked section for bending moments. This can be deduced from Equations 4.3.2 to 4.3.6.

$$\sigma = \frac{N}{A} + \frac{M}{W} \quad (4.3.2)$$

$$A=bh \quad (4.3.3)$$

$$W= bh^2/6 \quad (4.3.4)$$



Equations 4.3.3 and 4.3.4 are substituted in Equation 4.3.5.

$$\sigma = \frac{N}{bh} + \frac{M}{bh^2/6} \quad (4.3.5)$$

$$\sigma = f(h, h^2) \quad (4.3.6)$$

where  $N$  is the axial force;  $M$  is the moment;  $A$  is the cross sectional area and  $W$  is the section modulus.

Moreover, since the linear elastic analysis is performed, stresses can be defined with the linear function shown below.

$$\sigma = E\varepsilon, \text{ or} \quad (4.3.7)$$

$$E = (1/\varepsilon) \sigma \quad (4.3.8)$$

with this respect,

$$E = f(h, h^2) \quad (4.3.9)$$

Using Equations 4.3.6 to 4.3.9, the value  $h^{1.5}$ , which is between the values  $h$  and  $h^2$ , is chosen to take the thickness of the cracked elements into account by changing their elasticity moduli.

$$h < h^{1.5} < h^2 \quad (4.3.10)$$

In following equations, the steps for calculation of the crack depth are given.

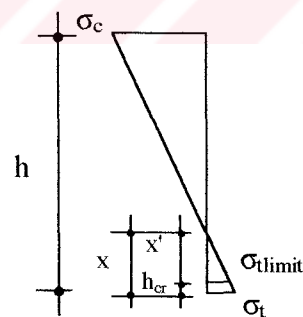


Figure 4.3-3 Stresses at Section of an Element

$$\frac{\sigma_t}{\sigma_t + \sigma_c} = \frac{x}{h} \quad (4.3.11)$$

where  $\sigma_t$  and  $\sigma_c$  are the tension and compression stresses, respectively;  $h$  is the thickness of the element;  $x$  is the depth of the tension region; and  $h_{cr}$  is the crack depth.

$$x = \frac{\sigma_t}{\sigma_t + \sigma_c} h \quad (4.3.12)$$

$$\frac{\sigma_{limit}}{\sigma_t} = \frac{x'}{x} \quad (4.3.13)$$

$$x' = \frac{\sigma_{limit}}{\sigma_t} x \quad (4.3.14)$$

$$x = x' + h_{cr} \quad (4.3.15)$$

$$h_{cr} = x - x' \quad (4.3.16)$$

$E_{cr}$ , which is the modulus of the elasticity of the cracked elements, can be obtained using the relationship between  $E$  and  $h$ .

$\sigma \sim h^{1.5}$  (assumption) and  $\sigma \sim E$ , then, it can be said that  $E \sim h^{1.5}$  and similarly,  $E_{cr} \sim h_{cr}^{1.5}$ . Using these equations and proportions, the modulus of elasticity of the cracked elements is obtained taking the crack depth into account.

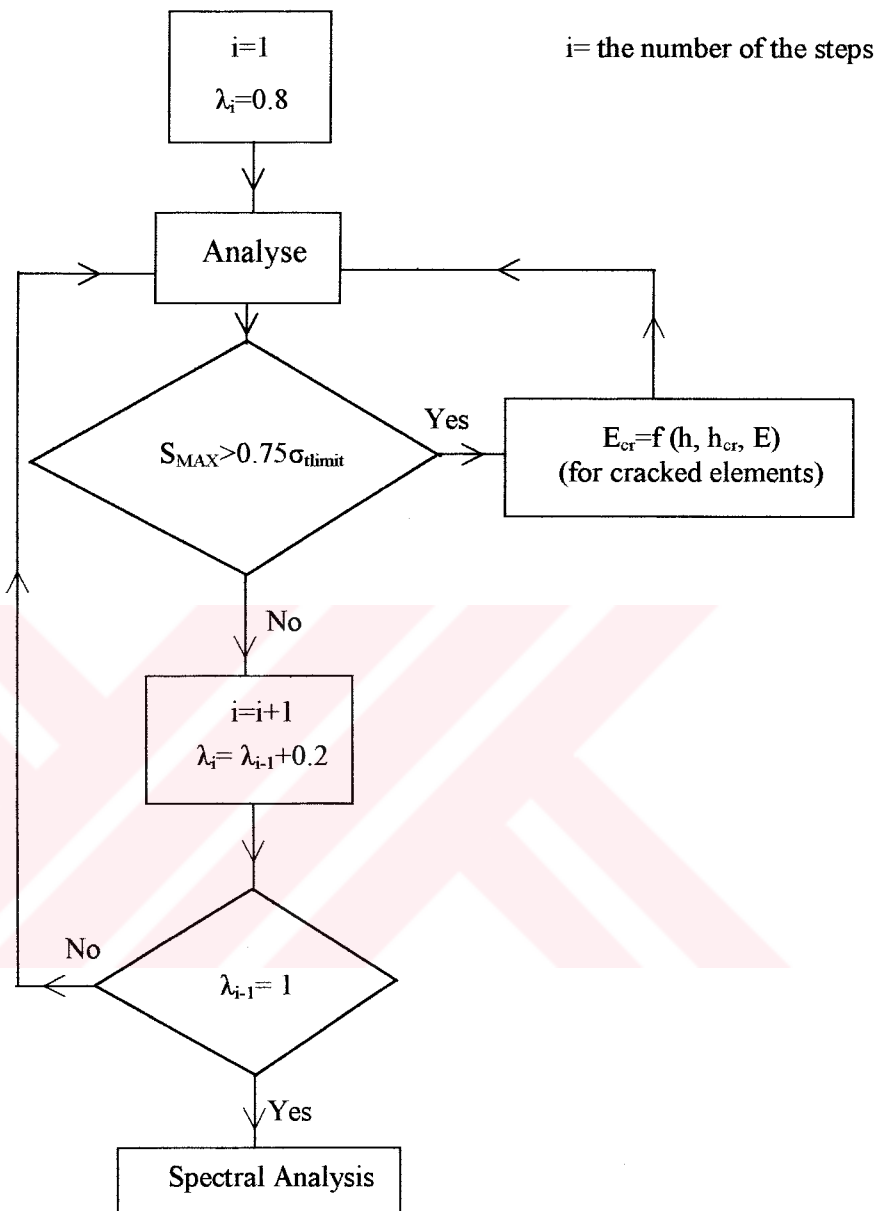


Figure 4.3-4 The Flow Chart to Determine the Cracks occurring under the Self-weight of the Structure

At the second stage, after determining the model including cracks under its self-weight by following the flow chart in Figure 4.3-4, the spectral analysis of the cracked model is performed. The procedure for the spectral analysis is given in Figure 4.3-5.

In the spectral analysis, the structure is subjected to an acceleration increment with a constant ratio like the Load Increment Method. The

propagation of the cracks through the structural elements with the effect of the acceleration increment is determined for each acceleration value. As the increment of the acceleration, a very low value, namely 0.02g is selected. Because, when larger increments are taken, high local stress concentrations, 5 or 6 times of the crack tension strength limit, are obtained in the structure in the spectral analysis. This is not realistic, because an element cannot take stresses larger than its strength limit. From the same reason, the earthquake acceleration 0.04g is subjected to the First Model as the initial acceleration value. For this value, no additional crack is observed. Therefore, the value is increased to the value of 0.06g where some minor cracks start to occur.

The principal stresses for all elements are calculated. If the principal stress of any element exceeds the strength limit (11.25 MPa for compression and 1.05 MPa for tension), the element is assumed as cracked.

At each acceleration value, the elements having principal tension (or compression) stress higher than the limit values are determined. The elasticity modulus of these elements is decreased taking the effect of the crack depth into account with the method explained above.

The model is analysed at the same acceleration to let the cracks to propagate. When the cracking stops, the acceleration is increased for the next step. The flow chart of this procedure is shown in Figure 4.3-5. This procedure is continued until the crack propagation stops at acceleration 0.4g. By doing so, the vulnerability of the structure at acceleration, which is the highest one recorded at least two times during 500 years term, is obtained (Durukal, 2001).

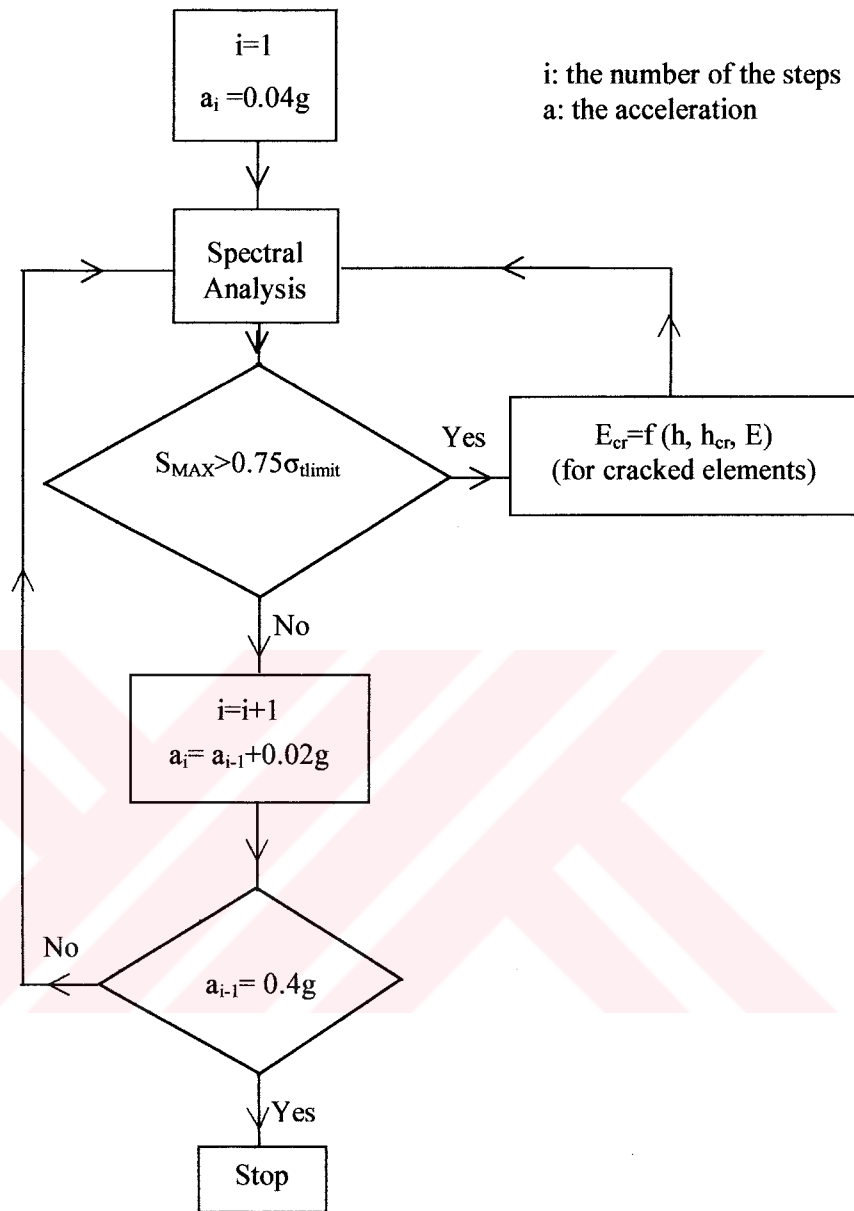


Figure 4.3-5 The Flow Chart of the Spectral Analysis for the Smearred Crack Modelling

The earthquake effects are investigated in the X and Y-direction separately, and the results of these two earthquakes are obtained.

The shape of the response-spectrum curve is taken from the Analysis Requirements for Earthquake Resistant Building in the Specifications for Structures to be Built in Disaster Areas (Turkish Earthquake Code). This code specifies design spectra with the curve shown in Figure 4.3-6. This code defines

the equations for each range of the spectrum curve for four different soil types. More information about the spectral analysis is given in Section 4.2.3.

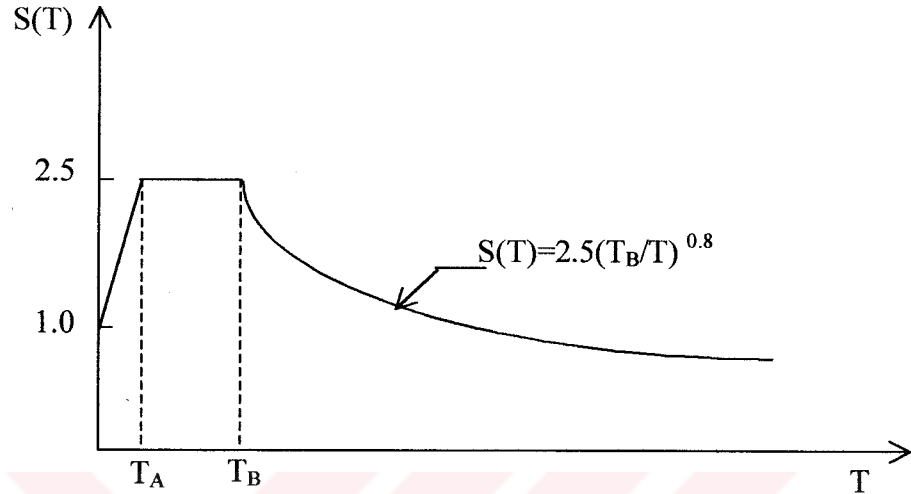


Figure 4.3-6 The Curve of Spectrum Coefficient according to the Turkish Earthquake Code

In this figure,  $T_A$  and  $T_B$  denote the characteristic periods depending on the soil types,  $T$  is the period of the structure and  $S(T)$  is the spectrum coefficient.

Changes in the stresses are determined for both solid and shell elements at acceleration values 0.1g, 0.2g, 0.3g, and 0.4g, while the earthquake is applied in the X and Y-directions separately. The results of analysis for above accelerations are given for  $S_{11}$  and  $S_{22}$  stresses (see Section 5.2.1), where  $S_{11}$  denotes the hoop stress for shell elements and the stress in the X-direction for solid elements, while  $S_{22}$  denotes the radial stress for shell elements and the stress in the Y-direction for solid elements.

This analysis procedure is also obtained for the first alternative model, M3, to investigate the effect of the stronger east and west arches to the dynamic vulnerability of the structure. Results of this analysis is also given for  $S_{11}$  and  $S_{22}$  stresses in Section 5.2.2.



# CHAPTER 5

## RESULTS AND FINDINGS

### 5.1. Results of the Static Analysis

The maximum principal stress resultants of three models, namely M1, M2 and M3 (see Section 4.1), are discussed, in this Section. The Smearred Crack Modelling Method is used for modelling the cracks of M1 and M3, and the Discrete Crack Modelling Method is used for M2. The number of the steps of the analyses is reached to nearly 20 for M1 and M3, when the collapse condition is reached. On the other hand, this increases to do nearly 30 steps for M2. Since the all iterations cannot be shown, the maximum principal stress distributions of M1 and M3 are given for three load factors. By doing so, it is possible to compare the changes in stresses under the increasing load factors in a more efficient way. However, one more load factor is given for M2. This is because, the analysis in this case stops at load factor 1.8 instead of 1.2, which is load factor obtained from M1 and M3.

The maximum principal stress distributions and the crack propagations of M1, M2, and M3 under the static loads are given in Figures 5.1-1 to 5.1-5. The variation of the vertical displacements versus the load factors is given for M1, M2, M3, and M4 in Figure 5.1-16.

#### 5.1.1. Static Analysis of the First Model

As the first case, the First Model, M1 is calculated, and the crack propagation through the structure is investigated. At this model, the initial cracks occur at the connection regions of the main semidomes to the secondary semidomes even at load factor 0.8. The elasticity moduli of the cracked elements decrease and the iteration is continued with the same load factor to let

the cracks propagate. This process is carried out until the propagation of cracks stop. Then, the load factor is increased to the value of 1.

When the load factor is 1, new cracks start to occur at some parts of the tympanum walls, and the main piers, which continue to propagate up to load factor 1.2. Since the propagation of the cracks at both the tympanum walls and the main piers is limited to a very small area relative to the whole structural part, they do not lead to the collapse of the structure. Hence, their distribution is not shown in the corresponding figures.

Some more cracks occur again at the connection region of the secondary semidomes to the main semidomes at load factor 1.2. At this load value also, more cracks are initiated at the connection region of the crests of the main semidomes to the main arches. Moreover, some cracks are observed at some random regions of the west semidome. These cracks continue to propagate under this load level for further steps and after a few more iterations, the cracks at the main west semidome increase extremely. Ultimately, the cracks cover one third of the surface of the west semidome, and hence the analysis is stopped (Figures 5.1-1 and 5.1-4). The stress distributions of the main structural parts are discussed separately in sequel.

### ***The Main Dome***

At load factor 0.8, compression stresses spread over at both the apex and the perimeter parts of the main dome (Figure 5.1-2). However, tension stresses are observed around the middle part of the main dome in the circumferential direction (Figures 5.1-2 and 5.1-3). The maximum value for compression and tension stresses is about 0.13 MPa at load factor 1. These tension stresses propagate through the main dome slowly, and their values just reach to 0.22MPa at the collapse load factor (Figure 5.1-4).

### ***Semidomes***

The stress distributions of both main semidomes are similar to each other until the collapse load factor is reached. Both tension and compression

stresses are observed over the main semidomes (Figure 5.1-2). However, tension stresses develop at almost all the surfaces of the secondary semidomes except a small region. Their maximum value is observed at the connection regions between the main semidomes and secondary semidomes. After taking these cracks into account, their propagation keeps continuing for further steps. Hence, the tension stresses increase and/or convert from compression to tension at the neighbouring uncracked elements (Figures 5.1-3 and 5.1-4). Moreover, it is observed that tension stresses at the connection regions between the main semidomes and the secondary arches, and at the bottom surfaces of the crests of the main semidomes where they are connected to the main arches are higher than the crack tension strength limit at further steps. After the cracks caused by these tension stresses are imposed on the model, tension stresses at the crests of the main semidomes are increased more. However, this increase at the west semidome is faster than the other one. As a result, the cracks propagate extremely fast through the middle part of the west main semidome, and finally it collapses before the other main structural elements at load factor 1.2 (Figure 5.1-4).

The same failure is not observed for the east main semidome, although their mechanical properties are identical. Apparently, the maximum stress of the east main semidome is around 0.53 MPa, which is the almost half of the crack tension strength limit. The additional secondary semidome on the east side of the structure is the effect for asymmetry. The other reason for the asymmetric failure at the main semidomes is that some restorations are included in the model, such as the higher west arch, four blinded windows at the west, and asymmetric ribs on the west side of the main dome, which change the symmetry of the model according to the north-south-axis. These are not visible in the figures, except for four blinded windows, since the figures are in the plan view. Four blinded windows are shown as the projections on the west side of the main dome and are seen for example in Figure 5.1-3.

### *Arches, Pendentives and Piers*

Principal tension stresses spread through almost all the arches, pendentives and upper parts of the piers until the collapse condition. The directions of these principal stresses do not depend on directions in either global or local axes. Since these stresses are almost in the same stress range, 0 - 0.26MPa, the variation of them cannot be observed in Figures 5.1-2 to 5.1-4. The highest tension stress occurs at the top of the key region of the north and south arches and its value is 0.45 MPa. This stress value is observed at a very limited region. Relatively very small tension stresses occur at the rest of the arches.

Tension stresses concentrate at four pendentives as compared to the arches and piers, reaching to the value of 0.34 MPa at load factor 1.2.

Tension stresses at some regions of the piers are higher than the crack tension strength limit. However, these stresses do not cause any important effect for the structure, because they occur at very small regions relative to the main structural parts. Moreover, the cracks caused by these stresses propagate for only a few steps. Therefore, they are not shown in figures. Compression stresses generally spread over the bottom parts of the piers and their highest value is 0.56 MPa.

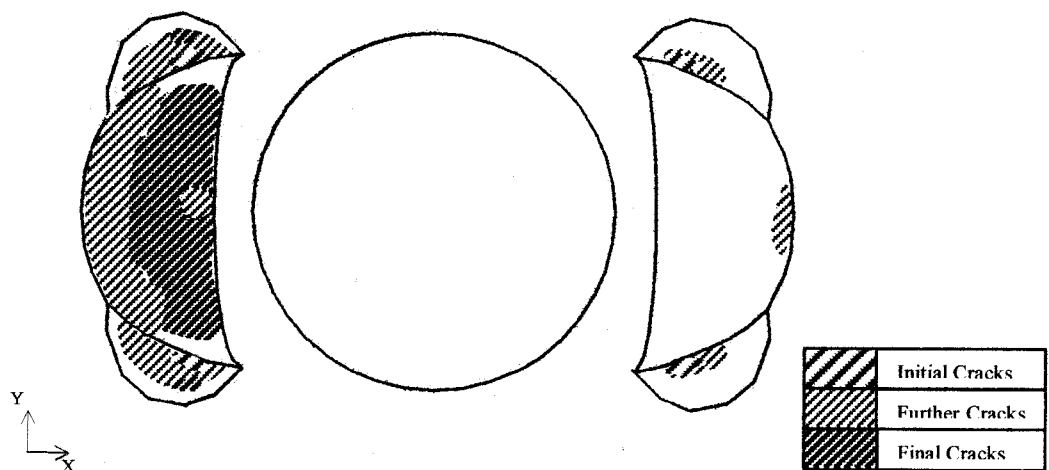


Figure 5.1-1 The Crack Propagation through M1 for the Collapse Load Factor,  $\lambda=1.2$

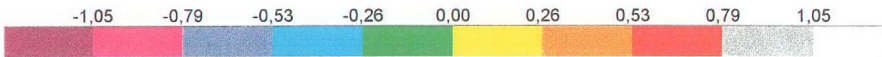
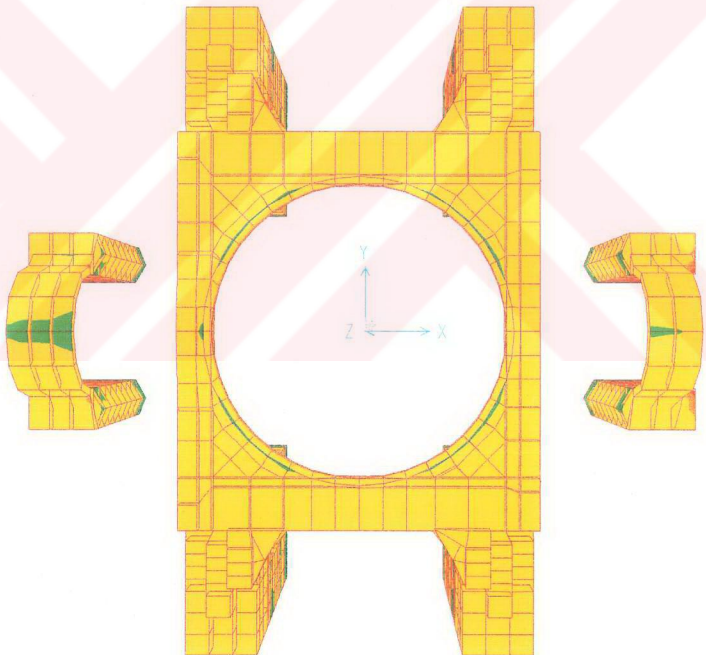
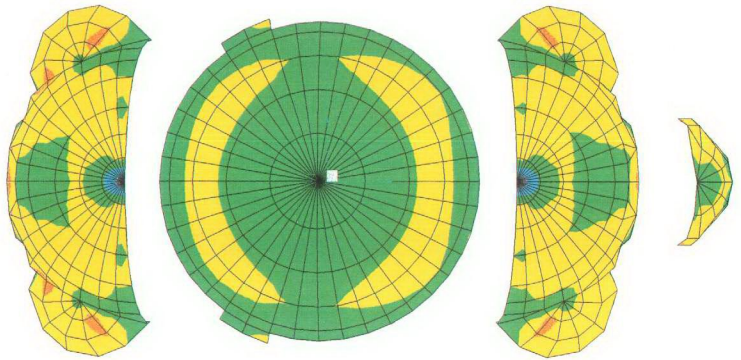


Figure 5.1-2 The Maximum Principal Stress Distribution through M1,  $\lambda=0.8$ , (MPa)

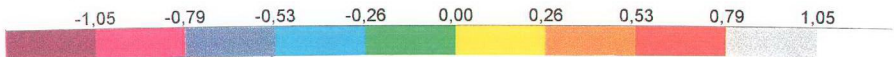
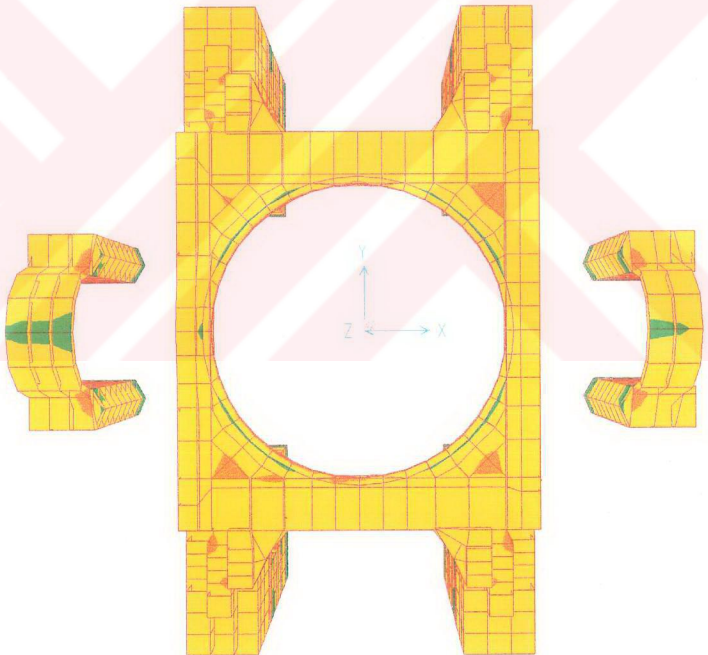
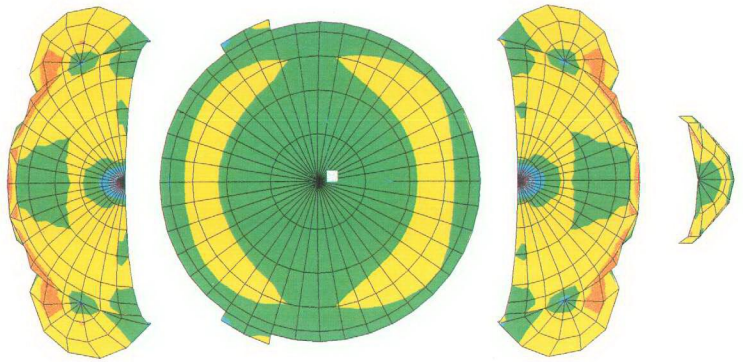


Figure 5.1-3 The Maximum Principal Stress Distribution through M1,  $\lambda=1$ , (MPa)



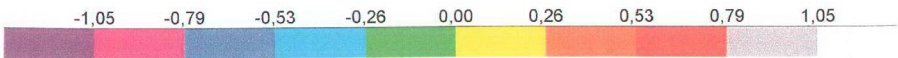
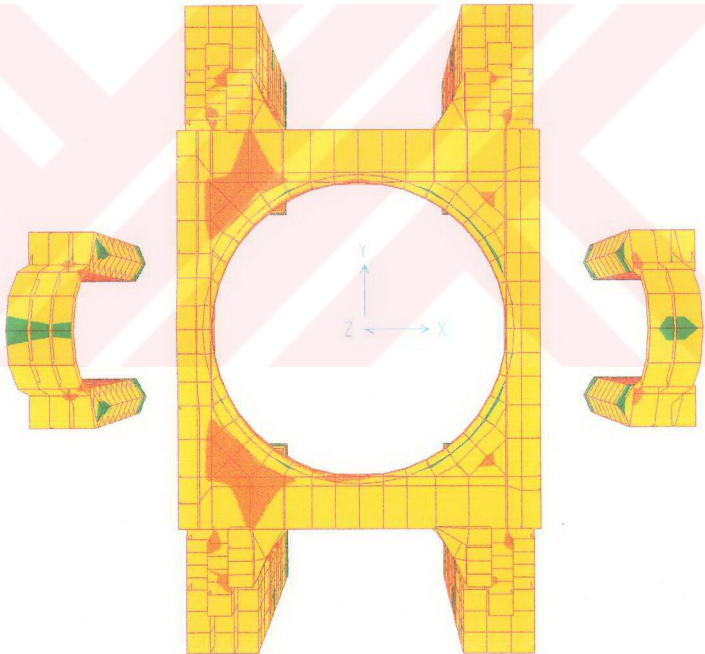
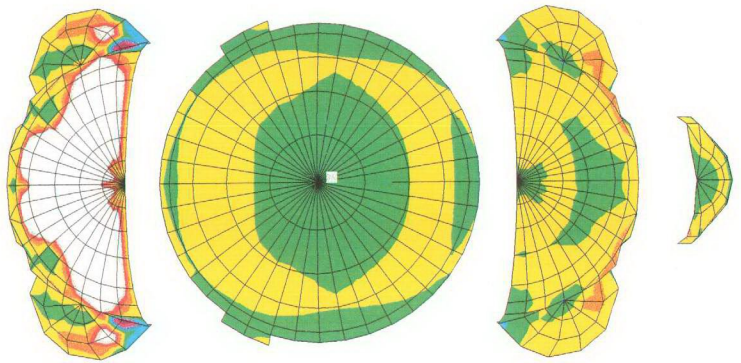


Figure 5.1-4 The Maximum Principal Stress Distribution through M1,  $\lambda=1.2$ , (MPa)



### 5.1.2. Static Analysis of the Second Model

As the second case, the static analysis is carried out in the Second Model, M2. The crack propagation of the model until it collapses by using the Load Increment Method. Different from M1, the Discrete Crack Modelling Method is used to take cracks into account in the model. Because it is time consuming to modify the mesh of the models, this method is preferred to use only for M2, which has the smallest number of the finite elements considered in this study.

The initial cracks are first observed at the connection region of the crests of the main semidomes where they connect to the east and west main arches at load factor 0.8 (Figure 5.1-5). After these cracked parts of the main semidomes are removed from the model, the crack propagation at the crests of the main semidomes stop. Since there is no other crack at the structure, the load factor is increased to the value of 1.

At load factor 1, some more cracks are observed at the piers, and these cracks develop further until load factor 1.8 (Figure 5.1-5). Besides, cracks start to occur at the main dome at this load factor. After a few calculation steps, more cracks develop in the piers. However, the cracks at the main dome propagate faster than the other main structural parts and finally, the main dome collapses. This means that, the removed parts, i.e. cracks, are covered one third of the surface of the main dome at load factor 1.8.

Four graphics are given to observe the redistribution of stresses of the model more clearly, because the collapse load factor is higher than that obtained in the previous model. Since there is not much difference among the stress distributions through the model at the lower load factors, the stress results of the different load factors are chosen from the previous case for demonstration.

#### *The Main Dome*

The stress distributions through the main dome are similar for both M1 and M2 until their collapse load factors (Figures 5.1-2 to 5.1-4 and Figures

5.1-6 to 5.1-9). Compression stresses develop at the apex and the perimeter of the main dome, whereas the other parts are covered with tension stresses between load factors 0.8 and 1.6 (Figures 5.1-6 to 5.1-8). The only difference that is observed at these stress distributions is the magnitudes of the stresses where tension stresses increase.

Tension stresses at the main dome increase fast at load factor 1.8 and they cover almost all of the main dome surface. When the cracks caused by the tension stresses cover one third of the main dome surface at load factor 1.8, the analysis stops and the structure is considered as collapsed (Figure 5.1-9). Although, a circumferential and almost symmetrical tension stress distribution is observed through the main dome for the previous load factors, its east part collapses first. This may be caused by the effects mentioned in Section 5.1.1.

#### ***Semidomes***

Since the thinner secondary domes are not included in this model, tension stresses at the main semidomes, especially at their perimeter parts, are not affected by the increment of the load as much as that in the previous analysis case. The initial cracks occur at the connection regions between the crests of the main semidomes to the arches at load factor 0.8 (Figures 5.1-5 and 5.1-6). After these regions are removed from the model, the tension stresses at their neighbouring elements increase slightly (Figures 5.1-7 and 5.1-8). However, the tension stresses develop faster at the main dome for further steps. Even, when the main dome collapses, the highest tension stress at the semidome is limited with the value of 0.79 MPa (Figure 5.1-9).

#### ***Arches, Pendentives and Piers***

The arches, pendentives and piers are covered by tension stresses, utmost 0.26 MPa, at the beginning (Figure 5.1-6). Tension stresses are concentrated at the top of the pendentives relative to that of the arches (Figures 5.1-7 and 5.1-8). However, they do not exceed the value of 0.53 MPa even at load factor 1.8 (Figure 5.1-9). In other words, no crack is observed at these regions even though the main dome collapses.



Figure 5.1-5 The Crack Propagation through  $M_2$  for the Collapse Load Factor,  $\lambda=1.8$

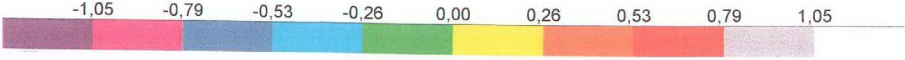
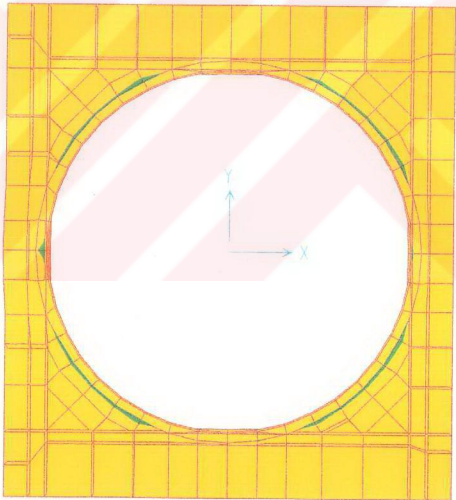
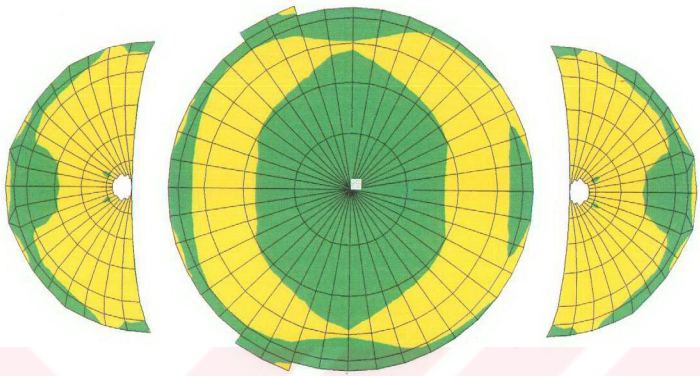


Figure 5.1-6 The Maximum Principal Stress Distribution through M2,  $\lambda=0.8$ , (MPa)

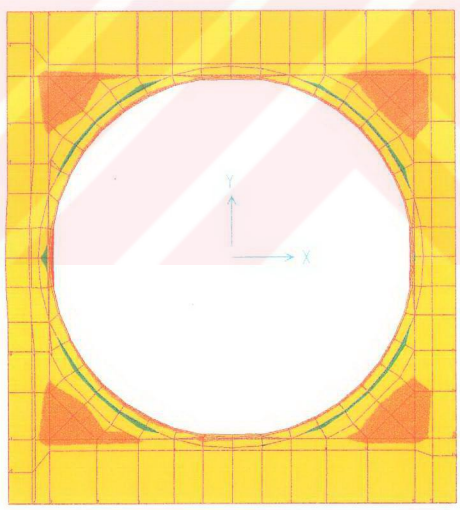
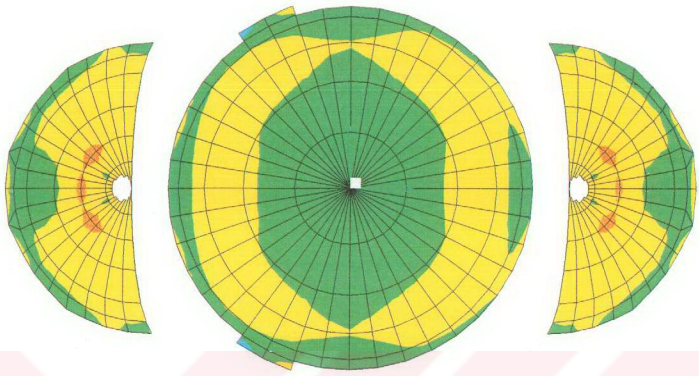


Figure 5.1-7 The Maximum Principal Stress Distribution through M2,  $\lambda=1.2$ , (MPa)



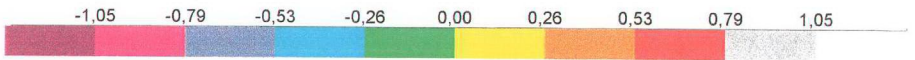
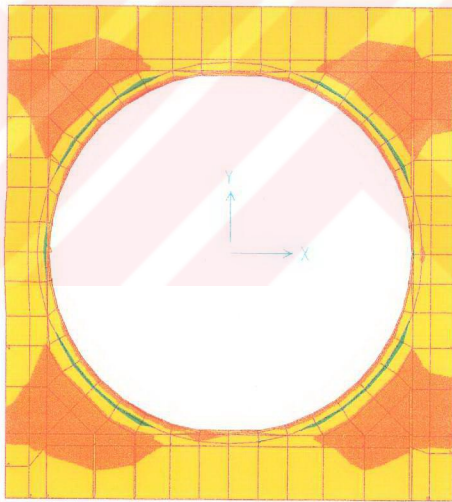
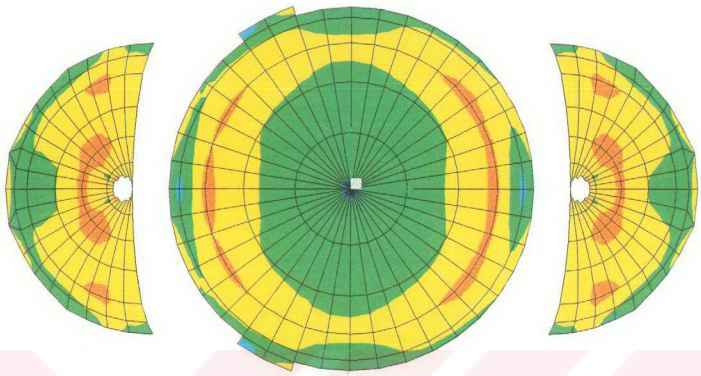


Figure 5.1-8 The Maximum Principal Stress Distribution through M2,  $\lambda=1.6$ , (MPa)

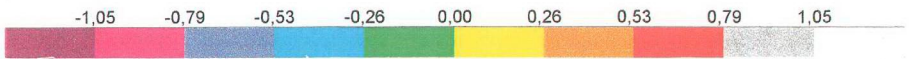
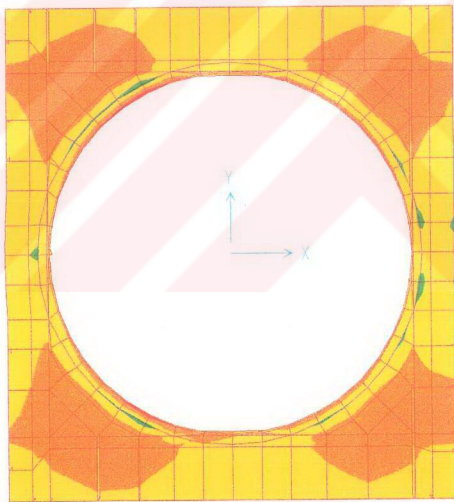
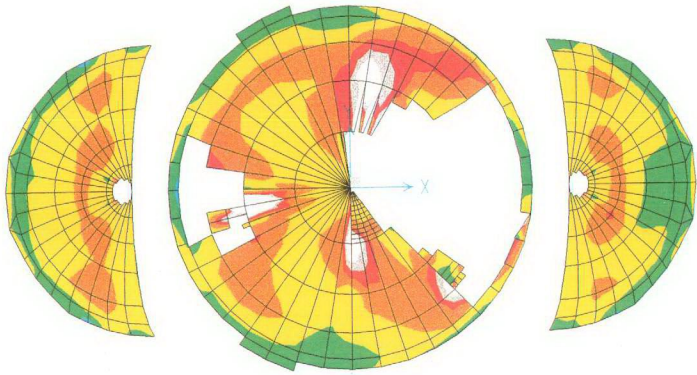


Figure 5.1-9 The Maximum Principal Stress Distribution through M2,  $\lambda=1.8$ , (MPa)



### 5.1.3. Static Analysis of the Third Model

The same analysis procedure performed for M1 is applied for M3. In this case, the crack propagation through the structure is observed with the Load Increment Method, and cracks are taken into account by using the Smeared Crack Modelling Method.

M3 is created for the investigation with arches that are as strong as those at the north and south. Hence, the east and west arches in M3 has the same rigidity as those in that of north and south.

The collapse behaviour of M3 is similar to that obtained for M1 with some differences in the stress distribution (Figure 5.1-13). The west semidome collapses before the other structural parts in both cases. Moreover, the collapse load factor is 1.2 like that of M1. On the other hand, the elements at the crests of the main semidomes of M3 do not crack at the beginning whereas these elements are cracked at M1, because M3 has stronger arches. On the other hand, M3 performs better under the spectral loading as compared with M1 as will be shown later. Results of the spectral analysis are given in Section 5.2.2. The stress distributions of the model for the static analysis are given in Figures 5.1-11 to 5.1-13.

The initial cracks start at the secondary semidomes where they are connected to the main semidomes, similar to M1. For the following load steps, the cracks at these regions propagate through the main semidomes. As mentioned above, the further development of these cracks cause the collapse of the west main semidome. The crack propagation for the collapse load factor is given in Figure 5.1-10. Additionally, the crack propagation of M1, M2, and M3 are given in Figure 5.1-14 to compare the collapse behaviour of the models. The maximum principal stress distributions of M1 and M3 are given together at their collapse load factor to see easily the effect of the stronger arches to the stress distribution (Figure 5.1-15).

In the case of M1, the initial cracks start at the secondary semidomes, then propagate to the main semidomes (Figure 5.1-1 or 5.1-14a). For the further

steps, cracks occur at the crest of the main semidomes. Finally, the west main semidome collapses, because of the cracks propagating through the middle part of the west main semidome from both the west secondary semidomes and the crest of the west main semidome. However, in the case of M3, the initial cracks start at the secondary semidomes same as that of M1 (Figure 5.1-14c). For the following steps, the propagation of cracks changes. Here, the initial cracks propagate towards the perimeter parts and the crest of the west main semidome. Because of the extreme cracks over the middle part of the west main semidome, it collapses. At the collapsed stage, both the middle part and the crest of the west main semidome have cracks, but they initiate from the secondary semidomes. The west main semidome collapses before the east one at both cases, because the crack propagation there is faster. This is most probably caused by the asymmetry of the model.

### *The Main Dome*

At load factor 0.8, both tension and compression stresses occur at the top surface of the main dome, while their value are in the same range with those obtained for M1 and M2 (Figure 5.1-11). However, the tension stresses develop at a wider region in the middle part of the main dome in the circumferential direction, as compared with the previous models. Here compression stresses occur at the apex in the east-west direction and at its perimeter randomly. Stress distribution changes slightly until the collapse load factor (Figures 5.1-11 and 5.1-12).

The tension stresses of the main dome reach to the value of 0.66 MPa at the collapse load factor. Therefore, no crack is observed at the main dome during the analysis for this case (Figure 5.1-13).

### *Semidomes*

Stress distribution of the semidomes is almost similar to that of M1 for load factors 0.8 and 1.0 (Figures 5.1-11 and 5.1-12). Tension stresses are concentrated at the connection regions of the main semidomes to the secondary

semidomes and to the secondary arches. Since cracks caused by these tension stresses are taken into account, the tension stresses at the middle part of the main semidomes, especially at the west one, increase for further steps. Finally, the west main semidome collapses in the same load as M1. However, the west main semidome has higher tension stresses than that of M1 at the collapse load factor (Figure 5.1-13).

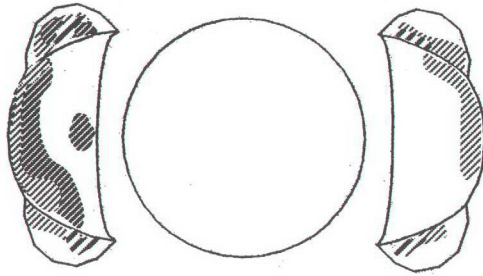
### *Arches, Pendentives and Piers*

Stress distribution through M3 is almost the same as M1 with respect to the main arches, pendentives, and piers. The highest tension stress is observed at the pendentives. These tension stresses propagate through the arches and top of the main piers for the higher load factors. However, they do not exceed the value of 0.79 MPa.

Higher tension stresses occur at the inner surfaces of the east and west main arches relative to the north and south arches at the beginning. These tension stresses cause more cracks for following steps. Although these cracks occur through the main arches, they do not propagate as much as those at the west main semidome and they do not affect the stability of the structure.

Cracks also occur at the secondary arches, where the main semidomes are connected, at load factor 1.2 and these cracks propagate at a wide region until the west main semidome collapses (Figure 5.1-13).

Some more cracks are also observed at some regions through the main piers at the beginning of the analysis, however, they are limited in very small regions and stop after a few iterations.



	Initial Cracks
	Further Cracks
	Final Cracks

Figure 5.1-10 The Crack Propagation through M3 for the Collapse Load Factor,  $\lambda=1.2$

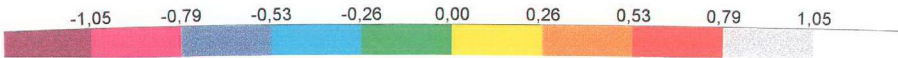
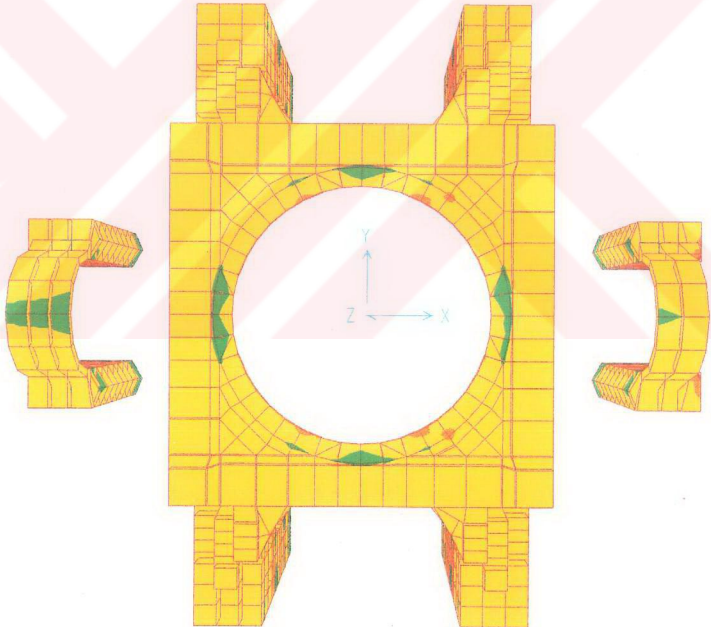
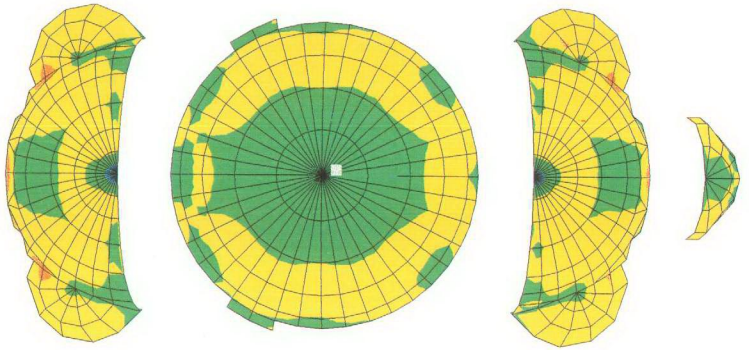


Figure 5.1-11 The Maximum Principal Stress Distribution through M3,  $\lambda=0.8$ , (MPa)



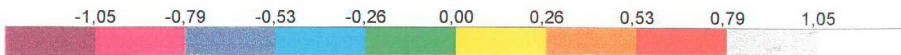
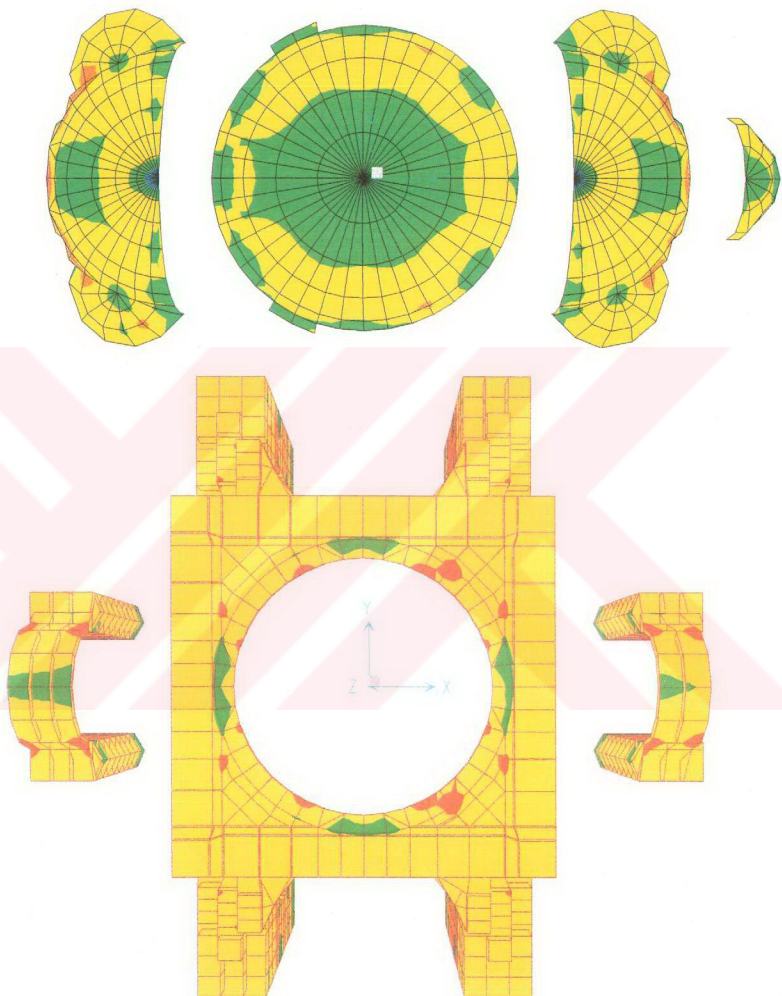


Figure 5.1-12 The Maximum Principal Stress Distribution through M3,  $\lambda=1$ , (MPa)

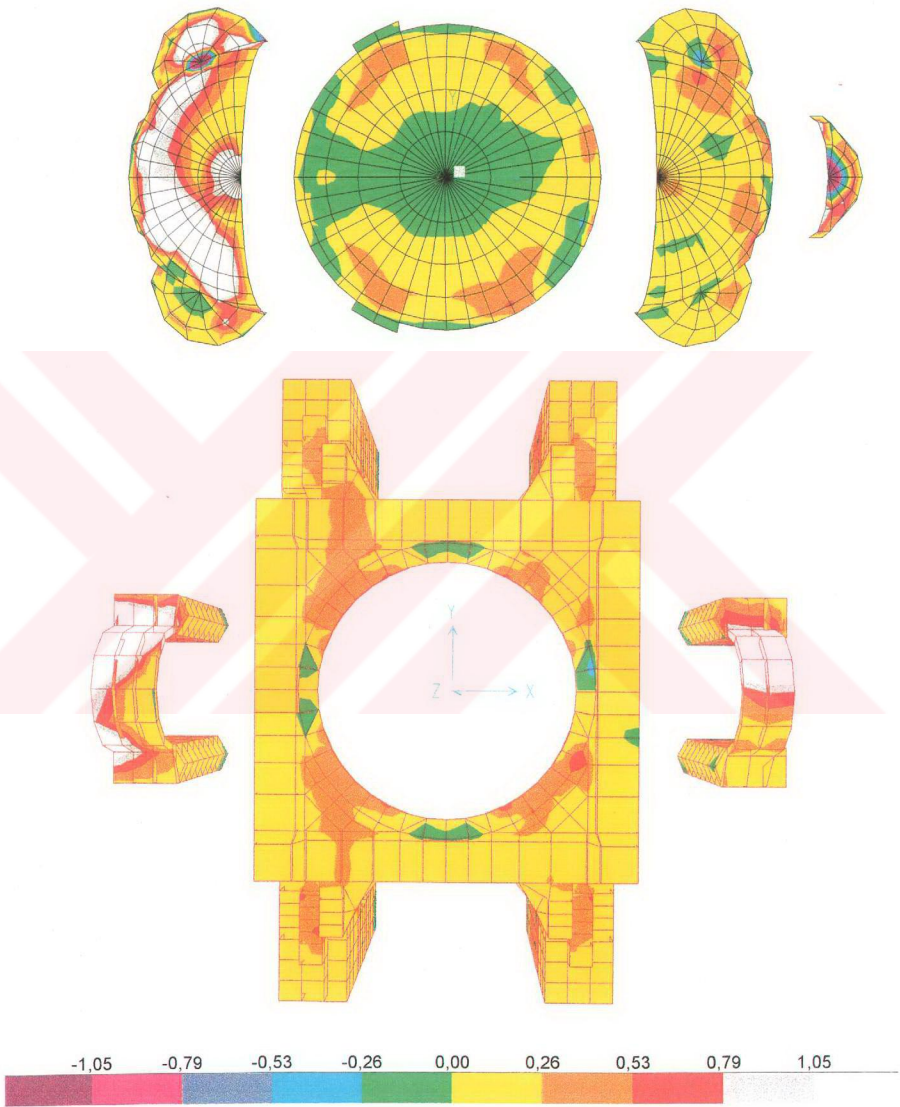
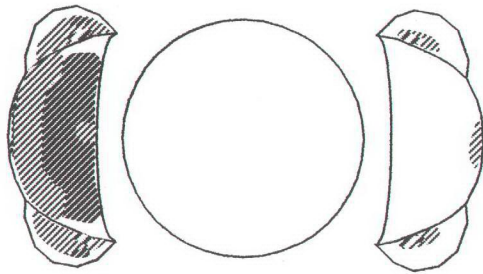
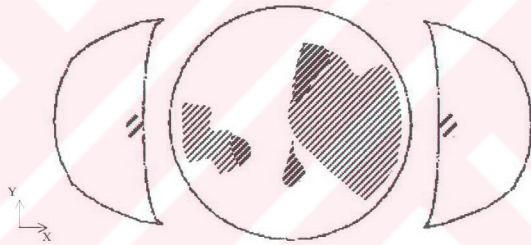


Figure 5.1-13 The Maximum Principal Stress Distribution through M3,  $\lambda=1.2$ , (MPa)

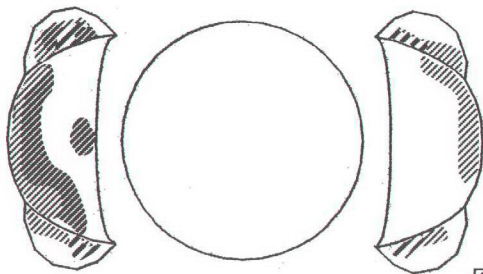




(a) M1



(b) M2



(c) M3




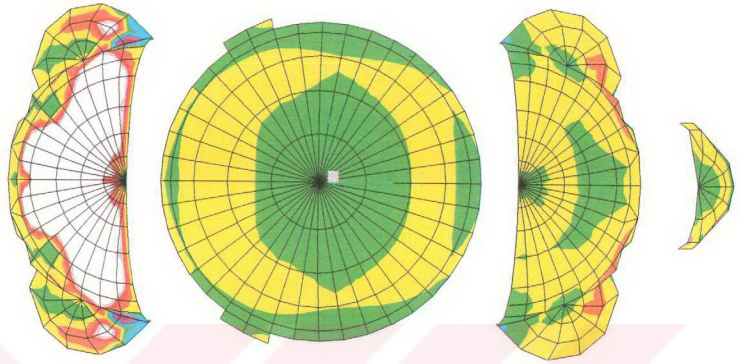
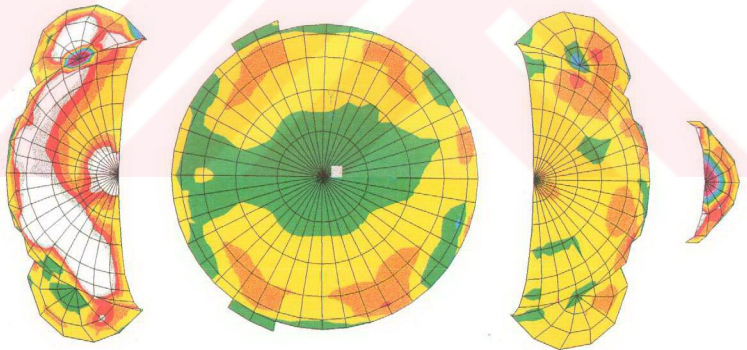
	Initial Cracks
	Further Cracks
	Final Cracks

Figure 5.1-14 The Crack Propagation through M1, M2, and M3 for the Static Analysis



M1



M3

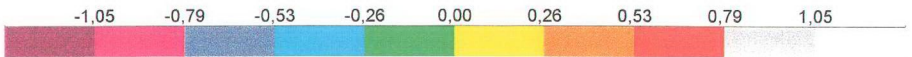


Figure 5.1-15 The Collapse Conditions for M1 and M3 for the Static Analysis (MPa)

#### 5.1.4. Static Analysis of the Fourth Model

As another alternative, M4, a ring is placed between the top of the windows and the main dome and its effect on the crack propagation, in other words, on the collapse behaviour, is investigated using the Load Increment Method. Same as M1 and M3, cracks are imposed on the model using the Smearred Crack Modelling Method. In this case, cracks start at the connection regions between the main semidomes and the secondary semidomes, as in M1. Furthermore, the collapse behaviour of the model is also same as M1 under the static loads. This means that the ring does not work efficiently to delay neither the collapse load factor nor the crack propagation. This is because the west main semidome collapses when the stresses of the main dome are smaller than the crack strength limit. Therefore, it can be said that this alternative model does not affect the collapse mechanism of the structure. However, it increases the tension stresses at the main dome slightly because of the displacement restrictions. Since there is not a visible change between the stress distributions of M1 and M4, no figures are given for those of M4. The plot that shows the variation of the vertical displacements at the apex of the main dome versus the load factors is given for all four models considered in this study (Figure 5.1-16).

The displacements are calculated at each step starting with load factor 0.8 until the collapse load factor. In these plots, the horizontal lines show the regions where the cracks propagate. Although the load factor is not increased, the vertical displacement of the structure increases at the steps which cracking occurs. However, these displacements are smaller than those occurring at the increment of the load factor. Since the collapse load factor of the Second Model is the highest among the all models used in this study, the highest displacement is obtained in this model. On the other hand, the values obtained in the First and Fourth Models are almost same.

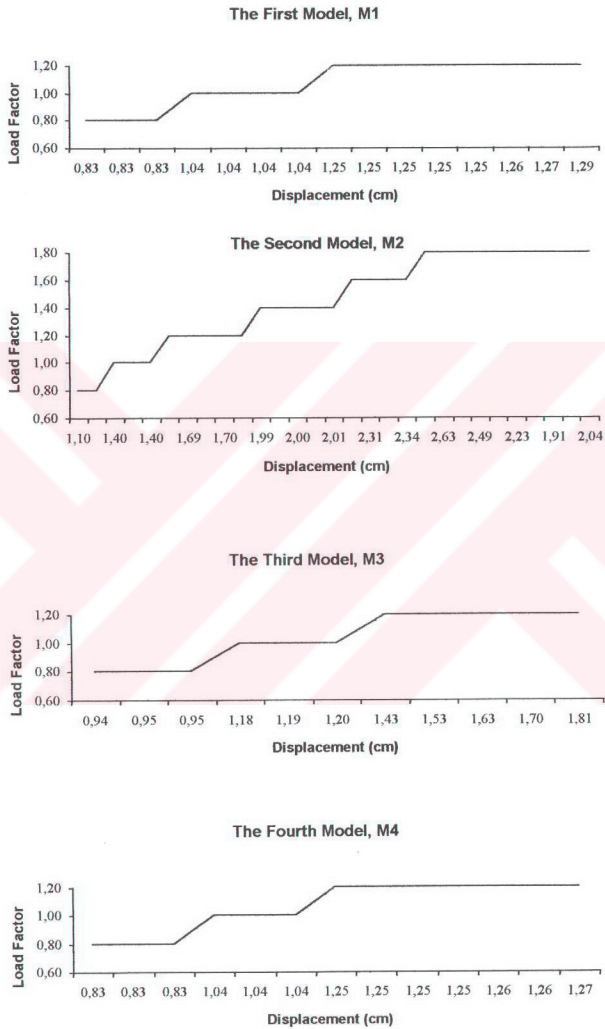


Figure 5.1-16 The Variation of the Vertical Displacement versus Load Factors for M1, M2, M3, and M4

## 5.2. Results of the Spectral Analysis

The First and Third Models are investigated from the spectral point of view. The main purpose of this part of the analysis is to obtain the stress distributions, and hence the critical regions, throughout M1 and M3 at the earthquake accelerations 0.1g, 0.2g, 0.3g and 0.4g, which are applied to the structure in the X and Y-directions, separately. Also, the crack propagation is obtained by using the Acceleration Increment Method, which is based on the Load Increment Method. Cracks are taken into account utilising the Smeared Crack Modelling Method. The Acceleration Increment Method is similar to the static analysis carried out for M1, but this time different assumptions are used for the Smeared Crack Modelling Method as described in Section 4.3.2.

The crack propagation under the effect of accelerations 0.1g, 0.2g, 0.3g and 0.4g in the X-direction is given in Figures 5.2-3 a, b, c and d. The crack propagations for the same accelerations in the Y-direction, are not given in the figure, because the cracked regions are not wide.

$S_{11}$  and  $S_{22}$  stress resultants of M1 under the effects of accelerations 0.1g, 0.2g, 0.3g and 0.4g in the X and Y-directions separately are given in Figures 5.2-4 to 5.2-13. For M3, only the stress resultants of acceleration 0.4g in the X and Y-directions separately are given in Figures 5.2-14 to 5.2-17, since there is no important differences among the results for other accelerations. It must be noted that the stress distributions given in the figures belong to the steps in which crack propagation stops. Therefore, the regions where the tension stress exceeds the crack tension strength limit are not given in figures.

### 5.2.1. Spectral Analysis of the First Model

#### A. Earthquake in the X-Direction

Before starting the spectral analysis, cracks caused by the self-weight of the model are obtained. By doing so, the dynamic vulnerability of the structure while it includes the cracks under its self-weight can be obtained at the end of



the spectral analysis. The static analysis is started with load factor 0.8, since the cracks develop first at this load value. In this case also, the initial cracks start at the connection regions of the main semidomes to the secondary semidome. After decreasing the modulus of elasticity of the cracked elements, the analysis is continued with the same load factor. When the cracks stop to propagate, the load factor is increased to the value of 1. Some more cracked elements are determined at the region mentioned before for this load factor. After taking the cracks into account, the procedure is carried out until the development of the cracks stop at  $\lambda=1$ . Afterwards, the spectral accelerations are applied to the structure. At the first acceleration, 0.1g is applied to the structure but in this case the tension stresses at some regions of the model are 5 ~ 6 times higher than the crack tension strength limit. Since this is not acceptable, the starting value is chosen as 0.04g. For this value, no additional crack is observed. Therefore, the value is increased to the value of 0.06g where some minor cracks start to occur. After imposing these cracks on the model, the model is analysed again for the same acceleration value, 0.06g. When no more crack is observed for the value of 0.06g, the acceleration is increased for the next step. This procedure is followed until the crack propagation stops at acceleration 0.4g. The acceleration is not increased beyond this value.

At acceleration 0.1g, the cracks at the secondary semidomes continue to propagate (Figure 5.2-3a), and additional cracks observed under its self-weight occur at the crests of the main semidomes and the connection region of the main semidomes to the secondary arches. These cracks continue to propagate for acceleration 0.2g (Figure 5.2-3b). At acceleration 0.3g, they cover all over the secondary semidomes, and the cracks at the crests of the main semidomes propagate through their middle parts (Figure 5.2-3c). The structure does not collapse even at acceleration 0.4g. Despite the fact that all the elements at the secondary semidomes and almost all the elements at the main semidomes have cracks (Figure 5.2-3d). This is because the most of the cracks do not propagate totally throughout the depth of the elements. Hence, these elements can still carry loads because the crack depth is taken into account (see Section 4.3.2).

The increase of the horizontal displacement at the apex of the main dome in the X-direction versus the accelerations is given in Figure 5.2-1.

Cracks, which are imposed on the model by decreasing the elasticity moduli to be able to consider the crack depths, cause an increase in the period of the model. This is because the structure becomes softer. Consequently, the higher periods are obtained for the higher accelerations (Figure 5.2-2). The period of M1 starts with 0.51 second for acceleration 0.1g and increase to 0.57, 0.81 and finally to 1.04 second for accelerations 0.2g, 0.3g, and 0.4g, respectively. The results of the analysis are discussed in detail at the following for each structural part.

#### ***The Main Dome***

*S<sub>11</sub> Stress Resultants:* Both tension and compression stresses develop at the main dome for acceleration 0.1g. Tension stresses are observed in the circumferential direction on the northern and southern parts of the main dome. Nevertheless, they do not exceed the crack strength limit. Maximum compression stress values are around 0.53 MPa, whereas tension stresses are around 0.26 MPa at the same acceleration (Figure 5.2-4).

Tension stresses spread over a wider area for higher accelerations (Figures 5.2-5 to 5.2-7). However, compression stresses develop at the apex of the main dome in the east-west direction reaching the perimeter at acceleration 0.4g, are observed. No crack is observed at the main dome until acceleration 0.4g (Figure 5.2-7). However, cracks start to occur at this acceleration, and propagate at following steps where they spread widely over the northern and southern parts of the main dome. After imposing the cracks at these regions on the model, the tension stresses at their neighbouring elements increase and the highest tension stress reaches to 0.95 MPa, when the crack stop at acceleration 0.4g.

*S<sub>22</sub> Stress Resultants:* Almost all the surface of the main dome is covered by compression stresses except for two small regions on its eastern and



western sides at acceleration 0.1g (Figure 5.2-8). In addition, more tension regions occur at the north and south of the main dome at acceleration 0.2g (Figure 5.2-9). These tension stresses develop over the surface of the main dome with except the apex and some perimeter parts at accelerations 0.3g and 0.4g (Figures 5.2-10 and 5.2-11). However, their values reach only to 0.5 MPa at the main dome even at acceleration 0.4g, when the cracks stop to propagate.

### *Semidomes*

*S<sub>11</sub> Stress Resultants:* Tension stresses develop along almost all the surface of the secondary semidomes at acceleration 0.1g (Figure 5.2-4). After taking these cracks into account, tension stresses progress through the main semidomes at further steps. Since the crests of the main semidomes are also cracked at acceleration 0.1g, tension stresses spread further from this region to middle parts (Figures 5.2-5 to 5.2-7). The development of the tension stresses at the main semidomes becomes faster at the following acceleration values. At acceleration 0.4g, most of the finite elements at the main semidome are cracked. Hence, they cannot carry loads as much as the uncracked elements. On the other hand, the tension stresses at the west semidome are higher than those at the east one as shown in Figure 5.2-7. This is because the elements at the west semidome are not cracked as many as those of the east semidome. Although all the elements of both semidomes have cracks for acceleration 0.4g, the structure does not collapse yet.

*S<sub>22</sub> Stress Resultants:* Tension stresses exceed the crack tension strength limit at the connection regions between the crests of the main semidomes and the main arches, and all over the secondary semidomes at acceleration 0.1g (Figure 5.2-8). At acceleration 0.4g, since the cracks are imposed on the model from the previous accelerations, tension stresses increase at the neighbouring elements of the regions mentioned before and the elements at the main and secondary semidomes are covered mostly by cracks (Figures 5.2-9 to 5.2-11).

### *Arches, Pendentives and Piers*

*S<sub>11</sub> Stress Resultants:* Compression stresses are observed at the top of the key regions of the north and south main arches, while tension stresses develop at the top surface of the main east and west arches, pendentives and some regions at the piers at acceleration 0.1g. (Figure 5.2-4). The highest tensile stresses are around 0.26 MPa. Besides, tension stresses at the inner surface of the key regions of the main arches are around 0.53 MPa.

The tension stresses spread towards the key regions of the north and south main arches. Also, the tension stresses in the adjacent elements of the pendentives increase at accelerations 0.2g and 0.3g and 0.4g (Figure 5.2-5 to 5.2-7). Cracks occur in a very limited region of the main south arch at acceleration 0.3g (Figure 5.2-6). Tension stresses at the other arches do not cause cracks. On the other hand, tension stresses at the piers close to their support regions increase extremely and cause cracks. These tension stresses convert to the compression or decrease at further steps, since cracks at the piers are taken into account.

At acceleration 0.4g, tension stresses are higher than the crack strength limit, and develop over a large area at the north and south main arches, and partially at the other arches. After the effects of these tension stresses are taken into account, tension stresses increase at the adjacent uncracked elements of the main arches. However, there is not a fatal damage at these regions in spite of the large amount of cracks.

Cracks also occur at the secondary arches where they are connected to the main semidomes at acceleration 0.4g, but they propagate slowly. Since they are not the main structural parts, the cracks, which occur due to these stresses, are not given in the figures. However, stress distributions through the secondary arches are given in Figures 5.2-4 to 5.2-7.

*S<sub>22</sub> Stress Resultants:* Tension stresses are observed at the top key regions of the east and west arches, pendentives and piers, and their highest

values are around 0.29 MPa at acceleration 0.1g. The maximum tension stress occurs at the top surface of the north and south main arches, which is 0.38 MPa at acceleration 0.4g. Therefore, these stresses do not cause to collapse even at this acceleration.

As it can be seen in Figures 5.2-4 to 5.2-7 and Figures 5.2-8 to 5.2-11, compression stresses develop at the key regions of the north and south main arches for  $S_{11}$  stresses at acceleration 0.1g (Figure 5.2-4). On the other hand, the compression stresses develop at the key regions of the east and west main arches for  $S_{22}$  stresses at the same acceleration (Figure 5.2-8).

### ***B. Earthquake in the Y-Direction***

The same accelerations are applied to M1 in the Y-direction. To begin with, the acceleration 0.1g is applied to M1 as in the X-direction. In this case, some additional minor cracks occur at the model. After imposing these cracks on the model, and let the new cracks propagate, the acceleration is increased to 0.2g, 0.3g and 0.4g. The stress distributions do not change much to show the effect of the earthquake subjected in the Y-direction. Hence, there are not widely propagated cracks to observe. The results of the analysis for  $S_{11}$  and  $S_{22}$  stress distributions are given only for acceleration 0.4g (Figures 5.2.12 and 5.2.13).

### ***The Main Dome and Semidomes***

*S<sub>11</sub> Stress Resultants:* Compression stresses develop all over the surface of the main dome, except for some small regions in the circumferential direction. The values of these tension stresses do not exceed 0.09 MPa even at acceleration 0.4g (Figure 5.2-12).

Both tension and compression stresses develop through the semidomes, while they both are limited with the value of 0.33 MPa.

*S<sub>22</sub> Stress Resultants* Tension stresses are limited with 0.09 MPa even at acceleration 0.4g and they occur only on the east and west sides of the main dome (Figure 5.2-13).

Tension stresses are observed at very small regions at the middle part of the main semidomes and their connection regions with the secondary arches, however their highest values are around 0.62 MPa (Figure 5.2-13). Tension stresses spread in the circumferential direction through the secondary semidomes in their middle part, but their value is limited to 0.13 MPa (Figure 5.2-13).

#### ***Arches, Pendentives and Piers***

*S<sub>11</sub> Stress Resultants:* Tension stresses spread over the east and west main arches, and partially pendentives, which are limited with 0.06 MPa at acceleration 0.4g (Figure 5.2-12). On the other hand, compression stresses occur over the north and south arches. A random stress distribution for tension and compression is observed over the piers, while the maximum tension stresses reach to the value of 0.5 MPa at some parts.

*S<sub>22</sub> Stress Resultants:* The surface of the key regions of the main arches is covered by compression stresses. Their values reach to 1.2 MPa at the east and west main arches, which is lower than the crack compression strength limit. At the other regions of the north and south arches, tension stresses are around 0.2 MPa (Figure 5.2-13) and tension stresses occurring through the piers do not exceed the value of 0.3 MPa.

### DISPLACEMENT VERSUS ACCELERATIONS

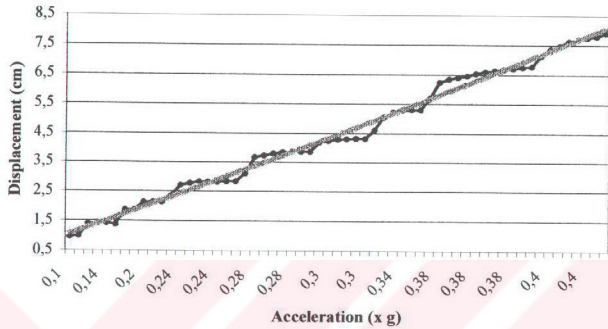


Figure 5.2-1 The Variation of the Horizontal Displacements in the X-direction at the Apex of the Main Dome versus the Accelerations for M1 under the Earthquake in the X-Direction

### PERIOD VERSUS ACCELERATIONS

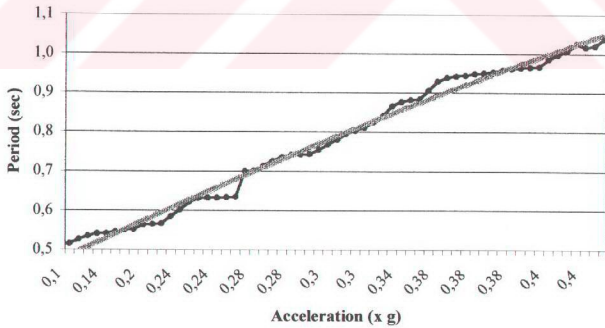
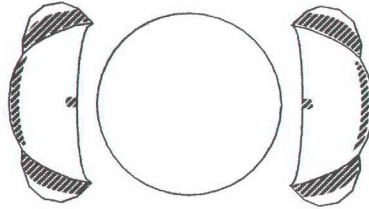
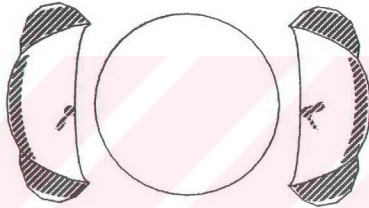


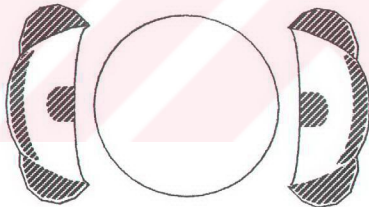
Figure 5.2-2 The Variation of the Period versus the Accelerations for M1 under the Earthquake in the X-Direction



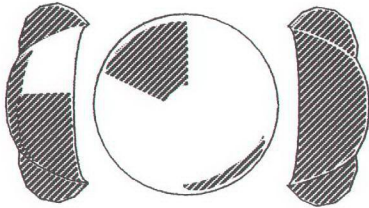
(a) 0.1g



(b) 0.2g



(c) 0.3g



(d) 0.4g



Figure 5.2-3 The Crack Propagation through M1 for the Spectral Accelerations



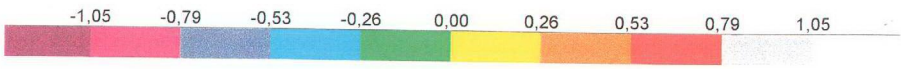
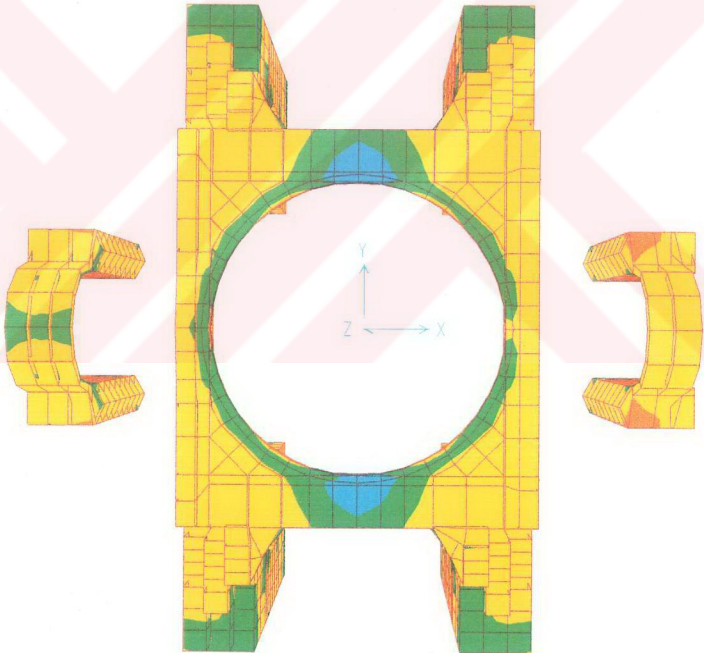
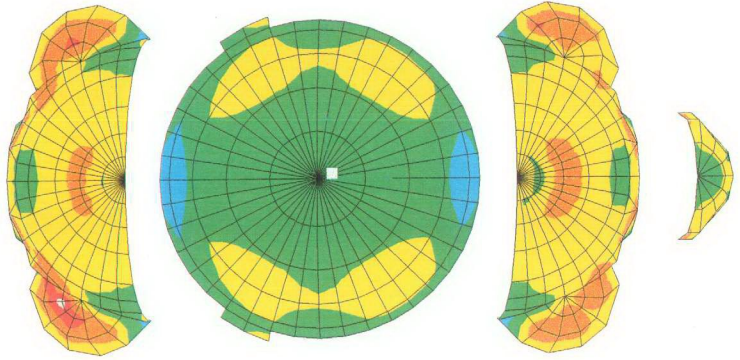


Figure 5.2-4  $S_{11}$  Stresses of M1 for Acceleration 0.1g in the X-Direction, (MPa)



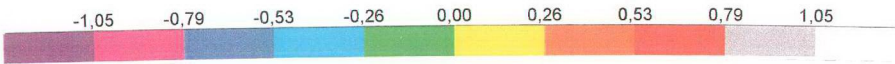
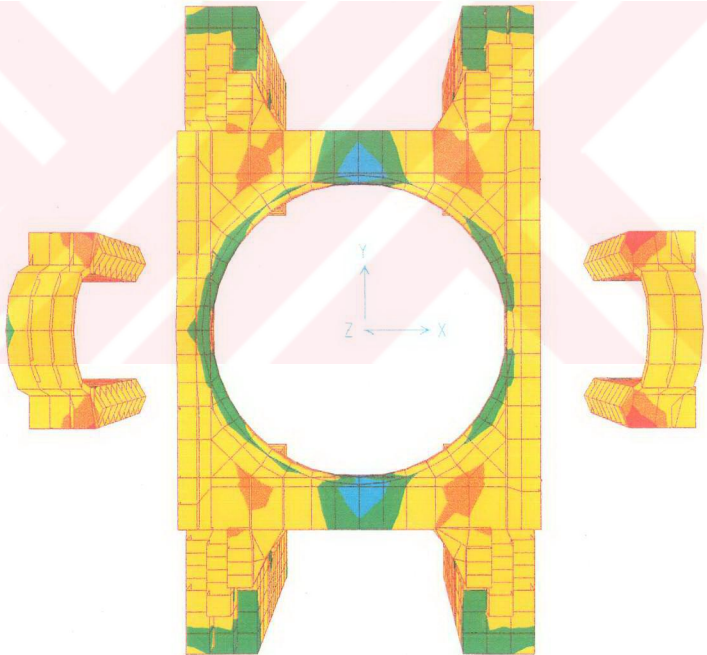
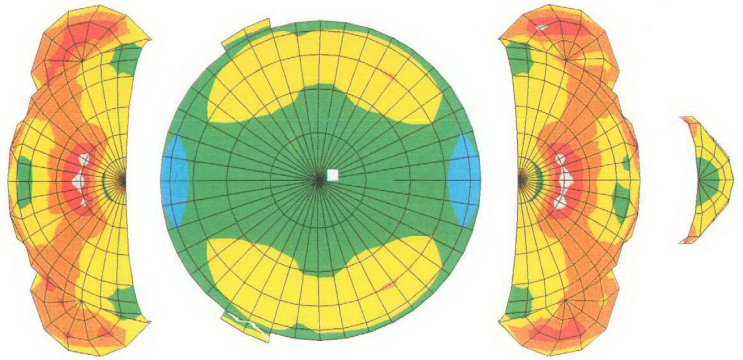


Figure 5.2-5  $S_{11}$  Stresses of M1 for Acceleration 0.2g in the X-Direction, (MPa)

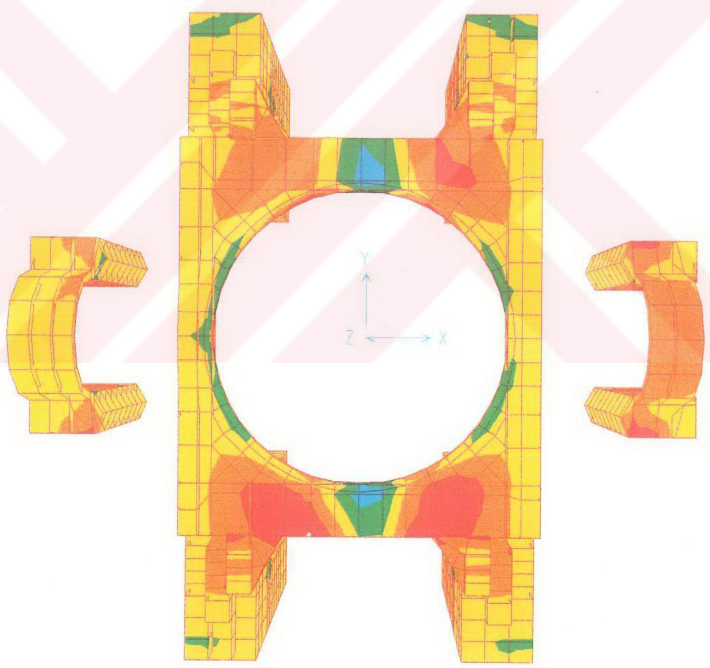
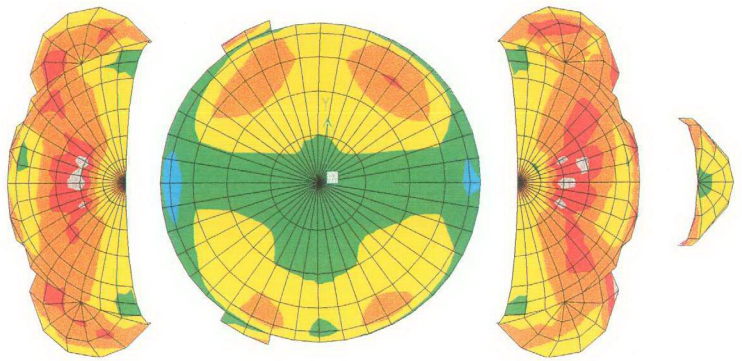


Figure 5.2-6  $S_{11}$  Stresses of M1 for Acceleration 0.3g in the X-Direction, (MPa)

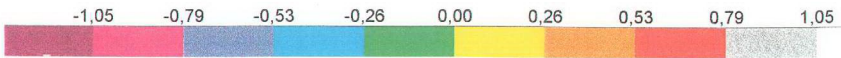
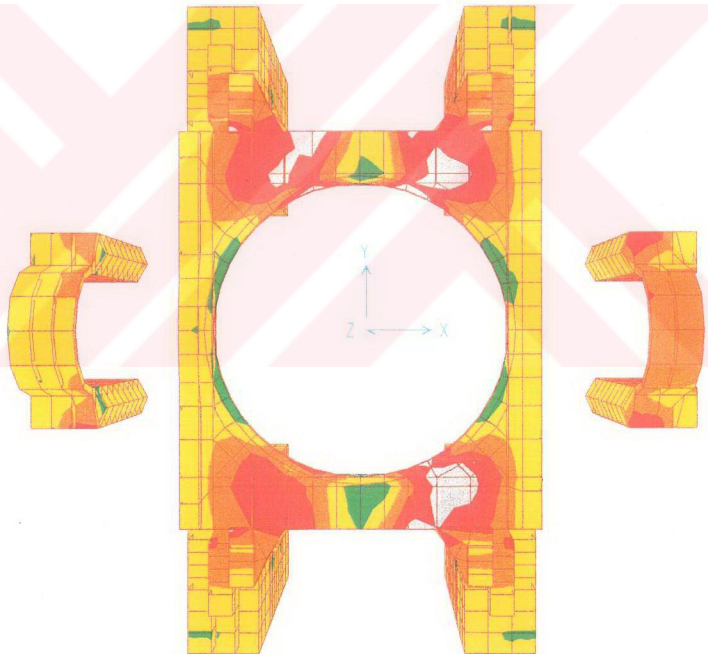
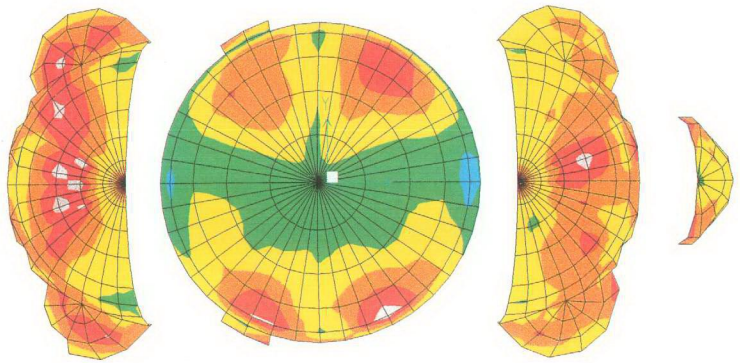


Figure 5.2-7  $S_{11}$  Stresses of M1 for Acceleration 0.4g in the X-Direction, (MPa)

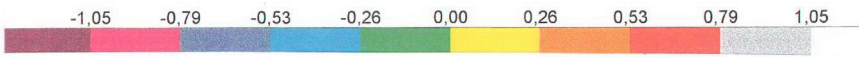
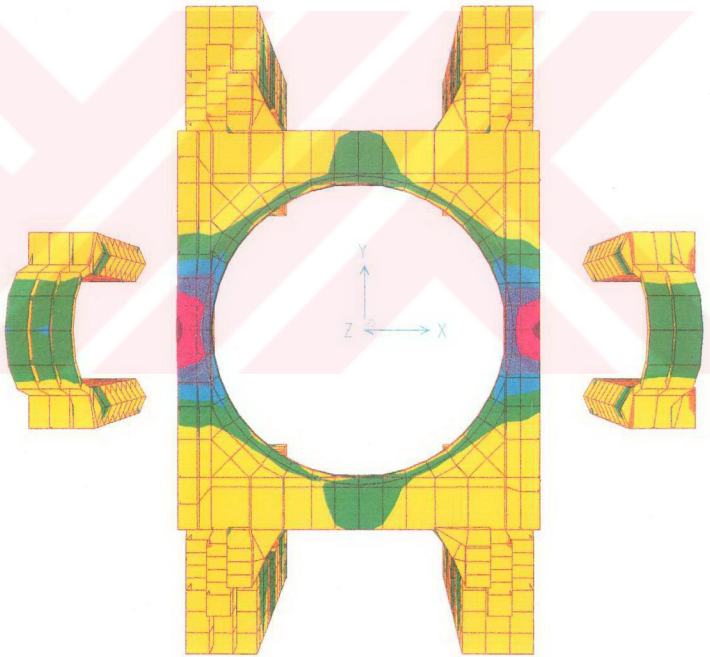
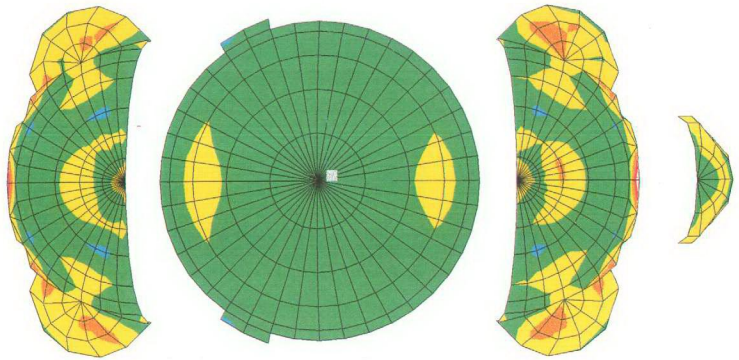


Figure 5.2-8  $S_{22}$  Stresses of M1 for Acceleration 0.1g in the X-Direction, (MPa)



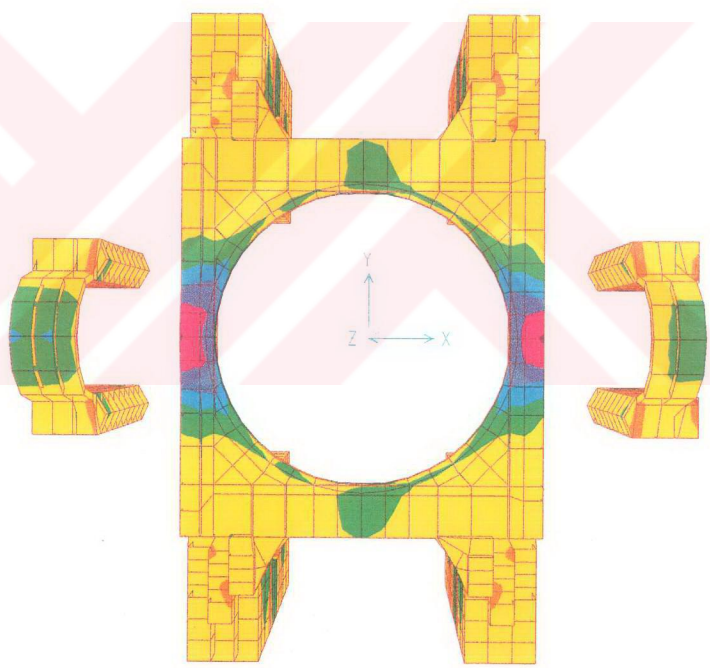
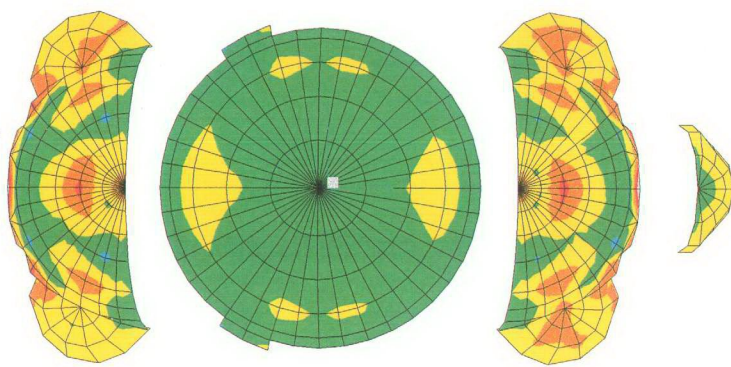


Figure 5.2-9  $S_{22}$  Stresses of M1 for Acceleration 0.2g in the X-Direction, (MPa)

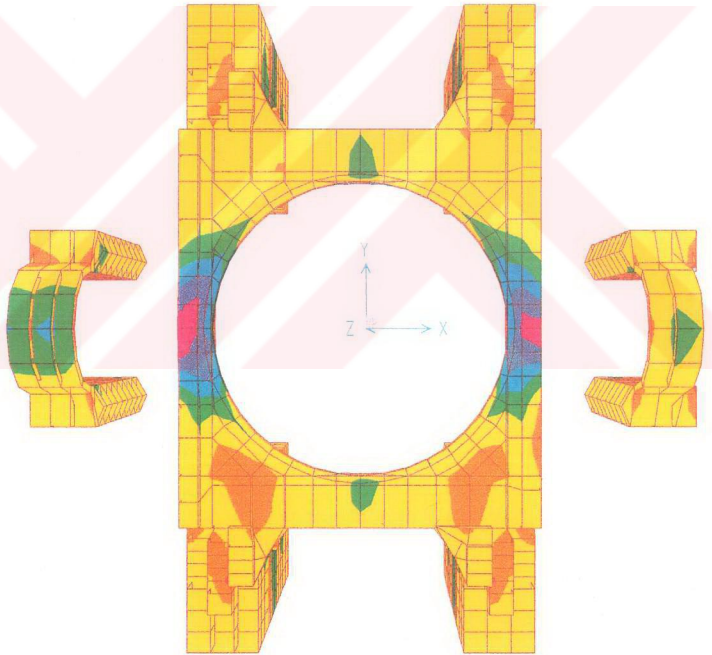
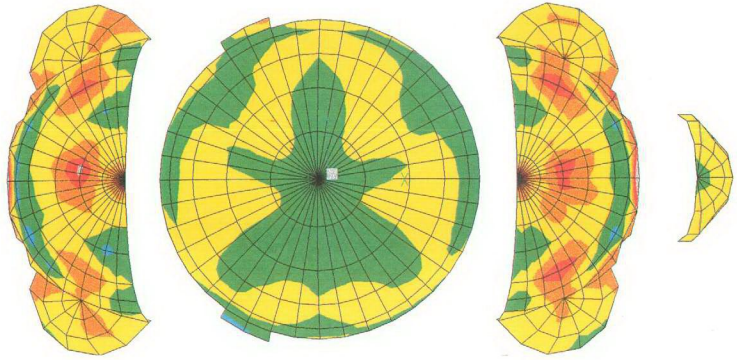


Figure 5.2-10  $S_{22}$  Stresses of M1 for Acceleration 0.3g in the X-Direction, (MPa)

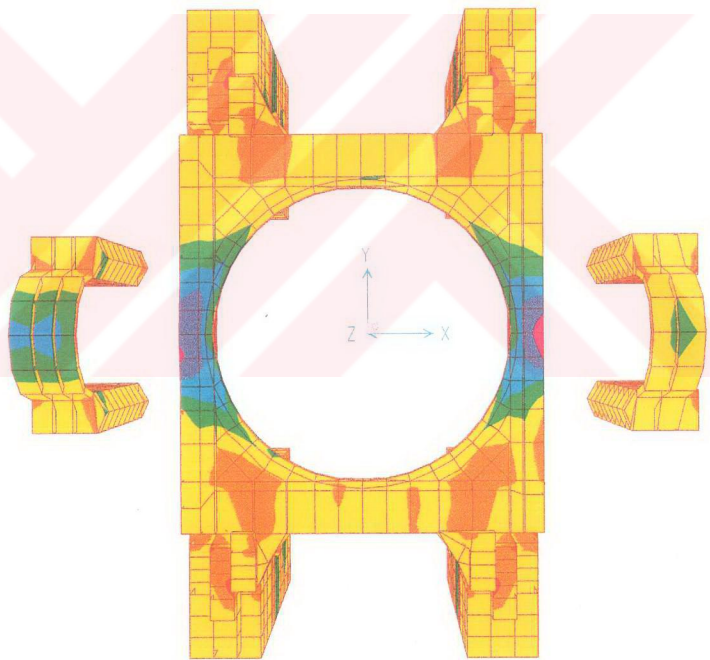
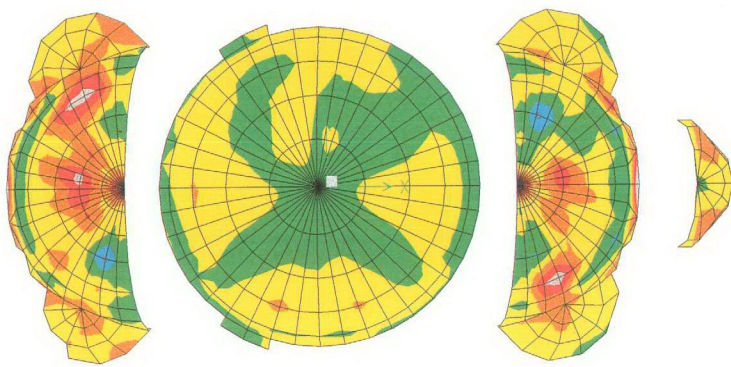


Figure 5.2-11  $S_{22}$  Stresses of M1 for Acceleration 0.4g in the X-Direction, (MPa)



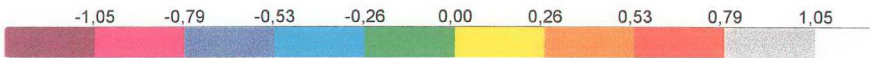
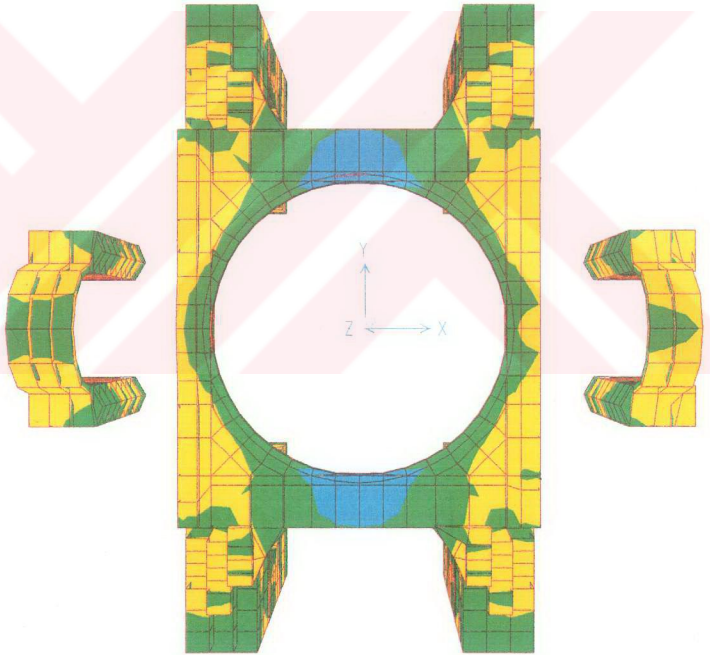
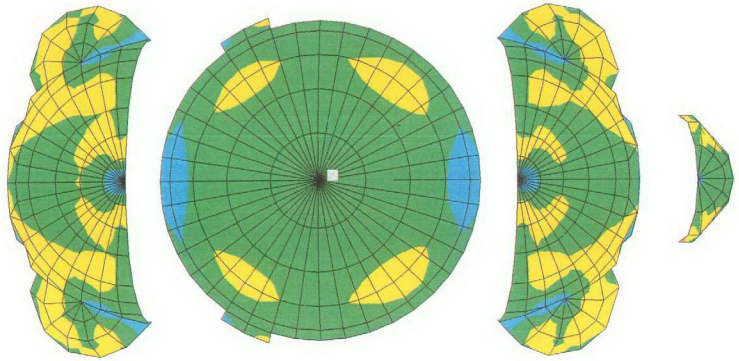


Figure 5.2-12  $S_{11}$  Stresses of M1 for Acceleration 0.4g in the Y-Direction, (MPa)

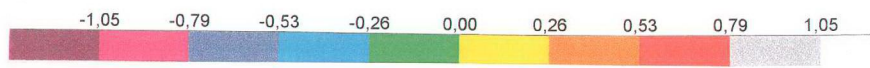
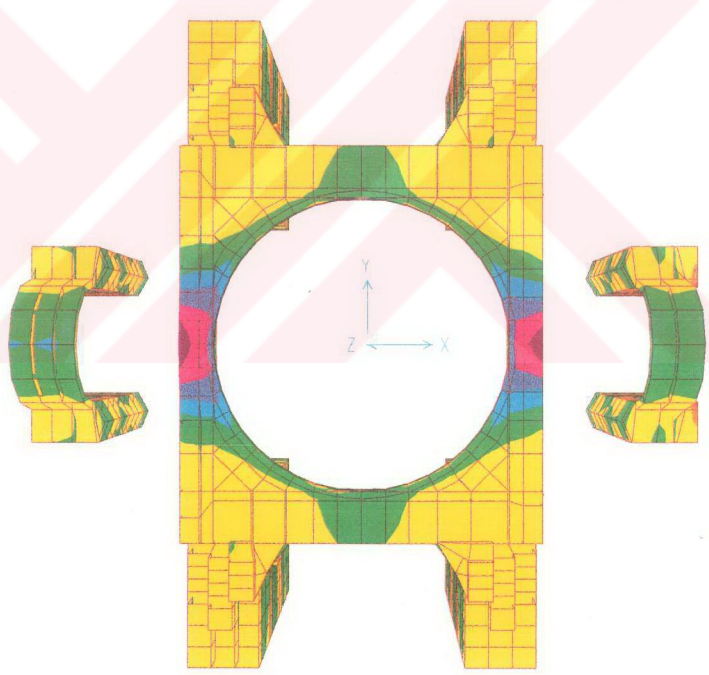
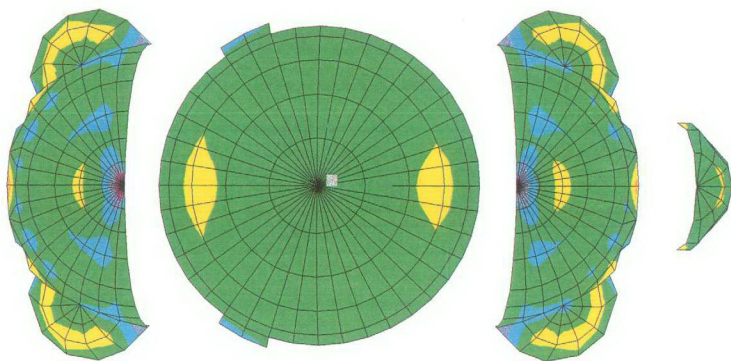


Figure 5.2-13 S<sub>22</sub> Stresses of M1 for Acceleration 0.4g in the Y-Direction, (MPa)

### 5.2.2. Spectral Analysis of the Third Model

The Third Model, M3, is also investigated from the spectral point of view to observe the effect of the strong arches instead of the weak main east and west arches. As seen in the previous analysis, the cracks are observed by using the Acceleration Increment Method. The cracks are taken into account by utilising the Smearred Crack Modelling Method for the assumption as in the spectral analysis carried out for M1 (Section 4.2.2).

$S_{11}$  and  $S_{22}$  stress resultants of the model are given only for acceleration 0.4g, which is subjected to the model in the X and Y-directions separately (Figures 5.2-14 to 5.2-17), because there is not much difference among the other stress resultants.

In this case, the period of the model is calculated as 1.55 second at accelerations 0.1g. Since no widely propagated cracks are observed in this model, the period of the model does not change even at acceleration 0.4g.

#### A. Earthquake in the X-Direction

*S<sub>11</sub> Stress Resultants:* The  $S_{11}$  stress distribution of the model at acceleration 0.4g is shown in Figure 5.2-14.  $S_{11}$  stress distributions of the domes of M1 and M3 (Figures 5.2-7 and 5.2-14) are given again in Figure 5.2-18 together to compare the effect of the stronger arches on the dynamic behaviour. In this case, a few cracks occur under the self-weight of the structure where the secondary semidomes are connected to the main semidomes. After taking these cracks into account, their propagation stops and no other crack is observed even at acceleration 0.4g. The maximum tension stress is 0.56 MPa, which occurs at the connection region of the main semidomes to the secondary arches and at the secondary semidomes (Figure 5.2-14 or 5.2-18). However, when the crack propagation stops at acceleration 0.4g, the maximum tension stresses of M1 is around 0.97 MPa at the secondary semidomes. This value is very close to the crack strength limit. (Figure 5.2-18). The cracks cover all the surfaces of the secondary semidomes and almost all the surfaces of the main semidomes and partially the north and south regions of the main dome in M1.

Tension stresses at the north and south arches do not increase as much as those obtained in M1. The maximum tension stress is 0.26 MPa even at acceleration 0.4g (Figure 5.2-14).

The stress distributions of M1 and M3 are given only for the domes to compare the effect of the stronger arches on the dynamic behaviour (Figure 5.2-18) This is because, a widely crack propagation is not observed through the main arches, pendentives and piers with respect to the domes.

*S<sub>22</sub> Stress Resultants:* From the same reason mentioned for *S<sub>11</sub>* stress resultants, the stress distributions of the domes in Figures 5.2-11 and 5.2-15 are given again in Figure 5.2-19 together. As can be seen from the figure, the tension stresses of M3 are much lower than those of M1.

#### **B. Earthquake in the Y-Direction**

Stress distributions of M3, when the earthquake is applied in the Y-direction, are almost the same as those in the X-direction. The results of the analyses, for *S<sub>11</sub>* and *S<sub>22</sub>* stress distributions are given in Figures 5.2-16 and 5.2-17.

*S<sub>11</sub> Stress Resultants:* Tension stresses occur at some middle parts of the main dome, however, their maximum value reaches only to 0.4 MPa.

Tension stresses occur at the main semidomes where they connect to the secondary arches, however, they neither propagate more nor exceed the crack strength limit even at acceleration 0.4g. They reach to the value of 0.56 MPa.

The key regions of the main arches are covered with compression stresses. On the other hand, tension stresses develop at the inner surfaces of the key regions of the north and south main arches. Nevertheless, their highest value is only 0.34 MPa.

*S<sub>22</sub> Stress Resultants:* Compression stresses spread over a wider region through the main dome relative to that of tension stresses. The maximum tension stress is 0.2 MPa.

Tension stresses increase along the connection regions of the main semidomes to the secondary arches. Nevertheless, their highest value, 0.56 MPa, is under the crack strength limit. Tension stresses of the secondary semidomes in circumferential direction, has the value of only 0.15 MPa.

Different from  $S_{11}$  stresses, compression stresses are concentrated on the east and west main arches instead of the north and south ones. The main arches, pendentives and piers are all stable even at acceleration 0.4g. The maximum tension stress at the pendentives is around 0.17 MPa, and the maximum tension stress that occurs at the north and south arches is 0.34 MPa at this acceleration.



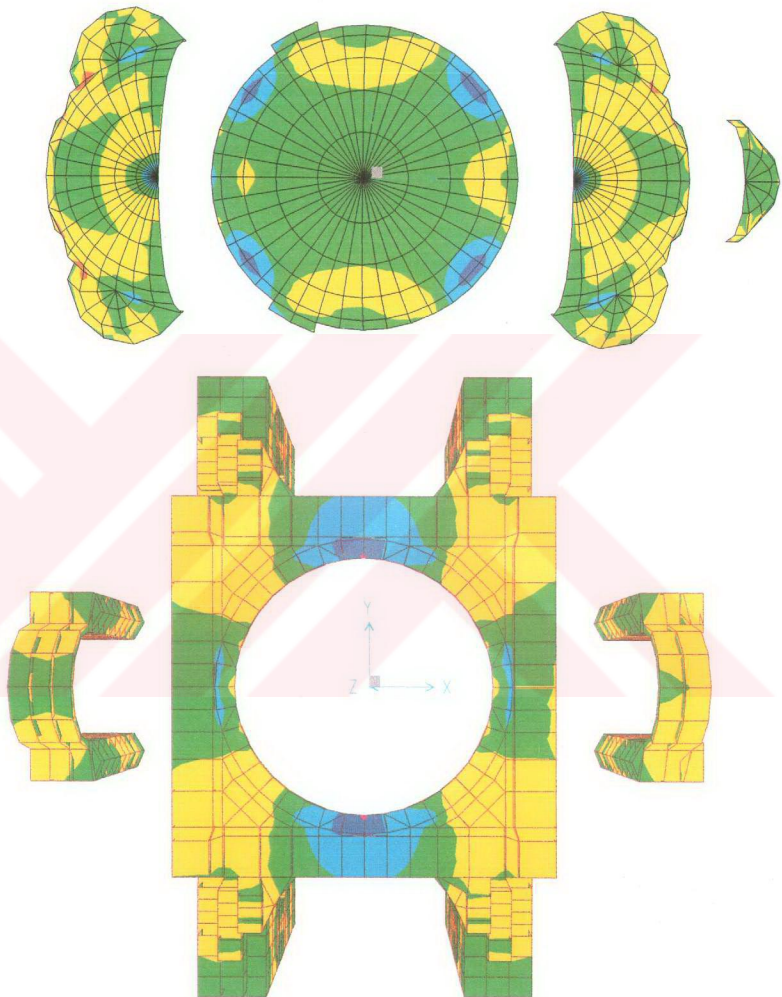


Figure 5.2-14  $S_{11}$  Stresses of M3 for Acceleration 0.4g in the X-Direction, (MPa)



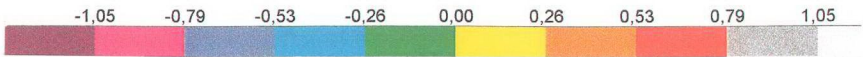
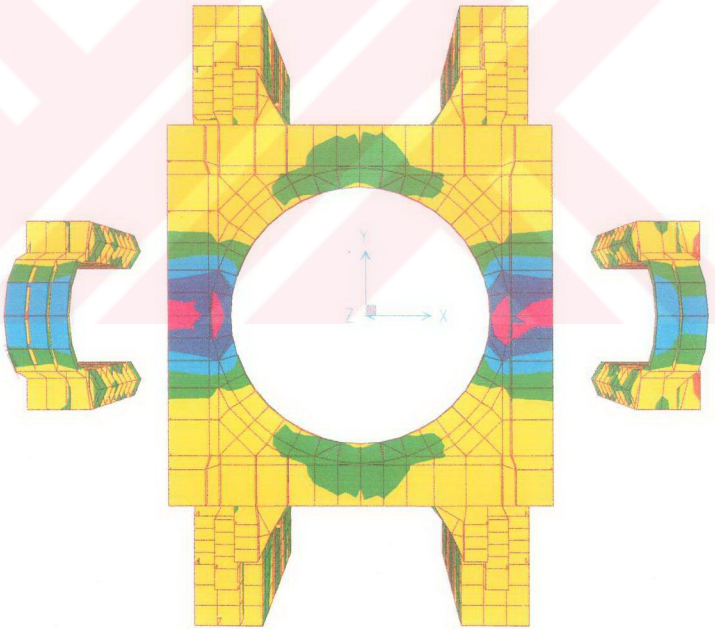
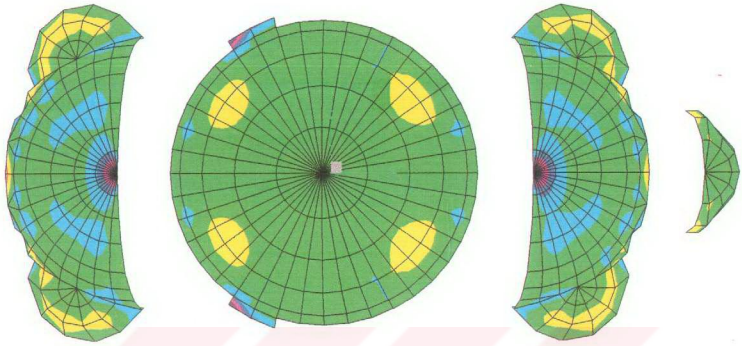


Figure 5.2-15  $S_{22}$  Stresses of M3 for Acceleration 0.4g in the X-Direction, (MPa)

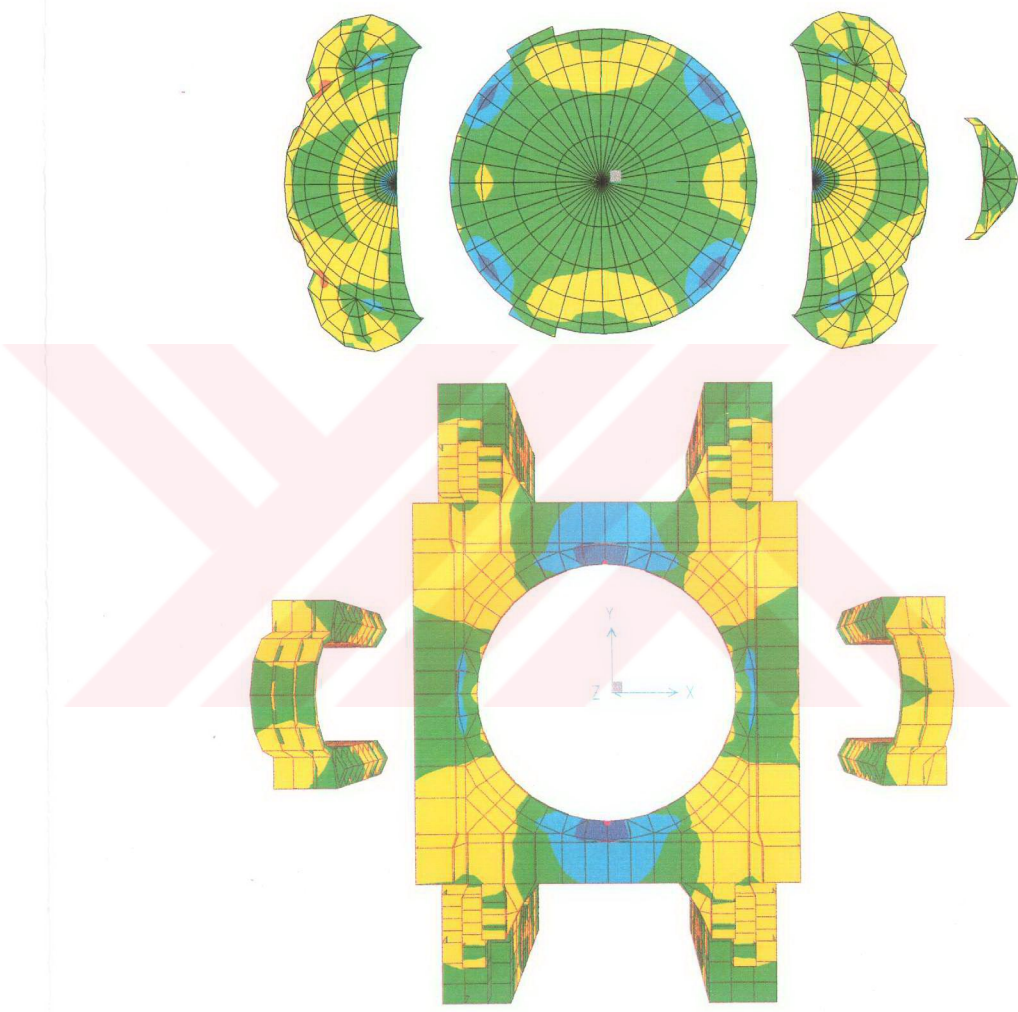


Figure 5.2-16  $S_{11}$  Stresses of M3 for Acceleration 0.4g in the Y-Direction, (MPa)

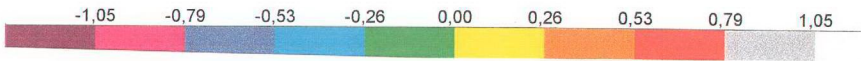
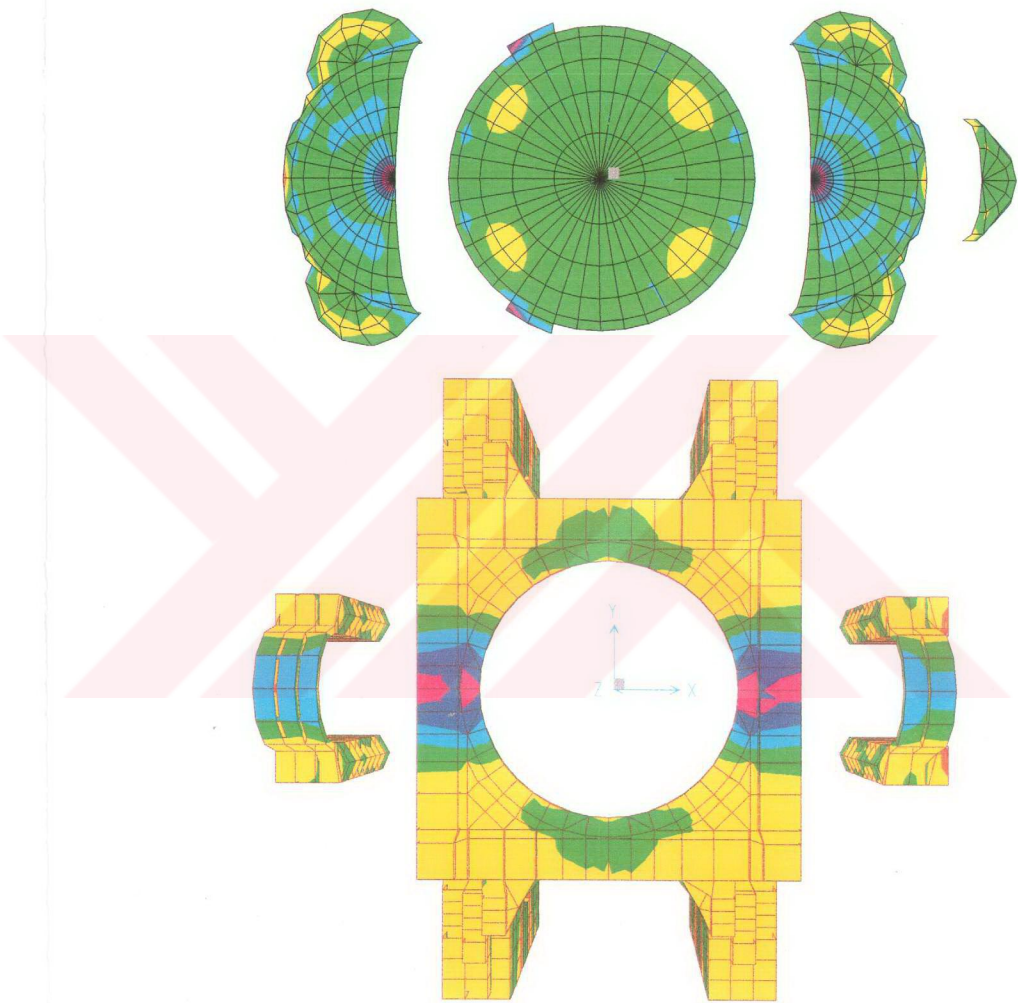
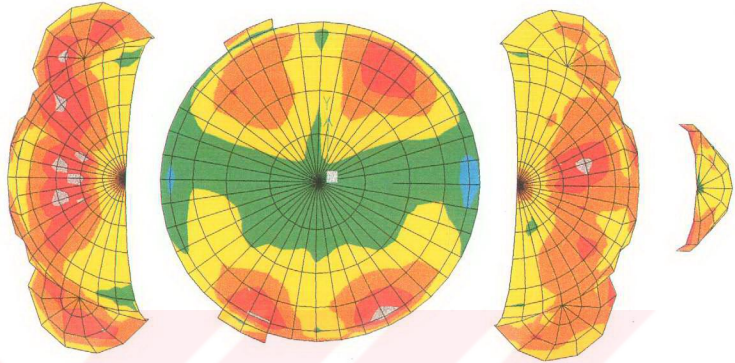
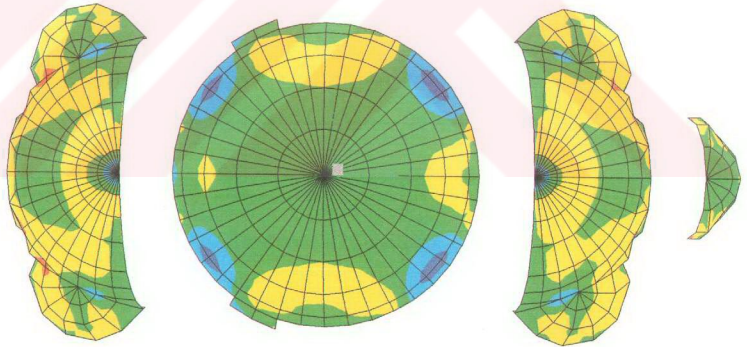


Figure 5.2-17  $S_{22}$  Stresses of M3 for Acceleration 0.4g in the Y-Direction, (MPa)



M1



M3

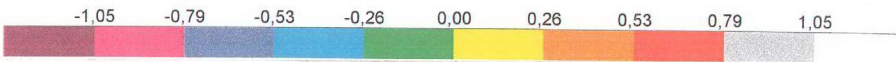
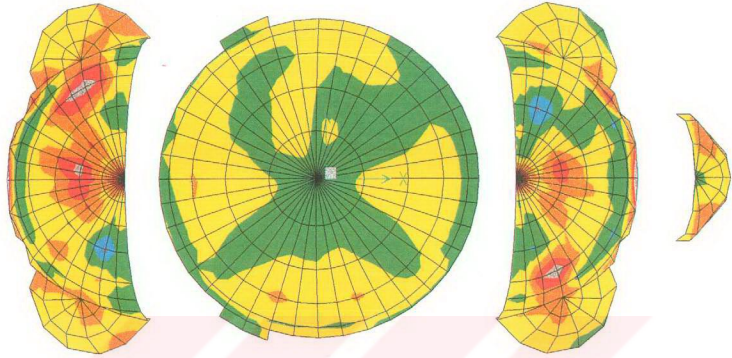
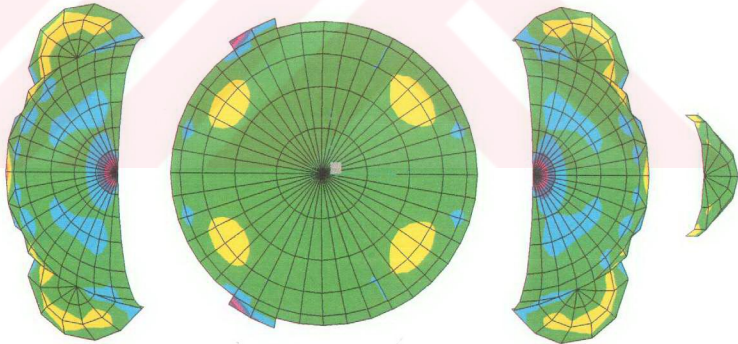


Figure 5.2-18  $S_{11}$  Stresses of M1 (upper one) and M3 for Acceleration 0.4g in the X-Direction, (MPa)





M1



M3

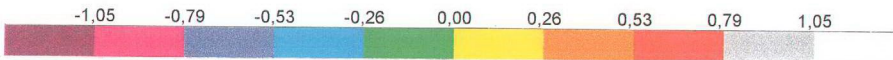


Figure 5.2-19  $S_{22}$  Stresses of M1 (upper one) and M3 for Acceleration 0.4g in the X-Direction, (MPa)

# CHAPTER 6

## DISCUSSION OF THE RESULTS AND CONCLUSIONS

The analyses carried out for Hagia Sophia in this study are divided into two parts. At the first part, crack propagation through the structure is investigated considering four computational models. These are;

- The First Model, M1, the whole structure
- The Second Model, M2, a smaller version of the first one
- The Third Model, M3, the first alternative model created in this study. In this model, the size of the east and west arches is increased to be equal to the size of the north and south arches.
- The Fourth Model, M4, the second alternative model created in this study. In this model, a steel ring is placed between the top of the windows and the main dome.

The First Model taken from the Kandilli Earthquake and Observatory Centre, was originally developed at the Princeton University. It was revised with respect of the material properties according to recent studies. The Model is composed of the main and the secondary load bearing parts. The Second Model is obtained from the first one by letting the secondary load bearing parts out of consideration, i.e. the Second Model includes only the main load bearing parts. The first alternative model M3 is created to investigate the effect of the main strong arches on the collapse behaviours of the structure under static and dynamic loads, whereas the second alternative model M4 is created to investigate the effects of a steel ring along the base of the main dome.

The effect of the crack propagation at the models on the collapse behaviour is investigated by using the Load Increment Method under static loading. For modelling



the cracks, two methods are used, namely the Smeared Crack Modelling and the Discrete Crack Modelling Methods.

The crack propagation at the First Model is obtained using the Load Increment Method. The cracks developing at each increment are introduced to the model using the Smeared Crack Modelling Method in the following step. Doing so, the collapse behaviour of the model and the collapse load value are obtained until failure. In this model, the initial cracks start at the secondary semidomes close to their connection region with the main semidome. Then, these cracks propagate through the main semidome. At the same time, new cracks develop at the crests of the main semidome with increasing load. These cracks propagate towards the perimeter of the main semidome. Finally the west main semidome collapses. From these observations, it can be concluded that the thinner secondary semidomes have major effect on both the collapse load and the collapse behaviour of the structure. The reason of cracking to start at the connection region of the semidomes is the fact that the thickness of the secondary semidomes is almost as half as that of the main semidomes. Since the structure is not fully symmetrical, the west semidome collapses before the east one at load factor 1.2. The additional secondary semidome at the east part of the structure effects the asymmetry. Another reason for the asymmetric failure is the effect of some restorations included in the model, such as the higher west arch, four blinded windows at the west, and asymmetric ribs at the west side of the main dome. All these effects change the symmetry of the model with respect of the north-south axis.

The Load Increment Method is used also for the Second Model to observe the crack propagation, whereas this time the Discrete Crack Modelling Method is considered. This method is chosen for the Second Model, which has the smallest number of finite elements among the models considered in this study. Because the method requires the modification of the mesh, it becomes very complicated and time consuming for the First Model, which is more complex. This time, the main dome collapses before other structural parts. This is different from the results of the static analysis of the other models. Cracking starts at the crests of the main semidomes. After imposing these cracks on the model, no more cracks are observed at the

semidomes. However, cracks occurring at the main dome propagate faster and the main dome collapses at load factor 1.8.

In the Third Model, the weaker west and east arches are replaced with stronger ones having the same rigidity as that of the north and south arches. However, this modification does neither increase the collapse load factor nor change the collapse behaviour. Conversely, tension stresses are distributed over a wider region at the first load factor, because the four strong arches surrounding the main dome restrict its displacements more. Initial cracks start at the secondary semidomes where they are connected to the main semidomes. These cracks propagate through the main semidomes. First, they spread over the perimeter of both main semidomes. The cracks at the west secondary semidomes spread faster than in other parts and they cover the middle part and the crest of the west main semidome. Finally, the west main semidome collapses because cracks cover almost one third of its surface the collapse condition (see Section 4) being reached.

According to the results obtained, there is no difference between the collapse behaviour of the First and Third Models under the static loads except the propagation of the cracks.

As the last alternative, the Fourth Model is created to investigate the effect of the steel ring placed between the top of the windows and the main dome. The collapse condition and the collapse behaviour of the Fourth Model are almost the same as those of the first one with except of some differences in the magnitudes of the stresses. Since the ring surrounding the main dome provides a radial confinement, tension stresses increase slightly, whereas the stress distribution does not change.

At the second part of the study, the First and Third Models are investigated from the spectral point of view. The response of a structure under the dynamic loads is affected by cracks existing and Hagia Sophia has already a lot of cracks. Unfortunately, no accessible records are available about these cracks. The cracked state of the First Model under its self-weight is obtained by the Load Increment Method. The procedure is started with load factor 0.08 and terminated when the

cracks stop to propagate at load factor 1. The dynamic vulnerability of this model is investigated using the Acceleration Increment Method, which is similar to the Load Increment Method. In the Acceleration Increment Method, the accelerations are increased with a factor incrementally and both the stress distributions and the crack propagation are determined at each increment. Cracks are imposed on the model at each acceleration value using the Smearred Crack Modelling Method under the different assumptions that are considered in the static analysis (see Section 4.3.2). The crack depth is taken into account in the analysis by reducing the elasticity moduli of cracked elements proportional to the crack depth and updating them accordingly. The procedure for the spectral analysis is started with acceleration 0.04g and finished when the crack propagation stops at acceleration 0.4g. 0.4g is the highest earthquake acceleration recorded at least two times during 500 years (Durukal, 2001).

At acceleration 0.1g, all the secondary semidomes and the perimeters of the main semidomes are cracked. Additionally, cracks occur at the crests of the main semidomes. These cracks spread through the middle part of the main semidomes for accelerations 0.2g, 0.3g and 0.4g. No cracks are observed at the main dome until the acceleration reaches the value 0.4g. At this acceleration, all the secondary semidomes, the east main semidome, almost all the surface of the west main semidome and partially, the main dome are cracked. In other words, the model has so many cracks at acceleration 0.4g. Nevertheless, the collapse has not been observed through the structure at this acceleration yet. This is because the depth of the cracks is considered in calculations and hence the cracked elements have still a load carrying capacity depending on their crack depths.

In the spectral analysis of the Third Model, the effect of the stronger arches on the dynamic vulnerability of the model is investigated. Like the procedure followed by the First Model, the Acceleration Increment Method is used to obtain the stress distributions of the model at each increment of the acceleration and the Smearred Crack Modelling Method is used to impose the cracks on the model. The Third Model performs very well under the spectral analysis. Only minor cracks are

observed at the secondary semidomes where they are connected to the main semidomes. This behaviour may be due to the period of the model, which increases from 0.51 second to 1.55 second after introducing stronger arches. Since the flexibility of the structure increases, it can endure acceleration 0.4g far better.

The period of the First Model increases at each acceleration value since cracks, which reduce the stiffness, are imposed on the model. In general, it can be said that the formation of cracks has the beneficial effect as it leads to the reductions in the natural frequencies during an earthquake. Consequently, considering crack propagation may have an important role to understand the real behaviour of a masonry structure.

When cracks are taken into consideration, the stress distribution changes through the structure. Stresses decrease in the cracked elements, hence their magnitudes increase in their neighbouring regions, which are still uncracked. Consequently, the collapse load factor can be obtained more realistically by following the propagation of cracks under incremental loading, which may be either static or dynamic.

Each part of the analyses, static or spectral, shows that the cracks of the First Model start at the secondary semidomes where they are connected to the main semidomes. For the following steps, the cracks spread through the main semidomes. However, at the Second Model, cracks start at the crest of the main semidomes where they are connected to the main arches, but the cracks at the main dome propagate faster and therefore, it collapses earlier, which means these regions require special attention in a retrofitting project.

The results also show that in the current state of the structure, strengthening of all semidomes has priority, if further cracks start to threaten the structure.

The top regions of the east and west main arches are also very critical. During the analyses performed at each part, cracks are observed at these regions. However, since the domes are the weaker parts of the structure as compared to the arches, the collapse condition is reached at the domes before the cracks at the arches propagate



widely. Nevertheless, the existing cracks at these regions have to be filled to prevent the collapse under a possible high ground motion.

Also according to the results of the spectral analyses, the risk of failure is high for the semidomes, while the main dome has no risk for itself even at acceleration 0.4g. Tension stresses of the secondary semidomes are higher than those at the other parts of the structure at acceleration 0.1g. The initial cracks start at the connection regions between the secondary and main semidomes and progress through the main semidomes. This is because the thickness of the secondary semidomes is about the half of that of the main semidomes. This shows that most probable collapse will initiate at the secondary semidomes propagating to the main semidomes. Therefore, strengthening of these parts is very important in a strengthening project in the way to relieve the main semidomes from high tension stresses.

Finally, cracks existing along the whole structure have to be investigated in detail and recorded, and the structure has to be investigated dynamically introducing these cracks in the analysis.

Following aspects are recommended to be considered in future research:

- Take the real cracked state of Hagia Sophia into account,
- Use the Discrete Crack Modelling Method in the First Model to compare both Crack Modelling Methods,
- Imply the Smeared Crack Modelling Method for the assumptions made in the dynamic analysis part (see Section 4.3.2) to the structure under static loads,
- Obtain the collapse load of the structure under dynamic loads,
- Investigate the effect of a ring placed between the top of the windows and the main dome (like in the Fourth Model) when the ring is prestressed, and finally
- Imply appropriate seismic isolation technics to the structure taking the critical regions determined in this study into account.

## REFERENCES

- Aoki, T.,** Kato, S. and Ishikawa, K., (1993), "Structural Characteristics of the Dome of Hagia Sophia from Measurement of Micro Tremor", Proceedings of the Strema International Symposium, Bath, UK, p. 115.
- Aoki, T.,** Kato, S., Ishikawa, K., Hidaka, K., Yorulmaz, M. and Çili, F., (1997), "Principle of Structural Restoration for Hagia Sophia", Strema 97, Spain.
- Atkinson, R. H.,** (1994), "In-place Evaluation of Masonry Materials", Proceedings of US - Italy Workshop on Guideline for Seismic Evaluation & Rehabilitation of Unreinforced Masonry Buildings, NCEER Report, p. 6/25.
- Bathe, K. J. and Wilson, E. L.,** (1976), Numerical Methods in Finite Element Analysis, Prentice-Hall Englewood Cliffs, N.J.
- Batur, A. ve Tanyeli, G.,** (1993), "1894 Depremi ve İstanbul'un Tarihi Yapılarındaki Hasar Üzerine Bir Örnekleme Çalışması: Ayasofya", 2. Ulusal Deprem Mühendisliği Konferansı, TMMOB Publication, The Chamber of Civil Engineering, İstanbul, p. 253.
- Binda, L.,** Roberti, G. M., Tiraboschi, C. and Abbaneo, S., (1994), "Measuring Masonry Material Properties", NCEER Report, p.6/3.
- Blasi, C.,** (2001), "Hagia Sophia: Geometry and Collapse Mechanisms", Studies in Ancient Structures, 2nd International Congress, Yıldız Technical University, Faculty of Architecture, p.323.
- Borrell, C. M.,** (1996), "Characterisation of the Mechanical Behaviour of Masonry", Structural Analysis of Historical Constructions, CIMNE, Barcelona, p. 87.
- Chen, W. -F. and Saleeb, A. F.,** (1994), "Constitutive Equations for Engineering Materials", Studies in Applied Mechanics, Vol.1 Elasticity and Modelling, 37A, Elsevier, USA.
- Croci, G.,** Cerone, M. and Visković A., (1997), "Analysis From a Historical and Structural Point of View of the Domes of Pantheon, Hagia Sophia and St. Peter", International Conference on Studies in Ancient Structures, Yıldız Technical University, p. 295.
- Çakmak, A. S.,** Moropoulou, A. and Erdik, M., (1998), "Dynamic Behaviour and Earthquake Response of Hagia Sophia", Compatible Materials for the Protection of European Cultural Heritage, Pact 55, ISSN: 0257-8727, p.31.
- Durukal, E.,** (1992), A Study on Structural Identification and Seismic Vulnerability Assessment of Ayasofya, M.Sc Thesis, Boğaziçi University, (unpublished).



**Durukal, E.,** Çakmak, A., Yüzügüllü, Ö., and Erdik, M., (1997), “Assessment of the Earthquake Performance of Hagia Sophia”, *Incomareh - Raphael, Studies in Ancient Structures*, Yıldız Technical University, Istanbul, p. 407.

**Durukal, E.,** Yüzügüllü, Ö. and Beyen, K., (1998), “Assessment of Mortar and Brick Properties of Hagia Sophia by Non-Destructive Testing Techniques - Non-Destructive Testing of Structural Materials in Historical Buildings”, *Compatible Materials for the Protection of European Cultural Heritage, Pact 55, ISSN: 0257-8727*, Istanbul, p. 221.

**Durukal, E.,** Erdik, M., Alpay, Y. and Celep U., (2001), “İstanbul’un Depremelliği”, *Türkiye Mühendislik Haberleri*, Vol. 2001-3, ISSN: 1300-3445, Ankara, p.11.

**Erdik, M.,** Durukal, E., Yüzügüllü, Ö., Beyen, K. and Kadakal, U., (1993), “Strong-motion Instrumentation of Hagia Sophia and the Analysis of Response to an Earthquake of 4.8 Magnitude”, *Structural Repair and Maintenance of Historical Buildings III, Proceedings of STREMA’ 93, 3rd International Conference*, Bath, UK, p. 99.

**Findell, K. L.,** Köyliüoğlu, H. U., and Çakmak, A. Ş. (1993), “Modelling and Simulating Earthquake Accelerograms using Strong Motion Data from the Istanbul, Turkey Region”, *Structural Repair and Maintenance of Historical Buildings III, Proceedings of STREMA’ 93, 3rd International Conference*, Bath, UK, p. 85.

**Gezi,** (1998), *Periodical*, p. 62.

**Gonçalves, T. D.,** (1998) “Compatible Renders for the Conservation of Ancient Buildings”, *Compatible Materials for the Protection of European Cultural Heritage, Pact 55, ISSN: 0257-8727*, p. 29.

**Jirásek, M.,** (2000), “Comparative Study on Finite Elements with Embedded Discontinuities”, *Computer Methods in Applied Mechanics and Engineering*, p.307.

**Karaesmen, E.,** (1993), “Structural Behaviour of Historic Masonry Domes of Major Importance: An Overview”, *Structural Repair and Maintenance of Historical Buildings III, Computational Mechanics Publications*, Southampton Boston, p.157.

**Karaveziroğlu, M.,** Papayianni, J., and Penelis, G. Gr., (1998), “Mortars and Grouts in Restoration of Roman and Byzantine Monuments”, *Compatible Materials for the Protection of European Cultural Heritage, Pact 56, ISSN: 0257-8727*, p. 219.

**Koyunlu, A.,** (1990), “Ayasofya Restorasyonu Genel Sorunları”, *Yapı*, Volume: 105, p. 47.

**Leftheris, B.P.,** Sapounaki, A., Stavroulaki, M.E., Tzanaki, E., Stavroulakis, G.E. (1998), “Effects of Material Modelling on the Modal Analysis of the Lighthouse in the Venetian Harbour of Chania”, *Compatible Materials for the Protection of European Cultural Heritage, Pact 55, ISSN: 0257-8727*, p. 231.

**Livingstone, R. A.,** Stutzman, P. E., Mark, R. and Erdik, M., (1992), "Preliminary Analysis of the Masonry of the Hagia Sophia Basilica", Materials Research Society, Spring Meeting, San Francisco, C. A, p.2.

**Mainstone, R. J.,** (1965), "The Structure of the Church of St. Sophia", Istanbul, Read at the Science Museum, London, p.23.

**Mainstone, R. J.,** (1988), "The Süleymaniye Mosque and Hagia Sophia", Int. Symposium on Sinan the Architect, Ankara, p.221.

**Mainstone, R. J.,** (1990), "Hagia Sophia: Justinian's Church of Divine Wisdom, later the Mosque of Ayasofya, in Istanbul", Journal of Structural Engineers, The Structural Engineer, Vol. 68, number 4, p.65.

**Mainstone, R. J.,** (1993), "The Structural Conservation of Hagia Sophia", Structural Repair and Maintenance of Historical Buildings III", Computational Mechanics Publications, Southampton Boston, p.3.

**Mark, R. and Westagard, A.,** (1988), "The First Dome of the Hagia Sophia: Myth vs. Technology", Domes from Antiquity to the Present, Proceedings of IASS- MSU Symposium, İstanbul, p.163.

**Mark, R., Çakmak, A. S., Hill, K., and Davidson, R.** (1993a), "Structural Analysis of Hagia Sophia: A Historical Perspective", Structural Repair and Maintenance of Historical Buildings III, Computational Mechanics Publications, Southampton Boston, p.33.

**Mark, R., Çakmak, A. S., Erdik, M. and Livingstone, R. A.,** (1993b), "The Structural Evaluation of Hagia Sophia in Istanbul", Public Assembly Structures From Antiquity to the Present, IASS Symposium, p. 113.

**Meyer-Christian, W.,** (1988), "Hagia Sophia, the Engineers Planning of Anthemios and Isidorus Reconstruction", Domes from Antiquity to the Present, Proceedings of IASS- MSU Symposium, İstanbul, p.173.

**Moropoulou, A., Çakmak, A. S. and Biscontin, G.,** (1998a), "Criteria and Methodology to Evaluate the Hagia Sophia Crushed Brick/Lime Mortars", Compatible Materials for the Protection of European Cultural Heritage, Pact 55, ISSN: 0257-8727, p. 39.

**Moropoulou, A., Kouli, M., Christaras, B. and Tsiourva, Th.,** (1998b), "Non-destructive Evaluation the Performance of Mortars on Historic Masonries", Compatible Materials for the Protection of European Cultural Heritage, Pact 55, ISSN: 0257-8727, p. 243.

**Moropoulou, A., Tsiourva, Th., Theoulakis, P., Christaras, B. and Kouli, M.,** (1998c), "Non-Destructive Evaluation of Pilot Scale Treatments for Porous Stone Consolidation in the Medieval City of Rhodes", Compatible Materials for the Protection of European Cultural Heritage, Pact 56, ISSN: 0257-8727, p.259.

**Mungan, İ.**, Türkmen, M. (1995), "Effect of the Arches and Semidomes on the Static and Dynamical Behaviour of the Central Dome in Hagia-Sophia", Proc. IASS Symp. Spatial Structures: Heritage, Present and Future, 1995, Vol. 2, Padova, ISBN 88-86281-10-2, p. 1253-1269.

**Mungan, İ.**, Türkmen, M., Yüksel, A. (1995), "Hagia Sophia: The Lightweight Dome of the Early Medieval Age, Proc. Int. Conf. Lightweight Structures in Civil Engineering, Warsaw Burska, p.739-741.

**Wiener, W. M.**, (1998), "İstanbul'un Tarihsel Topoğrafyası", Yapı Kredi Yayınları-1419, Toplumsal Tarih Araştırmaları Dizisi-7.

**Penelis, G. Gr.**, (1995), "Mortar and Grout", Mortars and Grouts in Restoration of Roman and Byzantine Monuments, The European Seminar on "Ancient and Traditional Mortar Technology and Their Importance in Conservation Projects", Thessaloniki, p. 91.

**Rossi, P. P.**, (1996), "Possibilities of the Experimental Techniques for the Structural Analysis of Historical Construction", EC Workshop on Non-destructive Testing To Evaluate Damage due to Environmental Effects on Historic Monuments, Trieste, Italy, paper number: 13.

**Rossi, P. P.**, (1997), "Experimental Techniques for the Structural Analysis of Historical Buildings", Geotechnical Engineering for the Preservation of Monuments and Historic Sites, Viggiani, Balkema, Rotterdam, p. 275.

**Rossi, P. P.** and Ventrucci, F., (1998), "Structural Assessment of St. Mark's Basilica, Venice", Compatible Materials for the Protection of European Cultural Heritage, Pact 55, ISSN: 0257-8727, p.277.

**SAP2000**, (1997), Integrated Structural Analysis and Design Software, Computer and Structures Inc., Berkeley, California.

**Singer, Ferdinand L.**, (1962), "Strength of Materials", Harper International Edition, New York, Evanston, and London, INT 35-06607.

**Smith, J. V.**, (1996), "Hagia Sophia: Advancement of Nonlinear Modelling", Senior Thesis, Princeton University, (unpublished).

**Spektra**, (1998), "Ayasoya'nın Deprem Performansı" İstanbul Anıtlar ve Müzeler Genel Müdürlüğü, İstanbul Röleve ve Anıtlar Müdürlüğü, Technical Report.

**Türkmen, M.**, (1994), "Ayasofya, Süleymaniye, Şehzade ve Mihrimah Tipi Cami Örtülerinde Yük Aktarımının Sonlu Eleman Metoduyla Çözümlemlenip İrdelenmesi", Ph.D Dissertation, Mimar Sinan University, (unpublished).

**Wilson, E. L.**, Der Kiureghian A., and Bayo E. P., (1981), "A Replacement for the SRSS Method in Seismic Analysis", Earthquake Engineering and Structural Dynamics, Vol. 9.